



Kent Academic Repository

Smith, Gregory (2019) *Properties of Knotted Solutions to Maxwell's Equations: An Exploration of Lipkin's Zilches in Vacuum Electromagnetic Fields, and a Multipole Expansion of the Vector Spherical Harmonics of Knotted Electromagnetic Fields.* Doctor of Philosophy (PhD) thesis, University of Kent,.

Downloaded from

<https://kar.kent.ac.uk/81514/> The University of Kent's Academic Repository KAR

The version of record is available from

This document version

UNSPECIFIED

DOI for this version

Licence for this version

UNSPECIFIED

Additional information

Versions of research works

Versions of Record

If this version is the version of record, it is the same as the published version available on the publisher's web site. Cite as the published version.

Author Accepted Manuscripts

If this document is identified as the Author Accepted Manuscript it is the version after peer review but before type setting, copy editing or publisher branding. Cite as Surname, Initial. (Year) 'Title of article'. To be published in *Title of Journal*, Volume and issue numbers [peer-reviewed accepted version]. Available at: DOI or URL (Accessed: date).

Enquiries

If you have questions about this document contact ResearchSupport@kent.ac.uk. Please include the URL of the record in KAR. If you believe that your, or a third party's rights have been compromised through this document please see our [Take Down policy](https://www.kent.ac.uk/guides/kar-the-kent-academic-repository#policies) (available from <https://www.kent.ac.uk/guides/kar-the-kent-academic-repository#policies>).



University of
Kent

PROPERTIES OF KNOTTED SOLUTIONS TO MAXWELL'S
EQUATIONS:
An Exploration of Lipkin's Zilches in Vacuum Electromagnetic
Fields; and a Multipole Expansion of the Vector Spherical
Harmonics of Knotted Electromagnetic Fields

A thesis presented by
Gregory Smith
to the
SCHOOL OF PHYSICAL SCIENCES,
UNIVERSITY OF KENT

In partial fulfilment of the requirements
for the degree of
Doctor of Philosophy in the subject of
PHYSICS

UNIVERSITY OF KENT
JUNE 2019

DECLARATION

University of Kent
PhD work Candidate Declaration

Candidate Name: Gregory Smith

Faculty: Faculty of Science

Thesis Title: Properties of Knotted Solutions to Maxwell's Equations: An Exploration of Lipkin's Zilches in Vacuum Electromagnetic Fields; and a Multipole Expansion of the Vector Spherical Harmonics of Knotted Electromagnetic Fields

Declaration to be completed by the candidate:

I declare that no portion of this work referred to in this thesis has been submitted in support of an application for another degree or qualification of this or any other university or other institute of learning.

Signed:

Date: January 16, 2020

COPYRIGHT

The author of this dissertation (including any appendices and/or schedules to this thesis) owns any copyright in it (the “Copyright”)¹ and he has given the University of Kent the right to use such Copyright for any administrative, promotional, educational and/or teaching purposes.

Copies of this dissertation, either in full or in extracts, may be made only in accordance with the regulations of the University Library of Kent. Details of these regulations may be obtained from the Librarian. This page must form part of any such copies made.

The ownership of any patents, designs, trade marks and any and all other intellectual property rights except for the Copyright (the “Intellectual Property Rights”) and any reproductions of copyright works, for example graphs and tables (“Reproductions”), which may be described in this thesis, may not be owned by the author and may be owned by third parties. Such Intellectual Property Rights and Reproductions cannot and must not be made available for use without the prior written permission of the owner(s) of the relevant Intellectual Property Rights and/or Reproductions.

Further information on the conditions under which disclosure, publication and exploitation of this thesis, the Copyright and any Intellectual Property Rights and/or Reproductions described in it may take place is available from the Head of School of Physical Sciences (or the Vice-President) and the Dean of the Faculty of Science, for Faculty of Science candidates.

¹This excludes material already printed in academic journals, for which the copyright belongs to said journal and publisher. Pages for which the author does not own the copyright are numbered differently from the rest of the thesis.

ACKNOWLEDGEMENTS

When I first talked to my supervisor, Professor Paul Strange, about undertaking a PhD in theoretical physics, hopefully involving mathematical knot theory, he said to me, ‘Greg, we are about to embark on an intellectual journey into the unknown!’. Before long, I realised he meant that entirely literally and that this project would take me on a route that would test me to my intellectual and emotional limits. I have seen the great cartoons summarising the journey of a PhD student’s evolution, from the happy, driven, enthusiastic student, to the stressed, confused, and frantic researcher, to finally the broken, exhausted wreck of a doctor-in-waiting that has given everything to this pursuit of knowledge. I can confirm that that cartoon is entirely accurate if not photographic in its ability to summarise every emotion I have been through to complete this thesis. This has been by far, the most difficult task I have ever undertaken for a number of reasons. I have, just about, managed to reach the end and obviously have a lot of people to thank for helping keep the parts of me together.

First of all, I would like to thank my supervisor for giving me the truest experience of what fundamental research is. We both started off with no knowledge of mathematical knots or had that much experience with classical electromagnetism, but I have managed, with his guidance, to publish half of the research (so far) and complete a PhD thesis in a very challenging area of mathematical physics.

Next I would like to say a big thank you to my family, some of which are no longer here with us. You have created the perfect environment for me as a child to question and enquire about the world around me. Sometimes it may not seem like the best outcome as I have changed from the happy blonde boy that loves everything, to one that is a bit hardened and grown-up. But without this up-bringing, I would not have

even considered undertaking a PhD in any subject, let alone thought one in mathematical physics was a possibility. Without the financial support too that both sets of grandparents provided through their own life's work - to earn enough so that all their children and grandchildren could have a good education - I could not have managed this. Thank you all so much. I miss you Granny, Grandad and Nanny.

Lastly, the biggest thank you of all goes to the person that has experienced every emotion that I have on this journey, not only from her own PhD, but now by having to be the wife riding alongside their partner doing the same self-inflicted damage to themselves. Dr. Joanna Thornton-Smith, I think it is a massive understatement to say that without you I could not have completed this thesis. You have helped me through the darkest moments in my life, you have proof read every page of this thesis and every paper I have submitted, and most importantly you have carried on telling me that I can do it when I thought it beyond the bounds of possibility. I am glad that we have had each other through the past few years, because tackling any of the things that we have had to without each other I think would have been impossible. You are the only one that will truly know what I have been through to get to this stage and to do that you would have endured a lot from me. I cannot thank you enough. I love you the mostest.

ABSTRACT

Classical Maxwell's equations have been fundamental to our understanding of physics since their inception in the 19th century. Any research which contributes to our understanding of them is of importance. In 1989, Ranāda introduced a topological formalism of Maxwell's equations in vacuum - investigating a set of solutions involving a mapping between spherical spaces projected into the electric and magnetic field lines - named the Hopf fibration. This research has been furthered by Ranāda and other prominent scientists to include: the family of torus knots within the field lines; a theory of the fundamental charge; and a description of the number of right and left handed photons. The Hopf fibration, embedded into charge-free electric and magnetic field lines as exact solutions to Maxwell's equations, is a central component to this body of work. Topological, classical electromagnetism is, therefore, an area that has the potential to further our understanding of Maxwell's equations.

This thesis describes a project that advances the knowledge of knotted electromagnetic fields and electromagnetism in two, distinct areas: zilches of unusual electromagnetic fields; and a multipole expansion on the vector spherical harmonics of the knotted electromagnetic fields. Zilches are a set of little-known conserved quantities within the charge-free Maxwell's equations. They were originally posited by Lipkin as new and potentially exciting - if their physical nature could be determined. This research examines the zilches in three unusual topologically non-trivial sets of electromagnetic fields - starting with the knotted solutions to Maxwell's equations. The results show a profound connection between the zilches and the fields' topology. It conjectures that this is the case for all integrable solutions. Alongside this, it is shown that the zilches can be written in terms of other, known conserved quantities of the fields.

The latter half of this thesis focuses on delivering a generalised multipole expansion of the vector spherical harmonics for the knotted electromagnetic fields, after outlining various flaws in the assumptions made by previous literature. Finally, the results from generating the generalised multipolar expansion coefficients are analysed and presented. A summary of the first 3680 coefficients are given in 18 equations - after noticing patterns occurring between them.

Firstly, this research further develops the area of knotted electromagnetic fields, providing a platform from which to generate them experimentally and to develop the theory further. Secondly, it sheds considerable light on the interpretation of the zilches and suggests a more central role in electromagnetism.

PUBLICATIONS

1. Smith, G and Strange, P. Properties of Null Knotted Solutions to Maxwells Equations. *Proc.SPIE*, 10120:10120 10120 6, 2017
2. Smith, G and Strange, P. Lipkins Conservation Law in Vacuum Electromagnetic Fields. *Journal of Physics A: Mathematical and Theoretical*, 2018

CONTENTS

Declaration	i
Copyright	ii
Acknowledgements	iii
Abstract	v
Publications	vii
1 Introduction	1
2 Background Theory	5
2.1 Mathematical Knot Theory and the Hopf fibration	5
2.1.1 Unknots, Knots, and Links	6
2.1.2 Knot Tabulation, Knots' Projections, and Reidemeister's Moves	7
2.1.3 Knot Classes	9
2.1.3.1 Torus Knots and the Torus	9
2.1.4 Knot Invariants	12
2.1.4.1 Crossing Number	12
2.1.4.2 Unknotting Number	12
2.1.4.3 Other Key Knot Invariants	12
2.1.5 The Hopf fibration	13
2.1.6 Stereographic Projection	16
2.2 Knotted Solutions to Maxwell's Equations	21
2.2.1 Bateman's Construction	22
2.2.2 An Extension to an Infinite Family of Solutions	27

2.2.3	Examples and Proofs	29
2.2.4	The Hopf fibration and the Electromagnetic Field	30
2.2.5	The Production of the Whole Family of Torus Knots as Solutions to Maxwell's Equations	32
2.2.6	Visualisation of the Electromagnetic Fields	34
2.2.7	Known Properties of Knotted Solutions to Maxwell's Equations	44
2.3	Summary	45
3	Zilches of Knotted Electromagnetic Fields	47
3.1	Lipkin's Zilches	49
3.2	Zilches in Knotted Electromagnetic Fields	51
3.2.1	Linking the Zilches to Topological Properties of the Fields . .	54
3.3	Zilches in Segmented Electromagnetic Fields	67
3.4	Zilches in 'Dripping' Electromagnetic Fields	70
3.5	Summary	73
4	The Generalized, Multipolar expansion of Knotted Electromagnetic Fields	74
4.1	Multipolar Expansion of the Vector Spherical Harmonics for the Hopf-Knotted Fields	75
4.1.1	Irvine and Bouwmeester's Multipole Expansion Method	77
4.1.2	The Derivation of Jackson's Multipole Expansion Coefficients	81
4.1.3	Irvine and Bouwmeester's Results Extended to Higher Knot Types	87
4.2	Generalised Multipolar Expansion of the VSH of the Knotted Solutions to Maxwell's Equations Method	91
4.2.1	Results from the Generalised Multipolar Method	95
4.2.2	Investigating the Patterns Occurring in the Multipole Coefficients	100
4.3	Summary	104
5	Conclusions	105
	Bibliography	109
A	Field Components for the Different $p - q$ knot-types	114
B	Multipole Coefficient Generation, $r^{-1}f_{l,m}$, for the V-VSH, for the Electric (C) and Magnetic (A) Vector Potentials	117

C Multipole Coefficient Generation, $r^{-1}f_{l,m}$, for the V-VSH, for the Electric (E) and Magnetic (B) Fields	120
D Multipole Coefficient Generation, $r^{-1}g_{l,m}$, for the W-VSH, for the Electric (A) and Magnetic (C) Vector Potentials	123
E Multipole Coefficient Generation, $r^{-1}g_{l,m}$, for the W-VSH, for the Electric (E) and Magnetic (B) Fields	126
F Multipole Coefficient Generation, $r^{-1}h_{l,m}$, for the X-VSH, for the Electric (E) and Magnetic (B) Fields, and the Electric (A) and Magnetic (C) Vector Potentials	130
G Tabulated Multipole Coefficients	133

LIST OF FIGURES

2.1	Examples of the different quantities within mathematical knot theory	7
		7
2.3	Examples of the three different projections of the trefoil knot	8
2.4	The three Reidemeister moves	8
		10
2.6	The toroidal direction is denoted by the blue arrow, the poloidal direction by the red arrow	10
2.7	Four examples of torus knots and their winding numbers	11
2.8	Removing one crossing from the $T(2, 3)$ knot and applying Reidemeister moves II and III to reveal the unknot.	13
2.9	The Hopf-map, η , and the pre-image, η^{-1}	16
2.10	Stereographic projection from $S^1 \rightarrow \mathbb{R}^1$	17
2.11	Stereographic projection from $S^2 \rightarrow \mathbb{R}^2$	18
2.12	Stereographic projection, $S^2 \rightarrow \mathbb{R}^2$, showing the warping of the sizes of latitude circles on the projection plane when taken closer to the north or south pole (shown as dotted lines)	19
2.13	Stereographic projection, $S^3 \rightarrow \mathbb{R}^3$, of the pre-image of the Hopf-map of a singular point from S^2	19
2.14	Stereographic projection, $S^3 \rightarrow \mathbb{R}^3$, of the pre-image of the Hopf-map of two points from S^2 , showing two linked circles - known as the Hopf-link	20
2.15	Stereographic projection, $S^3 \rightarrow \mathbb{R}^3$, of the pre-image of the Hopf-map of one complete latitude level of S^2 , showing all the linked circles form a torus surface	20
2.16	Stereographic projection, $S^3 \rightarrow \mathbb{R}^3$, of the pre-image of the Hopf-map of multiple points from three latitude levels of S^2 , showing multiple nested tori emerging	21

2.17	One latitude level of S^2 from the Hopf fibration projected into the electric, magnetic, and Poynting fields at time $t = 0$	33
2.18	The three levels of S^3 from the Hopf fibration projected into R^3	35
2.19	One magnitude level of the electric and magnetic scalar fields	36
	37	
2.21	The magnitudes of both the original and inside-out torus	38
2.22	The deformation of the scalar torus	38
2.23	Scalar plots of the electric and magnetic fields with differing trivial (p, q) -knots, projected at different magnitudes of $\phi_{1(2)}$	40
2.24	Scalar plots of the electric and magnetic fields with differing (p, q) -knots projected at different magnitudes of $\phi_{1(2)}$	41
2.25	Time evolution for three different knots projected into the electric and magnetic field lines	43
3.1	The p - q winding number tree showing the various combinations possible for $p = 1 - 10$ and $q = 1 - 10$	55
3.2	The results for Z^{000} when put in units per $\frac{1}{4(p+q)}E_{p,q} = pq\pi^2p!q!\epsilon_0E_0^2k^2/(2(p+q)!)$	56
3.3	The results for Z^{030} when put in units per $\frac{1}{4(p+q)}E_{p,q} = pq\pi^2p!q!\epsilon_0E_0^2k^2/(2(p+q)!)$	57
3.4	The results for Z^{110} when put in units per $\frac{1}{4(p+q)}E_{p,q} = pq\pi^2p!q!\epsilon_0E_0^2k^2/(2(p+q)!)$. These results are the same for Z^{220}	58
3.5	The results for Z^{330} when put in units per $\frac{1}{4(p+q)}E_{p,q} = pq\pi^2p!q!\epsilon_0E_0^2k^2/(2(p+q)!)$	59
3.6	The results for Z^{110} with the components highlighted using the colour coding system described in the text body that are used for calculating the crossing and unknotting numbers for torus knots	64
3.7	The results for $c(T(p, q))$ with the components highlighted using the colour coding system described in the text body that are used for calculating the crossing and unknotting numbers for torus knots	65
3.8	The results for $u(T(p, q))$ with the components highlighted using the colour coding system described in the text body that are used for calculating the crossing and unknotting numbers for torus knots	66

3.9	Segmented surfaces for: a. $(p, q) = (1, 1)$, $\phi_2 = 0.20$, giving one surface; b. $(p, q) = (4, 2)$, $\phi_2 = 0.005$, giving two surfaces; c. $(p, q) = (1, 5)$, $\phi_2 = 0.005$, giving five surfaces; d. $(p, q) = (3, 3)$, $\phi_2 = 0.005$, giving three surfaces; e. $(p, q) = (1, 5)$, $\phi_1 = 0.005$, giving five surfaces; f. $(p, q) = (3, 3)$, $\phi_1 = 0.005$, giving three surfaces	68
3.10	Dripping surfaces for: a. $(p, q) = (1, 1)$, $\phi_2 = 0.20$, giving two surfaces; b. $(p, q) = (1, 3)$, $\phi_2 = 0.05$, giving four surfaces; c. $(p, q) = (4, 1)$, $\phi_2 = 0.04$, giving five surfaces; d. $(p, q) = (2, 3)$, $\phi_2 = 0.03$, giving five surfaces; e. $(p, q) = (1, 1)$, $\phi_1 = 0.29$, giving two surfaces; f. $(p, q) = (1, 3)$, $\phi_1 = 0.05$, giving four surfaces (the plotting grid has been chosen here to cut holes in the outer surface so as to view the inner surfaces, in reality this surface is closed)	71
4.1	The exact knot types and their p - q combinations that were calculated are shown in red, with the p - q winding number tree showing the various combinations possible for $p = 1 - 10$ and $q = 1 - 10$	94

LIST OF TABLES

2.1	Table displaying the densities of known, conserved quantities	44
2.2	Table displaying the conserved quantities in terms of the winding numbers of the fields, (p, q) , and the total energy of the fields, $E_{p,q}$	45
3.1	Table displaying the numerical components of zilch for a variety of the winding numbers of the fields, (p, q)	52
3.2	The zilches in terms of the total energy of the field are completely related to the winding numbers of the field	53
3.3	The zilches in terms of known conserved quantities of the knotted fields	53
3.4	The values of the zilches for the various $p + q = 6$ knot-types and the results for calculating the number of pieces of surface, $N_{p,q}$	60
3.5	Conserved field properties and number of pieces of surface for the $(p, q) = (2, 3)$ segmented field	69
3.6	Examples to demonstrate the number of pieces of surface for $p + q = 5$	72
G.1	The Generalised Multipolar Coefficients For the Vector Spherical Harmonics, Knot type: $p=1; q=1$	134
G.4	The Generalised Multipolar Coefficients For the Vector Spherical Harmonics, Knot type: $p=1; q=2$	136
G.6	The Generalised Multipolar Coefficients For the Vector Spherical Harmonics, Knot type: $p=1; q=2$	137
G.8	The Generalised Multipolar Coefficients For the Vector Spherical Harmonics, Knot type: $p=1; q=3$	138
G.10	The Generalised Multipolar Coefficients For the Vector Spherical Harmonics, Knot type: $p=1; q=3$	139
G.12	The Generalised Multipolar Coefficients For the Vector Spherical Harmonics, Knot type: $p=1; q=4$	140

G.14 The Generalised Multipolar Coefficients For the Vector Spherical Harmonics, Knot type: $p=1; q=4$	141
G.16 The Generalised Multipolar Coefficients For the Vector Spherical Harmonics, Knot type: $p=1; q=5$	142
G.18 The Generalised Multipolar Coefficients For the Vector Spherical Harmonics, Knot type: $p=1; q=5$	143
G.20 The Generalised Multipolar Coefficients For the Vector Spherical Harmonics, Knot type: $p=1; q=6$	144
G.23 The Generalised Multipolar Coefficients For the Vector Spherical Harmonics, Knot type: $p=2; q=1$	147
G.25 The Generalised Multipolar Coefficients For the Vector Spherical Harmonics, Knot type: $p=2; q=1$	148
G.26 The Generalised Multipolar Coefficients For the Vector Spherical Harmonics, Knot type: $p=2; q=2$	150
G.28 The Generalised Multipolar Coefficients For the Vector Spherical Harmonics, Knot type: $p=2; q=2$	151
G.30 The Generalised Multipolar Coefficients For the Vector Spherical Harmonics, Knot type: $p=2; q=3$	152
G.32 The Generalised Multipolar Coefficients For the Vector Spherical Harmonics, Knot type: $p=2; q=3$	153

INTRODUCTION

Maxwell's equations are those that encompass all of classical electromagnetism, surviving every test put to them in the constantly changing landscape of scientific advancement [1]. They can be solved using standard techniques to produce solutions of monochromatic, wave-like electromagnetic radiation in vacuum [2]. They are celebrated as one of the great achievements of 19th century physics. Therefore, it is noteworthy, when science can produce another point from which to view and interpret them. In 1989, Ranãda introduced a topological formalism of Maxwell's equations to study a set of exotic solutions to Maxwell's equations [3], shown to be equivalent to previous solutions [4][5][6], in the form of a topological mapping - named the Hopf fibration [7]. The Hopf fibration is a mapping from the three-sphere, S^3 , to the two-sphere, S^2 [7], that, when projected into the electric and magnetic field lines, fills all of 3-dimensional real space, R^3 , with field lines that are loops, linked with each other *once*. When encoded in electric and magnetic fields lines via the Hopf fibration, the different latitudinal levels of S^3 appear as toroidal surfaces, nested inside one another - like Russian dolls. Ranãda's body of work showed that Maxwell's equations could be written in this topological framework, with the Hopf fibration underlying the field lines. It further demonstrated a quantization of the fundamental charge (3.3 times that of the electron charge), without the need for the Dirac monopole [3][8][9][10][11][12].² The research also characterised the number of right and left-handed photons - relating a quantum mechanical result to classical theory. The issue with Ranãda's method is that the topology of the field lines *is not preserved when propagating with time*. The Hopf fibration and its involvement in classical electromagnetic theory is of central importance to the advancement of a topological understanding of Maxwell's equations.

²The quantization of the fundamental charge is beyond the scope of this thesis.

In 2003, Bialynicki-Birula investigated a particular method of introducing vortex lines into electromagnetic fields, using a configuration originally developed in the early twentieth century, named *Bateman's construction* [13][6]. He explored the vortex lines in a set of *null* fields, discussed extensively by Robinson and Trautman [4][14] - named the *Robinson congruence*. These fields represented the velocity field that underlies Hopf-knotted fields. Robinson demonstrated that this field was constant, with time allowing the field lines to be transported along them without breaking. Irvine followed this paper by showing that the condition enforced by Bateman's construction, named the *null condition* (forcing the electric and magnetic fields to remain perpendicular to each other), was vital to ensuring that the topology of the field lines within the Hopf-knotted electromagnetic fields was preserved with propagation in time - and not dependant on the helicity of the field [15]. Kedia bolstered this research [16] by utilising a theorem from complex analysis, showing that under a particular set of conditions the powers of two complex functions when applied (the initial inputs to Bateman's construction for the Hopf fibration) were the winding numbers associated with the family of torus knots [17]. This allowed Kedia to demonstrate the infinite family of torus knots appearing within the electromagnetic field lines. Irvine published two papers outlining a multipolar expansion method applied to the Hopf-knotted fields[18][15], leading to a suggestion for their experimental realisation. The second of these papers extended this work to include the whole family of torus-knotted fields. Fully understanding these unusual electromagnetic fields would provide a real advance in the theory of electromagnetism - and beyond. As these exact solutions are found to have converging total energy, when considered over all space, they also provide a unique opportunity to examine other areas of electromagnetism that are poorly understood. The research presented here provides advancement in *both* areas.

This thesis is divided into three main chapters: Background Theory; Zilches of Knotted Electromagnetic Fields; and The Generalised, Multipolar Expansion of the Knotted Electromagnetic Fields. The first chapter aims to set the scene for the reader - explaining the underlying theory that forms the base for the investigations that follow. It provides a break-down of the basics of knot theory, to allow the reader a complete understanding of a mathematical knot. It then builds to discuss the nature of different spaces (spherical space) through which the Hopf fibration is defined. The Hopf fibration is then described in detail - mathematically. A method is provided by which to view this mapping in R^3 - stereographic projection. It moves on to show

how the Hopf fibration can be projected into the electric and magnetic field lines, via Bateman's construction. This construction has the added benefit, in comparison to Ranāda's method, that the topology projected into the field lines is preserved for all time, because of the enforced *null* condition at time, $t = 0$. More advanced solutions are demonstrated involving the theorem that enables the powers of two complex numbers to represent the winding numbers of the family of torus knots, allowing an infinite set of solutions to be encoded within the electromagnetic field lines. A novel method for viewing the topology is demonstrated through scalar field representation. Finally, the conserved properties of the sets of solutions are shown to be related to the total energy of the fields and their winding numbers.

The second chapter contributes to the body of work concerning a set of conserved quantities within vacuum electrodynamics, named the zilch of the field. Zilches were first introduced by Lipkin, in 1964, and promised to be a new, potentially exciting, quantity, the physical nature of which was not yet understood. This chapter explores the zilches in three, different, unusual electromagnetic fields - starting with the set of knotted solutions to Maxwell's equations. It will be demonstrated that the zilches have a deep connection to the topology of the charge-free dynamic fields, when such fields have solutions that have converging total energy. It will also be demonstrated that the zilches can be written entirely in terms of the other, known conserved quantities of the fields and their winding numbers: energy, momentum, angular momentum and helicity. This research differs from the current literature - not only because it examines the zilches in unusual fields that have converging total energy, and because it produces results for more than just Z^{000} - but it also facilitates a more in-depth understanding of the connection between the zilches and the fields.

The third chapter tackles one of the leading papers on knotted electromagnetic theory, by Irvine and Boumeester, that demonstrates a method of conducting a multipole expansion on the vector spherical harmonics, leading to the suggestion of a method for experimentally verifying such a set of fields [18]. It is the contention of this chapter that an initial assumption by Irvine and Boumeester invalidated the method used and, therefore, their results. An extension to higher knotted solutions is developed, using their original method, in an attempt to produce an equation given by Irvine in a subsequent paper [15]. This process achieves differing results. Because of the failure to find satisfactory results in this area, this chapter moves to develop a general

multipole expansion of the vector spherical harmonics. In doing so, patterns are discovered in the multipole coefficients that could help summarise them. These patterns are explored, defined and checked for the first 3680 multipole coefficients emanating from the first 49 different knot combinations, across four fields: electric, magnetic, electric vector potential and magnetic vector potential. This chapter summarises these coefficients in 18 equations, via the patterns discovered.

Finally, this thesis will culminate in a concluding chapter, summarising the results and suggesting routes for further work.

BACKGROUND THEORY

This chapter aims to cover the foundation theory upon which this research is built. It is broken down into two, main sections: Mathematical Knot Theory and the Hopf fibration; and Knotted Solutions to Maxwell's Equations. The first section covers the basics needed to understand knot theory and the equations that are used to understand the topological connections given in Chapter 3. It concludes with a discussion of the mathematical construction of the Hopf fibration, describing what it is and a way to view it in three dimensions of space. The second section outlines a novel way to reformulate Maxwell's equations - through a method called *Bateman's construction* - which allows the null electromagnetic fields' associated velocity field to remain constant with time. By employing this method, it will be shown that the Hopf fibration - and later the whole family of torus knots - can be projected into the electric and magnetic field lines as *exact* solutions to Maxwell's equations. A unique way of visualising the topology of these knotted fields is also given, as well as a few of the known properties of these solutions.

2.1 Mathematical Knot Theory and the Hopf fibration

In Mathematics, there is a whole field devoted to the theory of knots within Topology. Historically, mathematical knots were appreciated merely for their aesthetics. However, Lord Kelvin, in the 1860s, famously proposed a hypothesis that atoms could be differing knot-types within the fabric of the ether [19]. This idea led to the tabulation

of many differing knots by Tait [20], who suspected he was creating a table of elements. Since the Michelson-Morley experiment disproved the existence of the ether [21], chemists were less inclined to pursue mathematical knots, in a bid to tabulate the elements. Instead, mathematicians became increasingly intrigued by the potential of knots. Knot theory now sits as a sub-discipline within the area of Topology and has been shown to have many applications: from allowing the comprehension of the affects of knotting DNA strands; to facilitating the understanding of the handedness of polymers [22]. For this thesis, several aspects of knot theory have been utilised: within the construction of the knotted electromagnetic fields; and in the assessments of the zilches within the knotted electromagnetic fields. A solid understanding of the fundamentals of mathematical knots is integral to the reading of this thesis.

2.1.1 Unknots, Knots, and Links

Within knot theory, there are three, distinct quantities - unknots, knots and links [22]. To describe a mathematical knot, it is easiest to use an analogy. Imagine that someone is holding a shoelace and ties a knot in it, then glues the ends of the string together. This is a knot, as defined within mathematics, because there is no *possible* way of undoing the knot through manipulation of the shoelace - unless one cuts through it. When dealing with knots within mathematics, one should consider the shoelace to be infinitely thin and, therefore, a closed curve within Euclidean space (see figure 2.1(b) for an example of a knot - the trefoil). The unknot is such a loop - a closed loop - that, when completely unravelled, forms only a circle³ (see figure 2.1(a)). A link, as the name suggests, is where two or more unknots - or knots - are *linked* together, without intersecting at any point (see figure 2.1(c) and 2.1(d)). The unlink is the most basic form of link, it is comprised of two unlinked unknots. The next most basic link is the Hopf-link - made up of two linked unknots (see figure 2.1(c)). The Hopf-link is a central component of what is called the Hopf fibration, which appears in the electromagnetic field lines of a particular set of solutions to Maxwell's equations, and is the subject of section 2.1.5.

³The unknot is also known as the *trivial knot*.

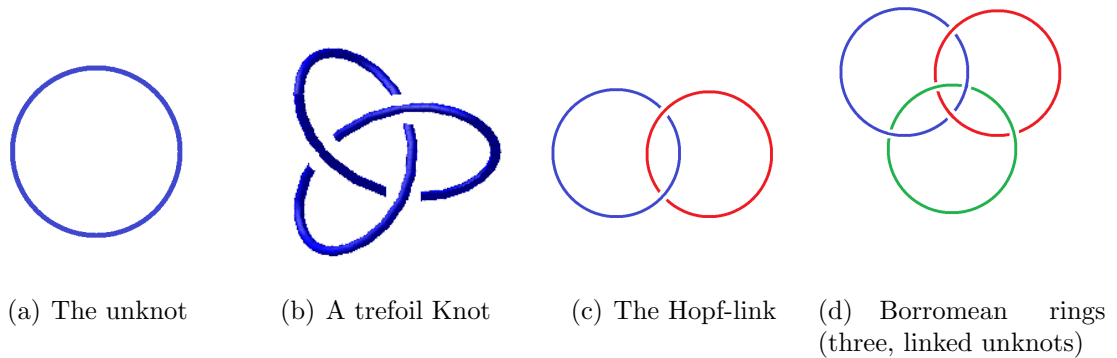


Figure 2.1: Examples of the different quantities within mathematical knot theory

2.1.2 Knot Tabulation, Knots' Projections, and Reidemeister's Moves

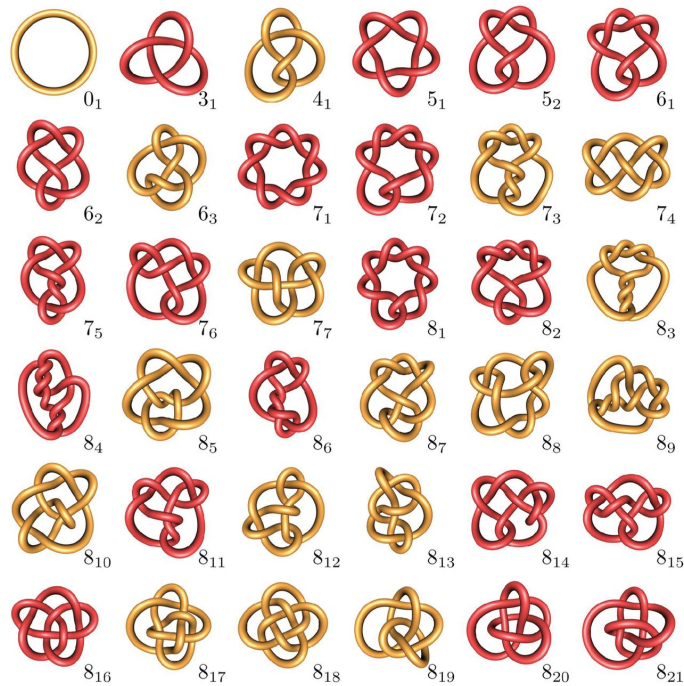


Figure 2.2: An example of a knot table⁴

The images that are displayed in knot tables are those of the most basic projection of each distinct knot (see figure 2.2). As knots sit within three-dimensional, Euclidean space, they can be observed from many angles. This means that, depending from which point of view a knot has been observed, it may not appear to be a specific knot

⁴Image sourced at [23].

(see figure 2.3). These points of view are called projections, and can be understood as an image of the knot, projected onto a two-dimensional plane located behind it. Understanding what tangle of lines equates to what knot is key to mathematical knots. The tabulated knots are those which show the minimum number of crossings⁵ - points at which the lines pass over each other. This means that, no matter what projection one is observing, the crossing number will never decrease, regardless of manipulation via the Reidemeister moves. The Reidemeister moves are a set of methods that allow one to untangle *sections* of the knot to reveal the least number of crossings (see figure 2.4).

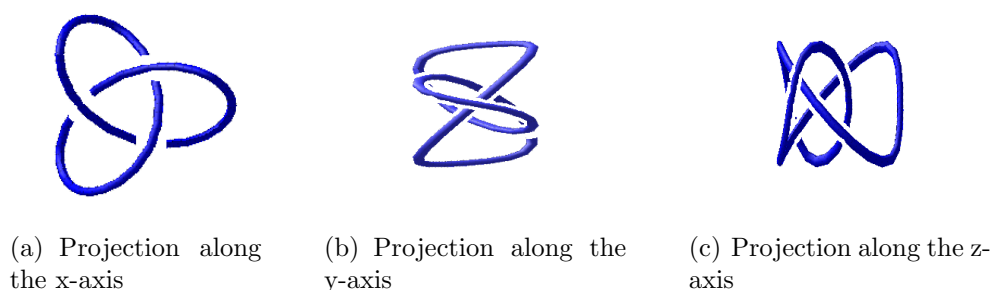


Figure 2.3: Examples of the three different projections of the trefoil knot

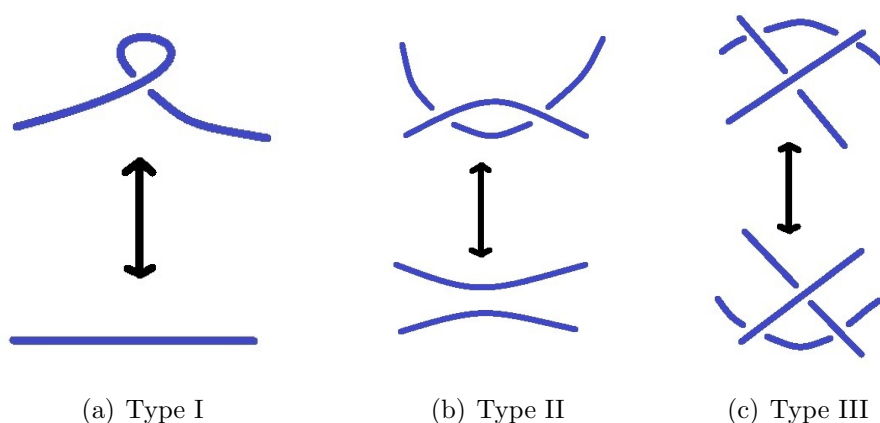


Figure 2.4: The three Reidemeister moves

The first Reidemeister move (Type I) allows the action of inserting in or removing a twist. The second move (Type II) facilitates the inclusion or removal of two crossings. The third move (Type III) permits moving a strand from one side of a crossing to the

⁵This is referred to as the *crossing number*.

other. A knot for which remaining crossings cannot be undone with the Reidemeister moves is called a *prime knot*. An example of a prime knot is figure 2.3(a), with a crossing number of 3. Figure 2.3(a) is the projection with the lowest possible crossing number. This is why the same knot in figure 2.2 has a label 3_1 - as per the Alexander-Briggs notation[22]. In figure 2.2 a table of knots is shown, including knots with up to eight crossings. The large number denotes the number of crossings the prime knot contains. The subscript denotes the order of the prime knots with the same crossing number.⁶ It is important to note that the mirror image of a prime knot is not included in the table, so each entry represents two knots - the knot and its mirror. Amphichiral knots exist.⁷ For such knots there is, obviously, only one representation.

2.1.3 Knot Classes

In 1978, Thurston proved that there are only three different classes of knots [24]: torus knots; satellite knots; and hyperbolic knots. The vast majority of the knots *discovered* have been hyperbolic. Some of the most thoroughly understood, however, are torus knots. Torus knots are central to research on higher knotted solutions to Maxwell's equations [16].

2.1.3.1 Torus Knots and the Torus

Torus knots are those knots that are acted out on a torus. A torus, T^n , is a surface defined within topology as a product of circles, S^1 ,⁸:

$$T^n = \underbrace{S^1 \times S^1 \times \dots \times S^1}_n. \quad (2.1)$$

The most common is the two-dimensional torus, T^2 , and is that surface over which the torus knots are defined. This surface is a subset of three dimensional real space,

$$T^2 \subset \mathbb{R}^3, \quad (2.2)$$

and can be written explicitly in Cartesian coordinates,

$$\left(R - \sqrt{x^2 + y^2}\right)^2 + z^2 = r^2, \quad (2.3)$$

and parametrically,

$$\begin{aligned} x &= (R + r \cos\theta)\cos\phi, \\ y &= (R + r \cos\theta)\sin\phi, \\ z &= r \sin\theta. \end{aligned} \quad (2.4)$$

⁶Although, torus knots tend to appear first before knots with twists.

⁷Amphichiral meaning equal to their mirror image.

⁸ S^1 is one dimensional spherical space and will be discussed in more detail in section 2.1.5

R is the distance from the centre of T^2 to the centre of the torus' tube structure (figure 2.6), r is the radius of the tube and θ and ϕ define the set of angles from the two circles of its construction, $\theta, \phi \in [0, 2\pi)$. Multiple surfaces can be created by adjusting the two radius parameters to fill all of \mathbb{R}^3 with nested tori (see figure 2.5). At the limits of $R, r \rightarrow \infty$, or when $R \rightarrow 1$ and $r \rightarrow 0$, two degenerate tori appear. The former is a line along the z -axis at the centre of the tori, representing the infinitely thick torus. The latter, a circle, or the infinitely thin torus, sits in the x - y -plane at the centre of the tubes. These toroidal surfaces will be shown to appear as solutions to Maxwell's equations in section 2.2.5.

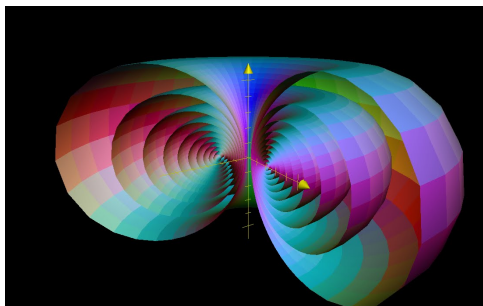


Figure 2.5: Nested tori sat in \mathbb{R}^3 ⁹

A curve that transits the smallest circumference around T^2 is called a meridian curve, and it can be described as wrapping around the torus in the poloidal direction. A curve that transits the largest circumference is called a longitude curve, and it can be described as wrapping around the torus in the toroidal direction (see figure 2.6).

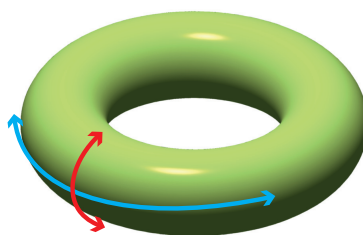


Figure 2.6: The toroidal direction is denoted by the blue arrow, the poloidal direction by the red arrow

The number of times the curve wraps itself around the torus, and in what direction,

⁹Image sourced at [25].

is indicated via the integer winding numbers, p and q . If the curve traverses a number of rotations in the poloidal direction, q indicates how many rotations have occurred. Another way to quantify this would be to count how many times the line crosses the longitude curve. The same is true for p , with respect to the toroidal direction and the meridian curve. For a torus knot to be produced, $(p, q) \geq 2$ and have to be co-prime, otherwise the result is a torus link.¹⁰ If either $(p, q) = 1$, the result is a trivial torus knot, as they are equivalent to the unknot. Consider the $p = 2, q = 3$ torus knot, $(2, 3)$. The line drawn on the surface of the torus crosses the longitude line three times and, therefore, is wrapping poloidally three times. The line also crosses the meridian line twice, therefore wrapping two times toroidally. This prescription produces the trefoil knot. Figure 2.7 demonstrates combinations of winding numbers, producing their respective torus knots.

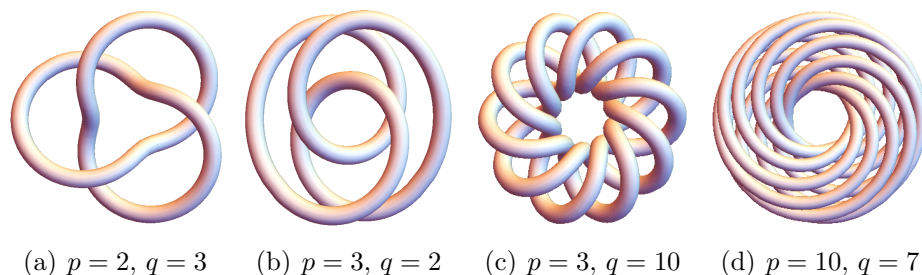


Figure 2.7: Four examples of torus knots and their winding numbers

Parametrically these knots can be defined by the following equations,

$$\begin{aligned} x &= (R + r \cos(qt)) \cos(pt), \\ y &= (R + r \cos(qt)) \sin(pt), \\ z &= r \sin(qt). \end{aligned} \tag{2.5}$$

Another construction of the family of torus knots utilises a connection between knots and singularities of complex maps from the three sphere to complex space, $S^3 \rightarrow \mathbb{C}$.¹¹ For a pair of complex numbers, u and v , where $u \pm v = 0$, where $(u, v) \in \mathbb{C}^2$ such that $|u|^2 + |v|^2 = 1$, such numbers produce a (p, q) -torus knot when p and q are co-prime [17].

¹⁰Co-prime means that (p, q) share no prime factors. This property is sometimes described as being *relatively prime*.

¹¹The three sphere, S^3 will be described in more detail in section 2.1.5.

2.1.4 Knot Invariants

When one considers mathematical knots, there are certain properties which will remain constant. These constants are called *knot invariants* and are topologically important. The knot invariants upon which this thesis focuses are: the crossing number; and the unknotting number for torus knots and links.

2.1.4.1 Crossing Number

The crossing number, $c(K)$, is determined by counting every time the line drawing out the knot projection passes over itself without intersecting. If the number of crossings is a minimum in all projections, and it is shown to be distinct from any knots with fewer crossings, then that is the crossing number for the knot. For the torus knots the crossing number is,

$$c(T(p, q)) = \min(p(q - 1), q(p - 1)). \quad (2.6)$$

2.1.4.2 Unknotting Number

The unknotting number, $u(K)$, states the number of crossings that need to be changed so that the knot can be manipulated into the unknot. This must be a minimum across all projections of the knot for it to be the unknotting number. Intuitively, one would suspect that a projection of a knot with the minimised number of crossings would give the unknotting number. This is not the case, and has been disproved [26]. The unknotting number for the torus knots is given by,

$$u(T(p, q)) = \frac{1}{2}(p - 1)(q - 1). \quad (2.7)$$

Consider the torus knot $T(2, 3)$. Its unknotting number is, $u(T(2, 3)) = 1$. Geometrically this involves changing one of the crossings in the knot and then applying two Reidemeister moves to manipulate the projection to become the unknot (see figure 2.8). All prime knots have $u(K_{prime}) = 1$.

2.1.4.3 Other Key Knot Invariants

The invariants just mentioned are those that are relevant to the later research in this thesis. That does not mean that they are the only, or most important invariants with regard to mathematical knot theory. The most notable invariants are that of the Alexander polynomial and the Jones polynomial [27][28]. The polynomials are

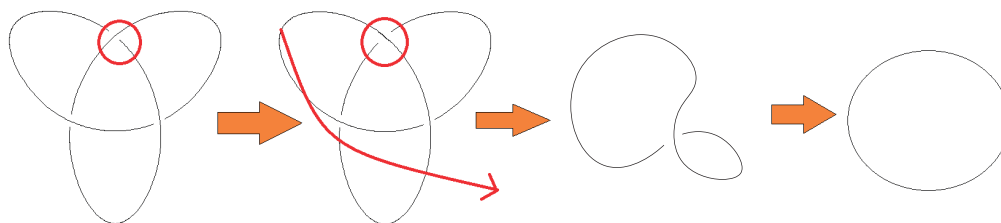


Figure 2.8: Removing one crossing from the $T(2,3)$ knot and applying Reidemeister moves II and III to reveal the unknot.

a great way to tell what type of knot one is looking at. To each knot a polynomial is assigned from its projection. No matter the projection given the polynomial will always be the same - hence, a knot invariant.

2.1.5 The Hopf fibration

In 1931, Hopf discovered a mapping between spherical spaces [29],

$$\eta : S^3 \rightarrow S^2. \quad (2.8)$$

This mapping is known by many names: the Hopf-map; the Hopf fibration; the Hopfion solution etc. It allowed a deeper comprehension of the three-sphere, S^3 . To understand the mapping, one must first appreciate the spaces that are used. The dimension of each spherical space is determined by how many dimensions the surface of the sphere contains. The first three spheres are S^0 , S^1 , and S^2 - also known as the zero-sphere, the one-sphere and the two-sphere respectively. The reason these spheres have been named first is because their forms are commonly known and easy to visualise. The zero-sphere is given by the equation,

$$\begin{aligned} S^0 &\subset \mathbb{R}^1 \\ x_0^2 &= 1, \end{aligned} \quad (2.9)$$

which gives the subset of values contained within one-dimensional, real space. The equation for the one-sphere, S^1 , is,

$$\begin{aligned} S^1 &\subset \mathbb{R}^2 \\ x_0^2 + x_1^2 &= 1, \end{aligned} \quad (2.10)$$

giving the unit circle contained in the plane. Finally, the two-sphere,

$$\begin{aligned} S^2 &\subset \mathbb{R}^3 \\ x_0^2 + x_1^2 + x_2^2 &= 1, \end{aligned} \quad (2.11)$$

giving the unit sphere contained in three-dimensional real space. The format continues indefinitely through the dimensions, with each spherical space being the subset of values within a real-valued space of one additional dimension,

$$\begin{aligned} S^n &\subset \mathbb{R}^{n+1} \\ \sum_{m=0}^n x_m^2 &= 1. \end{aligned} \tag{2.12}$$

The three-sphere is difficult to visualise, as it sits within \mathbb{R}^4 . Fortunately, there are techniques one can use to overcome this - such as stereographic projection.¹² One property of the spheres is that, sat at the equator of each, is the sphere of one less dimension.

The Hopf fibration is more than just a mapping between two topological spaces, it is a fibration over spheres. Within Algebraic Topology a fibration, by definition, is a surjective mapping between topological spaces that preserves the homotopy lifting property.¹³ A homotopy is a continuous mapping from one space to another. The most common example given is that of the ageing process on human appearance. The homotopy lifting property enables the continuous mapping to be *lifted* to the space *above* it.¹⁴

To understand the final equation of the Hopf fibration, one should understand a little about the set of numbers called *quaternions*, \mathbb{H} .

$$\mathbb{H} = \{q = w + xi + yj + zk \mid i^2 = j^2 = k^2 = ijk = -1\}. \tag{2.13}$$

Quaternions are an extension to complex numbers in that they have one, real scalar, w , and a vector composed of a set of special numbers - denoted by \mathbf{i} , \mathbf{j} and \mathbf{k} , whose coefficients, x , y and z , are real. These special numbers are called the fundamental quaternion units and have the property, $\mathbf{i}^2 = \mathbf{j}^2 = \mathbf{k}^2 = \mathbf{ijk} = -1$. It is important to note that they do not commute and, therefore, multiplicative order is essential. The quaternion units have the following multiplicative properties,

$$\begin{aligned} \mathbf{ij} &= \mathbf{k}, & \mathbf{ji} &= -\mathbf{k}, \\ \mathbf{jk} &= \mathbf{i}, & \mathbf{kj} &= -\mathbf{i}, \\ \mathbf{ki} &= \mathbf{j}, & \mathbf{ik} &= -\mathbf{j}. \end{aligned} \tag{2.14}$$

¹²See section 2.1.6.

¹³Surjective - many points from one space map to one point in another.

¹⁴For a more technical explanation of a fibration, refer to Chapter 7 of the book, *A Concise course on Algebraic Topology*, by May [30].

The three-sphere *is* the set of all unit quaternions,

$$S^3 = \{q = w + x\mathbf{i} + y\mathbf{j} + z\mathbf{k} \mid w^2 + x^2 + y^2 + z^2 = 1\}. \quad (2.15)$$

For this to be true, for $q \in S^3$ there is a $q^{-1} = w - x\mathbf{i} - y\mathbf{j} - z\mathbf{k}$ such that $q \cdot q^{-1} = w^2 + x^2 + y^2 + z^2 = 1$.¹⁵

The definition of the Hopf-map, η , is as follows,

$$\begin{aligned} \eta : S^3 &\rightarrow S^2 \\ \eta(q) &= q \cdot \mathbf{k} \cdot q^{-1} \\ &= (0, 2wy + 2xz, 2yz - 2wx, w^2 + z^2 - x^2 - y^2). \end{aligned} \quad (2.16)$$

Therefore, $\eta(q) \in \mathbb{R}^3$. The sum of each element squared adds to unity - which is just those set of values whose distance from the origin is 1, defining the unit two-sphere. Therefore, Hopf fibration has completely encoded the whole of the three-sphere onto the two-sphere and is a demonstration of surjective mapping.

This chapter presents the implementation of the Hopf fibration into the electromagnetic field lines. However, it does not rely upon the quaternionic formulation. The inclusion of the formulation is to demonstrate the nature of the mapping. A more common set-up is by noting that $\mathbb{R}^4 \in \mathbb{C}^2$ and $\mathbb{R}^3 \in \mathbb{C}^1 \times \mathbb{R}^1$. Therefore,

$$\begin{aligned} S^3 &= \left\{ (z_1, z_2) \in \mathbb{C}^2 \mid |z_1|^2 + |z_2|^2 = 1 \right\}, \\ S^2 &= \left\{ (z, x) \in \mathbb{C}^1 \times \mathbb{R}^1 \mid |z|^2 + x^2 = 1 \right\}. \end{aligned} \quad (2.17)$$

The Hopf-map is defined,

$$\eta(z_1, z_2) = \left(2 z_1 \bar{z}_2, |z_1|^2 - |z_2|^2 \right). \quad (2.18)$$

This definition becomes the same as that defined through the quaternionic formulation (see equation 2.16), if one allows $z_1 = w + iz$ and $z_2 = y + ix$. To understand the form the fibres take mapping from multiple points in S^3 to a singular point in S^2 , one should consider the effect of multiplying complex numbers together. A multiplication of one complex number by another (for example, $w = \lambda z$, where λ is complex) induces a rotation and a scaling factor in the range. For solutions to remain in S^3 , according to equation 2.17, the sum of the unit norm of the complex input functions,

¹⁵Here, the quaternionic arithmetic is rather straightforward and, therefore, will not be demonstrated.

w_1 and w_2 , has to equal unity. This imposes the condition, $|\lambda|^2 = 1$. This requirement yields a mapping to the same point in S^2 . Explicitly, if $\eta(z_1, z_2) = \eta(w_1, w_2)$ in S^2 , then $(w_1, w_2) = (\lambda z_1, \lambda z_2)$ in S^3 . Therefore,

$$\eta(w_1, w_2) = \left(2 \lambda z_1 \bar{\lambda} \bar{z}_2, |\lambda|^2 (|z_1|^2 - |z_2|^2) \right) = |\lambda|^2 \eta(z_1, z_2). \quad (2.19)$$

Because the set of all complex values that has $|\lambda|^2 = 1$ form the unit circle in \mathbb{C}^1 , it suggests that each point on S^2 has a fibre that is a circle in S^3 (See figure 2.9).

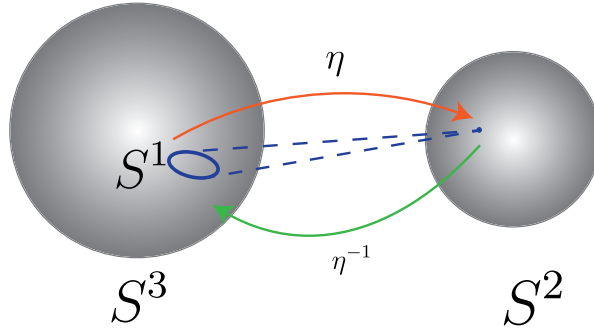


Figure 2.9: The Hopf-map, η , and the pre-image, η^{-1}

This means that λ takes the form $e^{i\psi}$. Considering the reverse map, with this form for λ , one can observe the pre-image of the Hopf fibration, but now in spherical coordinates:

$$\eta^{-1}(w_1, w_2) = \left(e^{i\frac{\phi+\psi}{2}} \cos\left(\frac{\theta}{2}\right), e^{i\frac{\phi-\psi}{2}} \sin\left(\frac{\theta}{2}\right) \right). \quad (2.20)$$

This takes a point on S^2 and gives the fibre from S^3 - the circle, S^1 . The next section gives an explicit breakdown of an effective method used to view this pre-image in \mathbb{R}^3 .

2.1.6 Stereographic Projection

The Hopf fibration is virtually impossible to imagine, as it sits within \mathbb{R}^4 . Fortunately, one can use a method called stereographic projection to visualise the Hopf fibration in \mathbb{R}^3 . Most simply, stereographic projection is a method used for visualising higher dimensional spaces in lower dimensions. It assigns two antipodal points to our spherical space: a north pole, from which the projection line emanates; and a south pole. The image produced in the projection space is a warped version of the original space.

Taking the space S^1 (the circle), sat in \mathbb{R}^2 (the x - y plane), a line can be drawn through the diameter of the sphere and be considered as \mathbb{R}^1 (or the x -axis). The y -axis also follows the diameter of S^1 , but orthogonal to \mathbb{R}^1 . One can assign the highest positive y -valued point on the sphere as the north pole, and the highest negative y -valued point as the south pole. A line is then projected from the north pole, through the surface of S^1 , onto the projection space, \mathbb{R}^1 (see figure 2.10). This gives a mapping from $S^1 \rightarrow \mathbb{R}^1$, and includes all points from S^1 - except that point at the north pole. The point at the north pole projects to $\pm\infty$ and, therefore, has to be added to complete the mapping.

$$\begin{aligned} p_1 : S^1 &\rightarrow \mathbb{R}^1 \cup \{\infty\} \\ p_1(x_1, x_2) &= \left(\frac{x_1}{1-x_2} \right). \end{aligned} \tag{2.21}$$

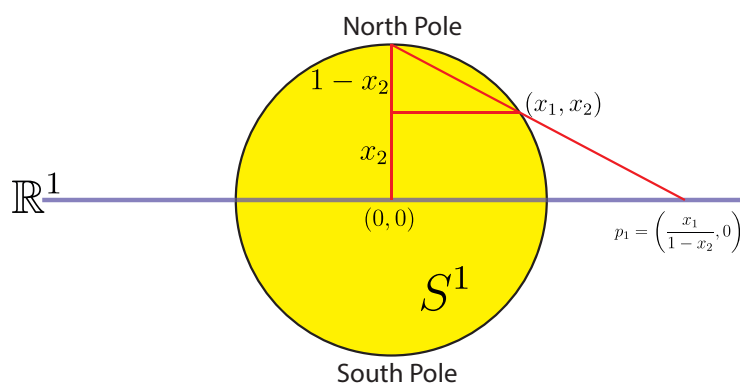


Figure 2.10: Stereographic projection from $S^1 \rightarrow \mathbb{R}^1$

The projection is calculated by employing trigonometry. Consider now the next dimension, S^2 (the sphere) embedded in \mathbb{R}^3 (see figure 2.11). The projection space, \mathbb{R}^2 (the x - y -plane), will be sat at the equator of the sphere, with the north and south poles located at the $+z$ and $-z$ axis, respectively. To give an analogy, the projection given in this set-up is equivalent to the geographical mapping of the Earth's surface to a world map. The mapping is calculated in the same way as the dimension below and takes on the following explicit form:

$$\begin{aligned} p_2 : S^2 &\rightarrow \mathbb{R}^2 \cup \{\infty\} \\ p_2(x_1, x_2, x_3) &= \left(\frac{x_1}{1-x_3}, \frac{x_2}{1-x_3} \right). \end{aligned} \tag{2.22}$$

For S^2 , we are still enforcing the conditions that $x_1^2 + x_2^2 + x_3^2 = 1$. If the plane to which we are projecting were considered to be \mathbb{C}^1 , then this sphere is called the *Riemann Sphere*.

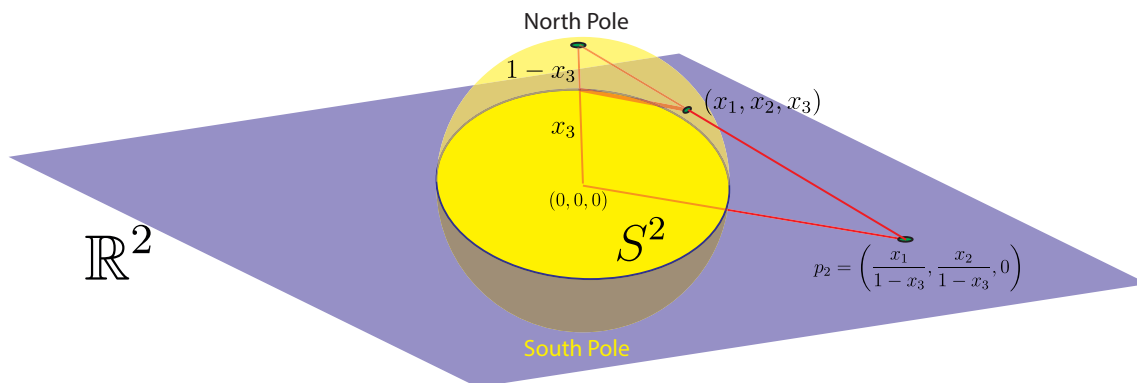


Figure 2.11: Stereographic projection from $S^2 \rightarrow \mathbb{R}^2$

The method of stereographic projection continues in this manner through the dimensions. The projection of $S^3 \rightarrow R^3$ therefore has the form:

$$p_3 : S^3 \rightarrow \mathbb{R}^3 \cup \{\infty\}$$

$$p_3(x_1, x_2, x_3, x_4) = \left(\frac{x_1}{1-x_4}, \frac{x_2}{1-x_4}, \frac{x_3}{1-x_4} \right), \quad (2.23)$$

with $x_1^2 + x_2^2 + x_3^2 + x_4^2 = 1$ for S^3 . The remarkable property of this mapping is that it is a conformal mapping, meaning that shapes and angles in the domain are preserved in the range. The projection warps the image of the space being projected, much in the same way that the map of the world distorts the areas of land masses, most notably towards to the north and south poles. In figure 2.12, one can see that projecting a line around the entire equator of S^2 gives the same sized circle as it sits at the projective plane. Projecting a line through all the points in a line of latitude closer to the north pole maps out to a much larger circle on the projective plane (see figure 2.12). Repeating for a latitude line closer towards the south pole maps out a smaller circle on the projective plane. There are limits: when trying to project through the poles, the south pole maps to the singular point at the origin, and north pole projects to infinity.

Stereographic projection, therefore, is a beneficial method for viewing S^3 , via the Hopf fibration. If one takes a composite function of the pre-image of the Hopf-map, η^{-1} , (equation 2.20) and its stereographic projection, p_3 , (equation 2.23) one finds for each point on S^2 there is a circle projected from its pre-image into \mathbb{R}^3 (See figure

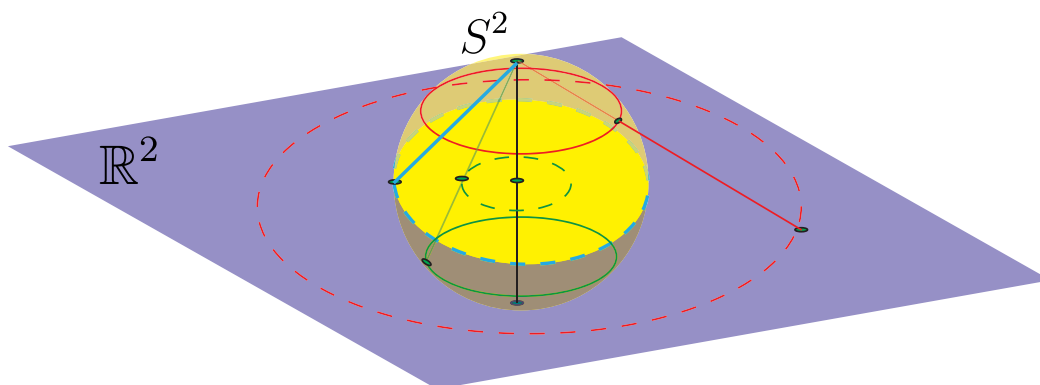


Figure 2.12: Stereographic projection, $S^2 \rightarrow \mathbb{R}^2$, showing the warping of the sizes of latitude circles on the projection plane when taken closer to the north or south pole (shown as dotted lines)

2.13). Explicitly, the mapping is:

$$p_3 \circ \eta^{-1} = \frac{1}{1 - \sin\left(\frac{\theta}{2}\right) \sin\left(\frac{\psi - \phi}{2}\right)} \left(\cos\left(\frac{\theta}{2}\right) \cos\left(\frac{\psi + \phi}{2}\right), \cos\left(\frac{\theta}{2}\right) \sin\left(\frac{\psi + \phi}{2}\right), \sin\left(\frac{\theta}{2}\right) \cos\left(\frac{\psi - \phi}{2}\right) \right). \quad (2.24)$$

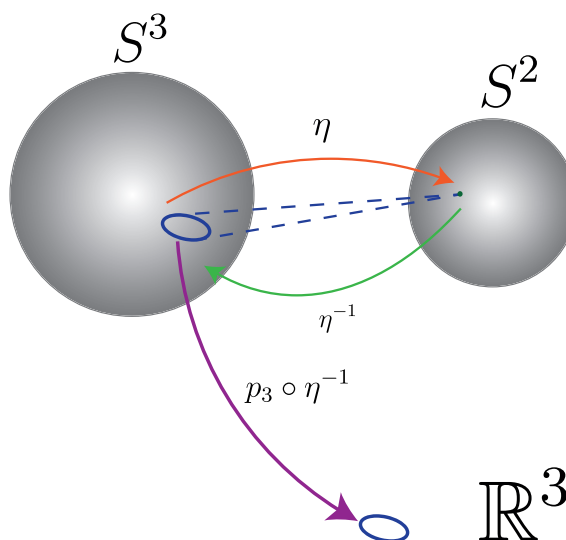


Figure 2.13: Stereographic projection, $S^3 \rightarrow \mathbb{R}^3$, of the pre-image of the Hopf-map of a singular point from S^2

If one takes more than one point from S^2 , the projection of the pre-images into \mathbb{R}^3 are multiple, non-intersecting circles that are all linked through a central point (see figure 2.14). As mentioned in section 2.1.1, these are known as *Hopf-links*.

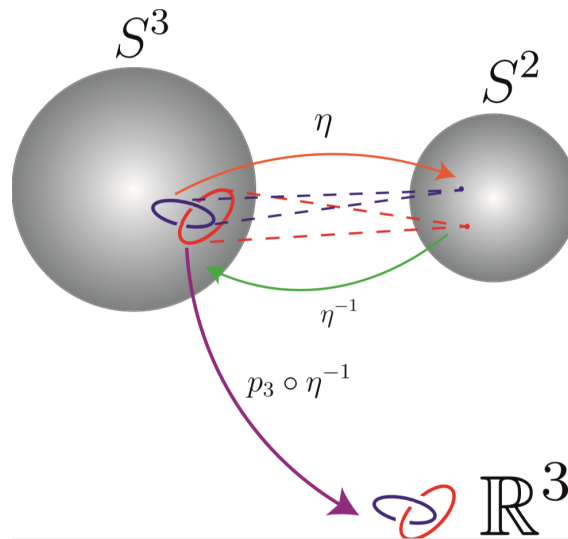


Figure 2.14: Stereographic projection, $S^3 \rightarrow \mathbb{R}^3$, of the pre-image of the Hopf-map of two points from S^2 , showing two linked circles - known as the Hopf-link

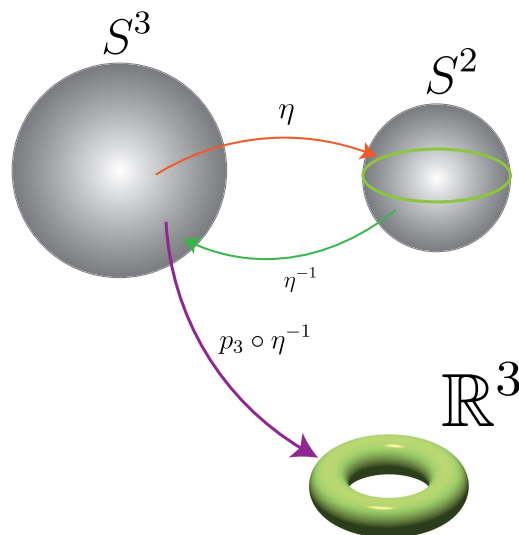


Figure 2.15: Stereographic projection, $S^3 \rightarrow \mathbb{R}^3$, of the pre-image of the Hopf-map of one complete latitude level of S^2 , showing all the linked circles form a torus surface

The structure becomes more defined when selecting latitudinal points on S^2 . Consider multiple points on the equator for example, these start to map out the surface of a torus, with all circles linked through its centre (see figure 2.15). If all points from the equator are considered, the projection is a torus surface, comprised of those Hopf-linked circles.

If one now takes multiple points from a selection of latitudinal levels of S^2 , the

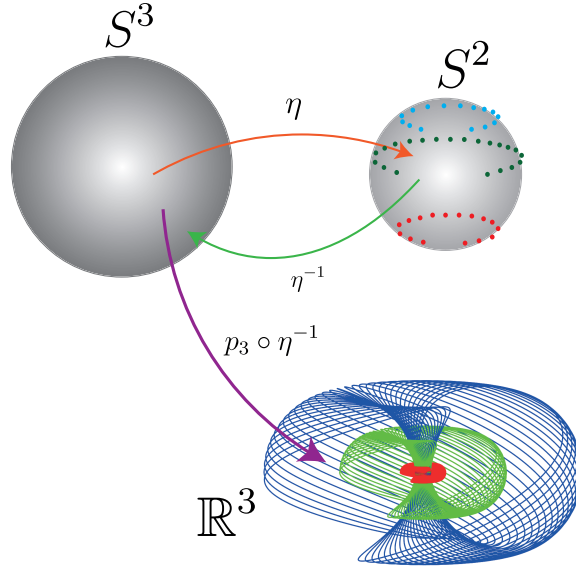


Figure 2.16: Stereographic projection, $S^3 \rightarrow \mathbb{R}^3$, of the pre-image of the Hopf-map of multiple points from three latitude levels of S^2 , showing multiple nested tori emerging

projections of their pre-images are that of multiple nested tori (like Russian dolls), comprised of the same circles that all link through their mutual centre (see figure 2.16). When considering the projection of all points from S^2 , the projection of the pre-image fills the whole of \mathbb{R}^3 with these nested tori. There are only two extra projections: a vertical line that is the torus that passes through infinity and represents the north pole; and a circle nested at the centre of all the tori (considered to be the infinitely thin torus), which represents the projection of the south pole.

For completeness, one can also determine the inverse stereographic projection, meaning taking a point from the projection plane and projecting back to the original space. With the previous examples, that would be a projection from a real space back to a sphere. Explicitly, the inverse stereographic projection from $\mathbb{R}^3 \rightarrow S^3$ is given by:

$$p_3(x_1, x_2, x_3) = \frac{1}{x_1^2 + x_2^2 + x_3^2 + 1} (2x_1, 2x_2, 2x_3, x_1^2 + x_2^2 + x_3^2 - 1). \quad (2.25)$$

2.2 Knotted Solutions to Maxwell's Equations

In 1989, Rañada realised a unique set of exact solutions to Maxwell's equations that encoded the Hopf fibration within the charge-free electric and magnetic field lines [3]. He extended this body of work to eventually suggest that this model could be used as

a topological description of the fundamental charge [8][9][10][11][12]. In 2008, Irvine and Bouwmeester conducted a multipole expansion on the vector spherical harmonics of this Hopfion-solution, leading them to suggest an experimental verification in the form of circularly polarised beams of light, with a further paper by Irvine extending these results to higher knot types [18][15]. A few years later Kedia, Bialynicki-Birula, Peralta-Salas and Irvine, reformulated the problem with the simpler method of Bateman's construction [16][6], previously employed by Bialynicki-Birula whilst analysing vortex lines in electromagnetic fields [13]. Kedia et al.'s paper managed to generalise Bateman's construction so that it could not only provide the Hopf-knotted solutions to Maxwell's equations, but also of torus knots and links (of which there are an infinite amount) by applying a theorem from complex analysis [17]. This area of Hopf-knotted and torus-knotted solutions to Maxwell's equations is a hugely exciting area of Physics research, with the Hopf fibration being viewed as a central geometrical object that permeates several disciplines within Physics. It has been found to have beneficial results in quantum computing, general relativity, and classical mechanics [31][32]. This thesis outlines the physical nature of an obscure set of conserved quantities within Maxwell's equations, named *zilches* - within the context of knotted electromagnetic fields, it also aims to improve upon the results of Irvine et al. to progress the research *closer* to experimentally producing these knotted pulses of light.

The following section will specifically deal with the method of Bateman's construction. Bateman's construction will provide a consistent method for generating solutions to Maxwell's equations. Once the electric and magnetic fields have been set up, the method for encoding the stereographic projection of the inverse Hopf-map will be introduced, followed by the extension to obtaining the infinite family of torus knots and links - that will appear within the field lines. Further to this, a breakdown of a selection of known properties of these unique solutions will be examined. An explanation of the scalar plots used for visualising them will also be provided.

2.2.1 Bateman's Construction

Bateman's construction and its use in setting up the Hopf fibration and torus knots in the electromagnetic fields, is essential to providing a consistent topological structure that is preserved with time. The reason for this is down to its ability to construct all null electromagnetic fields (which has been proven by Hogan [33]) with an association to what is called a null geodetic shear-free congruence [16]. The null condition demands that the electric and magnetic fields are continuously perpendicular to each

other, and of equal magnitude. What it does, mathematically, is most relevant when creating a tensor formulation of the fields. Without its enforcement, the fields could be classified as non-null. Consequentially - in some inertial reference frame - the electric or magnetic field could disappear. The null condition and its importance in relation to the time evolution of the Hopf-knotted and torus-knotted solutions to Maxwell's equations will be discussed further in section 2.2.2.

For these equations it is important to note that the international standard of units (S.I.) will be employed. The free field Maxwell's equations will be used. Finally, the fields will be adjusted to have a high degree of symmetry via,

$$\begin{aligned} \mathbf{E} &\rightarrow \mathbf{E}, \\ \mathbf{B} &\rightarrow \frac{1}{c}\mathbf{B}. \end{aligned}$$

The symmetrised Maxwell's equations, for a free field in a vacuum in S.I. units are, therefore,

$$\begin{aligned} \nabla \cdot \mathbf{E} &= 0, \\ \nabla \cdot \mathbf{B} &= 0, \\ \nabla \times \mathbf{E} &= -\frac{1}{c} \frac{\partial \mathbf{B}}{\partial t}, \\ \nabla \times \mathbf{B} &= \frac{1}{c} \frac{\partial \mathbf{E}}{\partial t}. \end{aligned} \tag{2.26}$$

\mathbf{E} is the electric field vector, \mathbf{B} is the magnetic field vector, c is the speed of light in a vacuum and t is time. Every other mathematical operator takes on their usual meaning.

Bateman's construction creates a complex vector field, \mathbf{R} , in dimensions (3+1) where the electric field and magnetic field are the real and imaginary parts, respectively,

$$\mathbf{R} = \mathbf{E} + i\mathbf{B}. \tag{2.27}$$

This is usually referred to as the Riemann-Silberstein vector [34], and assumes that the electric and magnetic fields themselves are comprised of real sets of numbers. It is important that Maxwell's equations can be retrieved from this equation, otherwise it would hold no meaning in reality. To retrieve the first two of Maxwell's equations, the divergence of the field will be taken and put equal to zero,

$$\nabla \cdot \mathbf{R} = \nabla \cdot (\mathbf{E} + i\mathbf{B}) = 0 = \nabla \cdot \mathbf{E} + i\nabla \cdot \mathbf{B}.$$

Taking the real and imaginary parts,

$$\nabla \cdot \mathbf{E} = \Re(\nabla \cdot \mathbf{R}) = 0, \quad (2.28)$$

$$\nabla \cdot \mathbf{B} = \Im(\nabla \cdot \mathbf{R}) = 0. \quad (2.29)$$

This, therefore, shows that the first two of Maxwell's equations can be retrieved from this complex vector field. Maxwell's next two equations are encompassed by:

$$\nabla \times \mathbf{R} = \frac{i}{c} \frac{\partial \mathbf{R}}{\partial t}. \quad (2.30)$$

Below, the straight forward proof is shown:

$$\begin{aligned} \nabla \times \mathbf{R} &= \nabla \times (\mathbf{E} + i\mathbf{B}) = \nabla \times \mathbf{E} + i(\nabla \times \mathbf{B}) = -\frac{1}{c} \frac{\partial \mathbf{B}}{\partial t} + i \left(\frac{1}{c} \frac{\partial \mathbf{E}}{\partial t} \right) \\ \nabla \times \mathbf{R} &= \frac{i}{c} \frac{\partial \mathbf{E} + i\mathbf{B}}{\partial t} = \frac{i}{c} \frac{\partial \mathbf{R}}{\partial t}. \end{aligned} \quad (2.31)$$

For this, newly constructed, complex vector field, Maxwell's equations can be summarised by the following,

$$\begin{aligned} \nabla \cdot \mathbf{R} &= 0, \\ \nabla \times \mathbf{R} &= \frac{i}{c} \frac{\partial \mathbf{R}}{\partial t}. \end{aligned} \quad (2.32)$$

It is then customary to express this newly constructed vector field in terms of a couple of complex scalar functions, $\alpha(x, y, z, t)$ and $\beta(x, y, z, t)$, using the following ansatz,

$$\mathbf{R} = E_0 \nabla \alpha \times \nabla \beta = \frac{i}{c} \left(\frac{\partial \alpha}{\partial t} \nabla \beta - \frac{\partial \beta}{\partial t} \nabla \alpha \right), \quad (2.33)$$

where E_0 is an arbitrary constant with units of electric field. These complex functions are dimensionless and, as will be demonstrated in the next section, can be written in terms of space-time coordinates, along with a scale factor, k . Equation 2.33 is important, as it enables one to check the validity of each form that α and β assume. This amounts to the following conditions:

$$\begin{aligned} \nabla^2 \alpha - \frac{\partial^2 \alpha}{\partial t^2} &= 0, \\ \nabla^2 \beta - \frac{\partial^2 \beta}{\partial t^2} &= 0, \\ \nabla \alpha \cdot \nabla \beta - \frac{\partial \alpha}{\partial t} \frac{\partial \beta}{\partial t} &= 0. \end{aligned} \quad (2.34)$$

To establish this, one must take the x -component of the left hand side of equation 2.33 and then square it to give:

$$(\nabla \alpha \times \nabla \beta)_x^2 = \left(\frac{\partial \alpha}{\partial y} \frac{\partial \beta}{\partial z} - \frac{\partial \beta}{\partial y} \frac{\partial \alpha}{\partial z} \right)^2. \quad (2.35)$$

Which after some manipulation looks like,

$$(\nabla\alpha \times \nabla\beta)_x = \left(\frac{\partial^2\alpha}{\partial y^2} + \frac{\partial^2\alpha}{\partial z^2} \right) \left(\frac{\partial^2\beta}{\partial y^2} + \frac{\partial^2\beta}{\partial z^2} \right) - \left(\frac{\partial\alpha}{\partial y} \frac{\partial\beta}{\partial y} + \frac{\partial\beta}{\partial z} \frac{\partial\alpha}{\partial z} \right)^2. \quad (2.36)$$

If one then uses equations 2.34,

$$(\nabla\alpha \times \nabla\beta)_x = \left(\frac{\partial^2\alpha}{\partial t^2} - \frac{\partial^2\alpha}{\partial x^2} \right) \left(\frac{\partial^2\beta}{\partial t^2} - \frac{\partial^2\beta}{\partial x^2} \right) - \left(\frac{\partial\alpha}{\partial t} \frac{\partial\beta}{\partial t} - \frac{\partial\beta}{\partial x} \frac{\partial\alpha}{\partial x} \right)^2. \quad (2.37)$$

Expanding and then simplifying finally gives,

$$(\nabla\alpha \times \nabla\beta)_x = \frac{i}{c} \left(\frac{\partial\alpha}{\partial t} \frac{\partial\beta}{\partial x} - \frac{\partial\beta}{\partial t} \frac{\partial\alpha}{\partial x} \right). \quad (2.38)$$

The above, when repeated for the y and z coordinates, gives the right hand side of equation 2.33. It is important to check that the chosen ansatz meets the same requirements that the Riemann-Silberstein vector has demonstrated in equations 2.32.

$$\begin{aligned} \nabla \cdot (\nabla\alpha \times \nabla\beta) &= \left(\frac{\partial^2\alpha}{\partial x\partial y} \frac{\partial\beta}{\partial z} + \frac{\partial\alpha}{\partial y} \frac{\partial^2\beta}{\partial x\partial z} - \frac{\partial^2\beta}{\partial x\partial y} \frac{\partial\alpha}{\partial z} - \frac{\partial\beta}{\partial y} \frac{\partial^2\alpha}{\partial x\partial z} \right) + \\ &\quad \left(\frac{\partial^2\beta}{\partial y\partial x} \frac{\partial\alpha}{\partial z} + \frac{\partial\beta}{\partial x} \frac{\partial^2\alpha}{\partial y\partial z} - \frac{\partial^2\alpha}{\partial y\partial x} \frac{\partial\beta}{\partial z} - \frac{\partial\alpha}{\partial x} \frac{\partial^2\beta}{\partial y\partial z} \right) + \\ &\quad \left(\frac{\partial^2\alpha}{\partial z\partial x} \frac{\partial\beta}{\partial y} + \frac{\partial\alpha}{\partial x} \frac{\partial^2\beta}{\partial z\partial y} - \frac{\partial^2\beta}{\partial z\partial x} \frac{\partial\alpha}{\partial y} - \frac{\partial\beta}{\partial x} \frac{\partial^2\alpha}{\partial z\partial y} \right) \\ &= 0. \end{aligned} \quad (2.39)$$

All the terms cancel, as shown, to give $\nabla \cdot \mathbf{R} = 0$ where $\mathbf{R} = \nabla\alpha \times \nabla\beta$ and, therefore, the first two of Maxwell's equations. As with the previous form of \mathbf{R} , it is important to find the second set of Maxwell's equations - but using α and β . Starting with equation (2.33) and substituting equation (2.32) into it gives,

$$\begin{aligned} \frac{i}{c} \frac{\partial \nabla\alpha \times \nabla\beta}{\partial t} &= \nabla \times \mathbf{R} \\ &= \nabla \times \nabla\alpha \times \nabla\beta. \end{aligned} \quad (2.40)$$

Taking the left hand side first,

$$\begin{aligned} \frac{i}{c} \frac{\partial \nabla \alpha \times \nabla \beta}{\partial t} &= \frac{i}{c} \frac{\partial}{\partial t} \left[\left(\frac{\partial \alpha}{\partial y} \frac{\partial \beta}{\partial z} - \frac{\partial \beta}{\partial y} \frac{\partial \alpha}{\partial z} \right) \mathbf{x} + \left(\frac{\partial \beta}{\partial x} \frac{\partial \alpha}{\partial z} - \frac{\partial \alpha}{\partial x} \frac{\partial \beta}{\partial z} \right) \mathbf{y} + \left(\frac{\partial \alpha}{\partial x} \frac{\partial \beta}{\partial y} - \frac{\partial \beta}{\partial x} \frac{\partial \alpha}{\partial y} \right) \mathbf{z} \right] \\ &= \frac{i}{c} \left[\left(\frac{\partial^2 \alpha}{\partial t \partial y} \frac{\partial \beta}{\partial z} + \frac{\partial \alpha}{\partial y} \frac{\partial^2 \beta}{\partial t \partial z} - \frac{\partial^2 \beta}{\partial t \partial y} \frac{\partial \alpha}{\partial z} - \frac{\partial \beta}{\partial y} \frac{\partial^2 \alpha}{\partial t \partial z} \right) \mathbf{x} + \right. \\ &\quad \left(\frac{\partial^2 \beta}{\partial t \partial x} \frac{\partial \alpha}{\partial z} + \frac{\partial \beta}{\partial x} \frac{\partial^2 \alpha}{\partial t \partial z} - \frac{\partial^2 \alpha}{\partial t \partial x} \frac{\partial \beta}{\partial z} - \frac{\partial \alpha}{\partial x} \frac{\partial^2 \beta}{\partial t \partial z} \right) \mathbf{y} + \\ &\quad \left. \left(\frac{\partial^2 \alpha}{\partial t \partial x} \frac{\partial \beta}{\partial y} + \frac{\partial \alpha}{\partial x} \frac{\partial^2 \beta}{\partial t \partial y} - \frac{\partial^2 \beta}{\partial t \partial x} \frac{\partial \alpha}{\partial y} - \frac{\partial \beta}{\partial x} \frac{\partial^2 \alpha}{\partial t \partial y} \right) \mathbf{z} \right]. \end{aligned}$$

Here, the algebra has brought the partial differential operator, $\frac{\partial}{\partial t}$, into the brackets. In the same way that, that operation has occurred, the process of bringing an applied operator outside of the brackets can be achieved. This gives,

$$\begin{aligned} \frac{i}{c} \frac{\partial \nabla \alpha \times \nabla \beta}{\partial t} &= \frac{i}{c} \left[\left(\frac{\partial}{\partial y} \left(\frac{\partial \alpha}{\partial t} \frac{\partial \beta}{\partial z} - \frac{\partial \beta}{\partial t} \frac{\partial \alpha}{\partial z} \right) - \frac{\partial}{\partial z} \left(\frac{\partial \beta}{\partial y} \frac{\partial \alpha}{\partial t} - \frac{\partial \alpha}{\partial y} \frac{\partial \beta}{\partial t} \right) \right) \mathbf{x} + \right. \\ &\quad \left(\frac{\partial}{\partial z} \left(\frac{\partial \beta}{\partial x} \frac{\partial \alpha}{\partial t} - \frac{\partial \alpha}{\partial x} \frac{\partial \beta}{\partial t} \right) - \frac{\partial}{\partial x} \left(\frac{\partial \alpha}{\partial t} \frac{\partial \beta}{\partial z} - \frac{\partial \beta}{\partial t} \frac{\partial \alpha}{\partial z} \right) \right) \mathbf{y} + \\ &\quad \left. \left(\frac{\partial}{\partial x} \left(\frac{\partial \alpha}{\partial t} \frac{\partial \beta}{\partial y} - \frac{\partial \beta}{\partial t} \frac{\partial \alpha}{\partial y} \right) - \frac{\partial}{\partial y} \left(\frac{\partial \beta}{\partial x} \frac{\partial \alpha}{\partial t} - \frac{\partial \alpha}{\partial x} \frac{\partial \beta}{\partial t} \right) \right) \mathbf{z} \right]. \end{aligned}$$

It becomes fairly obvious that this is a curl acting on a relation between α and β and time derivatives. The equation can therefore be written,

$$\frac{i}{c} \frac{\partial \nabla \alpha \times \nabla \beta}{\partial t} = \frac{i}{c} \nabla \times \left(\frac{\partial \alpha}{\partial t} \nabla \beta - \frac{\partial \beta}{\partial t} \nabla \alpha \right). \quad (2.41)$$

The dynamical parts of Maxwell's equations in terms of α and β are,

$$\nabla \times (\nabla \alpha \times \nabla \beta) = \nabla \times \left[\frac{i}{c} \left(\frac{\partial \alpha}{\partial t} \nabla \beta - \frac{\partial \beta}{\partial t} \nabla \alpha \right) \right]. \quad (2.42)$$

This equation, therefore, demonstrates the other form of the initial ansatz,

$$\mathbf{R} = \frac{i}{c} \left(\frac{\partial \alpha}{\partial t} \nabla \beta - \frac{\partial \beta}{\partial t} \nabla \alpha \right). \quad (2.43)$$

This shows $\nabla \alpha \times \nabla \beta$ has the same properties that are required by the Riemann-Silberstein vector (equation 2.32) and can return Maxwell's equations. There is one,

final property that needs to be constrained before any complex functions can be inserted into α and β for testing. The field should be a null-field,

$$\mathbf{R}^2 = 0. \tag{2.44}$$

To prove that the fields are, in-fact, null, the original form of our complex vector field will be substituted into the above equation,

$$\begin{aligned} \mathbf{R}^2 &= (\mathbf{E} + i\mathbf{B})^2 \\ &= \mathbf{E}^2 - \mathbf{B}^2 + 2i\mathbf{E} \cdot \mathbf{B} = 0. \end{aligned} \tag{2.45}$$

Taking the real and imaginary parts,

$$\begin{aligned} \Re(\mathbf{R}^2) &= \mathbf{E}^2 - \mathbf{B}^2 = 0, \\ \mathbf{E}^2 &= \mathbf{B}^2, \end{aligned} \tag{2.46}$$

$$\Im(\mathbf{R}^2) = 2\mathbf{E} \cdot \mathbf{B} = 0, \tag{2.47}$$

which quite clearly demonstrates the null-field conditions. This is also confirmed with the α and β configurations (equation 2.33).

This concludes the construction of the null complex vector field, \mathbf{R} , that has been shown to give Maxwell's equations and written in a way that combinations of complex scalar functions can be inserted. This allows for exploration of how they affect the nature of the electric and magnetic fields.

2.2.2 An Extension to an Infinite Family of Solutions

In 2013, Kedia et al. produced a remarkable extension to Bateman's construction method which, in the case of the knotted solutions to Maxwell's equations, produced the whole family of torus knots [16]. This method will be explained, before applying it to project the Hopf fibration and torus-knotted solutions into electromagnetic field lines. Starting with a couple of analytic functions of α and β ,

$$f(\alpha, \beta), \text{ and } g(\alpha, \beta). \tag{2.48}$$

One can define another function,

$$h(\alpha, \beta) = \frac{\partial f}{\partial \alpha} \frac{\partial g}{\partial \beta} - \frac{\partial f}{\partial \beta} \frac{\partial g}{\partial \alpha}. \tag{2.49}$$

If one considers the following form of \mathbf{R} ,

$$\mathbf{R} = \nabla f(\alpha, \beta) \times \nabla g(\alpha, \beta) = h(\alpha, \beta)(\nabla \alpha \times \nabla \beta), \tag{2.50}$$

it can be shown that,

$$\mathbf{R} = i \left(\frac{\partial f}{\partial t} \nabla g - \frac{\partial g}{\partial t} \nabla f \right) = h(\alpha, \beta) i \left(\frac{\partial \alpha}{\partial t} \nabla \beta - \frac{\partial \beta}{\partial t} \nabla \alpha \right). \quad (2.51)$$

Therefore, as this conforms to the conditions set by Bateman's construction, and returns the initial ansatz, the result is an equation that produces an infinite family of solutions, determined by α and β .

Now that the construction of an infinite family of solutions has been demonstrated, the null condition and its relevance to the time evolution of the fields should be further discussed. Underlying each null knotted electromagnetic field, there is a velocity field that transports the electric and magnetic field lines as if they were suspended in a flowing fluid. For the Hopfion solution the velocity field is commonly referred to as the *Robinson congruence* [4][35]. The preservation of the orthogonality of the fields (due to enforcing the null condition), within this fluid-like transportation, makes the fields shear-free - this is referred to as the *frozen field* condition [15]. At time $t = 0$, the velocity field is a tangent to the Poynting vector field and remains fixed in form as it moves at the speed of light in the $-z$ direction. The electric and magnetic field lines propagate along these straight lines given by the velocity field at this time. Therefore, to find the form of the electric and magnetic fields at a later time, it is only necessary to know the velocity field at $t = 0$. Irvine proved that, for the Hopf-knotted electromagnetic field setup, this null condition - present at $t = 0$ - is the key to the preservation of the topology within the field lines [15]. Previously, this was considered due to the conserved helicity of the field lines [3].¹⁶ Irvine gave an example of a field that, at $t = 0$, is not null, but has its helicity conserved. He showed that, over time, the topology of the fields was lost. This null condition is, therefore, hugely important in preserving the topology within the electromagnetic field lines. Because Bateman's construction enforces this condition, it is ideal for application within this research.

An interesting consequence, when considering a whole family of solutions, is that, across them all, the normalised Poynting field is always the same. To demonstrate this, consider the Poynting field [36] - given by,

$$\mathbf{S} = \frac{1}{\mu_0} (\mathbf{E} \times \mathbf{B}). \quad (2.52)$$

¹⁶Helicity is commonly used to determine the linking number or knottedness of the fields.

The normalised Poynting field is, therefore,

$$\tilde{\mathbf{S}} = \frac{(\mathbf{E} \times \mathbf{B})}{|\mathbf{E} \times \mathbf{B}|}. \quad (2.53)$$

This can be written in terms of the Riemann-Silberstein vector and its complex conjugate,

$$\begin{aligned} \tilde{\mathbf{S}} &= i \left(\frac{\mathbf{R} \times \mathbf{R}^*}{\mathbf{R} \cdot \mathbf{R}^*} \right) \\ &= i \frac{|h(\alpha, \beta)|^2 (\nabla \alpha \times \nabla \beta) \times (\nabla \alpha^* \times \nabla \beta^*)}{|h(\alpha, \beta)|^2 (\nabla \alpha \times \nabla \beta) \cdot (\nabla \alpha^* \times \nabla \beta^*)} \\ &= i \frac{(\nabla \alpha \times \nabla \beta) \times (\nabla \alpha^* \times \nabla \beta^*)}{(\nabla \alpha \times \nabla \beta) \cdot (\nabla \alpha^* \times \nabla \beta^*)}. \end{aligned} \quad (2.54)$$

No matter the forms of $f(\alpha, \beta)$, $g(\alpha, \beta)$, and therefore $h(\alpha, \beta)$, the normalised Poynting field remains unchanged for all members of that family. For the Hopf fibration, the normalised Poynting field, its constancy with time, and its relation to the electric and magnetic fields' deformations through the velocity field is further analysed in section 2.2.4.

2.2.3 Examples and Proofs

To further demonstrate the validity of Bateman's construction, one can consider an example involving circularly polarised plane waves. This example was originally demonstrated by Bialynicki-Birula and then by Kedia, et al., alongside the Hopf fibration solution - which will be described in section 2.2.4 [13][16]. The choices for the input functions are as follows:

$$\begin{aligned} \alpha &= kz - \omega t, \quad \beta = kx + iky, \\ f(\alpha, \beta) &= e^{i\alpha}, \quad g(\alpha, \beta) = \beta. \end{aligned} \quad (2.55)$$

Where k is the wave number and ω the angular frequency. It is now necessary to check that these choices of α and β are suitable inputs for the Riemann-Silberstein vector.

$$\begin{aligned} (\nabla \alpha)^2 - \left(\frac{\partial \alpha}{\partial t} \right)^2 &= 0, \\ (\nabla \beta)^2 - \left(\frac{\partial \beta}{\partial t} \right)^2 &= 0, \\ \nabla \alpha \cdot \nabla \beta - \frac{\partial \alpha}{\partial t} \frac{\partial \beta}{\partial t} &= 0. \end{aligned} \quad (2.56)$$

These, clearly, conform to the relations given by equations 2.34. The input functions can now be inserted into equation 2.50,

$$\begin{aligned} \mathbf{R} &= E_0 \nabla f(\alpha, \beta) \times \nabla g(\alpha, \beta), \\ &= E_0 (k\hat{\mathbf{x}} + i k\hat{\mathbf{y}}) e^{i(kz - \omega t)}. \end{aligned} \quad (2.57)$$

Where E_0 is an arbitrary constant with units of electric field. Breaking \mathbf{R} up into its real and imaginary parts for the electric and magnetic fields:

$$\begin{aligned}\mathbf{E} &= E_0(\cos(kz - \omega t)k\hat{\mathbf{x}} - \sin(kz - \omega t)k\hat{\mathbf{y}}), \\ \mathbf{B} &= E_0(\sin(kz - \omega t)k\hat{\mathbf{x}} + \cos(kz - \omega t)k\hat{\mathbf{y}}).\end{aligned}\tag{2.58}$$

Section 2.2.2 demonstrated that infinite families of solutions could be created where a function $h(\alpha, \beta) = \frac{\partial f}{\partial \alpha} \frac{\partial g}{\partial \beta} - \frac{\partial f}{\partial \beta} \frac{\partial g}{\partial \alpha}$. This led to a shared, unchanging, normalised Poynting field being observed across the whole family of solutions. For the circularly polarised fields, the normalised Poynting field is calculated via,

$$\begin{aligned}\tilde{\mathbf{S}} &= i \left(\frac{\mathbf{R} \times \mathbf{R}^*}{\mathbf{R} \cdot \mathbf{R}^*} \right) \\ &= k\hat{\mathbf{z}}.\end{aligned}\tag{2.59}$$

This result is exactly what one would expect and further corroborates the applicability of Bateman's construction for the purposes of examining electromagnetic fields.

2.2.4 The Hopf fibration and the Electromagnetic Field

This chapter has, so far, given the framework for understanding a new development of the electromagnetic field through Bateman's construction, alongside giving equations to view a noteworthy mapping from $S^3 \rightarrow S^2$, the Hopf fibration, in \mathbb{R}^3 , via stereographic projection. This thesis will now combine the contents of the previous sections to project the Hopf fibration into the electromagnetic field lines as exact solutions to Maxwell's equations. The input functions as stated by Bialynicki-Birula [13], and then by Kedia, et al. [16], give the form of the Robinson congruence that underlies the Hopf fibration, and are shown by,

$$\begin{aligned}\alpha &= -\frac{d}{b}, \quad \beta = -i \frac{a}{2b}, \\ f(\alpha, \beta) &= \frac{1}{\alpha^2}, \quad g(\alpha, \beta) = \beta,\end{aligned}\tag{2.60}$$

where,

$$a = kx - iky, \quad b = kct - i - kz, \quad d = k^2x^2 + k^2y^2 + k^2z^2 - (kct - i)^2.\tag{2.61}$$

Above, k is a scale factor with units of inverse distance and c is the speed of light. To make the forms comparable to the equations given for the Hopf fibration, this is written as,

$$\alpha = -\frac{k^2x^2 + k^2y^2 + k^2z^2 - (kct - i)^2}{kct - i - kz}, \quad \beta = -i \frac{kx - iky}{2(kct - i - kz)}.\tag{2.62}$$

These forms of α and β were furthered by Kedia et al. [16] to give the inputs to project the Hopf fibration into the electric and magnetic fields, and then extend them to an infinite family of results (see section 2.2.5).

$$\alpha = \frac{k^2 r^2 - k^2 c^2 t^2 - 1 + 2i kz}{k^2 r^2 - (kct - i)^2}, \beta = \frac{2(kx - i ky)}{k^2 r^2 - (kct - i)^2}, \quad (2.63)$$

where $r^2 = x^2 + y^2 + z^2$. The forms of α and β given here are, strangely, the inverse stereographic projection coordinates (see equation 2.25) when $t = 0$ - which is a projection from $\mathbb{R}^3 \rightarrow S^3$. This seems counter-intuitive since, to view the Hopf fibration mathematically, one has to take the stereographic projection of the inverse map of the Hopf-map. One can assume that this comes about through its relation to the Robinson congruence.

These equations now need to be tested for legitimacy for use within the Riemann-Silberstein vector (and, therefore, Maxwell's equations) according to equations 2.33 and 2.34.

$$\begin{aligned} (\nabla\alpha)^2 - \left(\frac{\partial\alpha}{\partial t}\right)^2 &= 0, \\ (\nabla\beta)^2 - \left(\frac{\partial\beta}{\partial t}\right)^2 &= 0, \\ \nabla\alpha \cdot \nabla\beta - \frac{\partial\alpha}{\partial t} \frac{\partial\beta}{\partial t} &= 0. \end{aligned} \quad (2.64)$$

Therefore, the following condition holds,

$$\nabla\alpha \times \nabla\beta = \frac{i}{c} \left(\frac{\partial\alpha}{\partial t} \nabla\beta - \frac{\partial\beta}{\partial t} \nabla\alpha \right). \quad (2.65)$$

Finally,

$$|\alpha|^2 + |\beta|^2 = 1. \quad (2.66)$$

This demonstrates that these combinations of α and β are coordinates on S^3 . When α and β get inserted into the Riemann-Silberstein vector,

$$\mathbf{R} = E_0 \frac{4}{(A + 2ikct)^3} \begin{pmatrix} (kct - kx - kz + i(ky - 1))(-kct - kx + kz + i(ky + 1)), \\ -i(kct + ky - kz + i(kx - 1))(-kct + ky + kz + i(kx + 1)), \\ 2(kx - iky)(-kct + kz + i) \end{pmatrix}, \quad (2.67)$$

where E_0 is an arbitrary constant with units of electric field. The components of the electric and magnetic fields are the real and imaginary parts of R , respectively:

$$E_x = -\frac{4E_0}{(A + 2ikct)^3} (A^4 - 2A^3 k^2 (y^2 + z^2 - ctz) - 12A^2 k^2 ct (kxy + z) + 24Ak^4 c^2 t^2 (y^2 + z^2 - ctz) + 16k^4 c^3 t^3 (-ct + kxy + z)), \quad (2.68)$$

$$E_y = -\frac{4E_0}{(A+2ikct)^3}(-2A^3k(kxy - z - 2ct) - 12A^2k^2ct(kx^2 + kz^2 - z) + 24Ak^3c^2t^2\left(kxy + \frac{2ct}{3} - z\right) + 16k^5c^3t^3(x^2 + z^2 - ctz)), \quad (2.69)$$

$$E_z = -\frac{4E_0}{(A+2ikct)^3}(-2A^3k(kx(ct - z) - y) - 12A^2k^2ct(ky(z - ct) - x) + 24Ak^3c^2t^2(kx(ct - z) - y) + 16k^4c^3t^3(ky(z - ct) - x)), \quad (2.70)$$

$$B_x = -\frac{4E_0}{(A+2ikct)^3}(-2A^3k(kxy + z - 2ct) - 12A^2k^3ct(czt - z^2 - y^2) + 24Ak^3c^2t^2\left(kxy + z - \frac{2ct}{3}\right) + 16k^5c^3t^3(ctz - z^2 - y^2)), \quad (2.71)$$

$$B_y = -\frac{4E_0}{(A+2ikct)^3}(A^4 - 2A^3k^2(x^2 + z^2 - ctz) - 12A^2k^2ct(-kxy + z) + 24Ak^4c^2t^2(x^2 + z^2 - ctz) + 16k^4c^3t^3(-ct - kxy + z)), \quad (2.72)$$

$$B_z = -\frac{4E_0}{(A+2ikct)^3}(-2A^3k(z - x - y) - 12A^2k^2ct(y + kx(z - ct)) + 24Ak^3c^2t^2(ky(z - ct) - x) + 16k^4c^3t^3(y + kx(z - ct))). \quad (2.73)$$

In the above, $A = \frac{1}{2}(k^2x^2 + k^2y^2 + k^2z^2 - k^2c^2t^2 + 1)$. If one considers these fields for fixed time, $t = 0$, they give the stereographic projection coordinates of the pre-image of the Hopf-map in the electric, magnetic, and Poynting fields. Each are orthogonal to each other and are centred at the origin (see figure 2.17).

$$\begin{aligned} \mathbf{E} &= \frac{4E_0}{(k^2x^2+k^2y^2+k^2z^2+1)^3}(k^2y^2 + k^2z^2 - k^2x^2 - 1, -2k(kxy - z), -2k(y + kxz)) \\ \mathbf{B} &= \frac{4E_0}{(k^2x^2+k^2y^2+k^2z^2+1)^3}(2k(kxy + z), k^2y^2 - k^2z^2 - k^2x^2 + 1, -2k(x - kyz)) \\ \mathbf{S} &= \frac{1}{\mu_0} \frac{16}{(k^2x^2+k^2y^2+k^2z^2+1)^5}(-2k(kxz - y), -2k(kyz + x), k^2x^2 + k^2y^2 - k^2z^2 - 1) \end{aligned} \quad (2.74)$$

This structure is preserved within the Poynting fields but deforms, with time, throughout the electric and magnetic fields. Although the field lines deform, the topology of the Hopf fibration remains with time, due to the field lines' translation via the velocity field.¹⁷

2.2.5 The Production of the Whole Family of Torus Knots as Solutions to Maxwell's Equations

Kedia, et al. [16] established that the whole family of torus knots could be produced within Bateman's constructed fields. They utilise a particular proof, originally expounded by Milnor [17], and later employed by Dennis, et al. [37] in their work on optical vortices in the zeroes of intensity in light beams. This proof showed that, if there is a pair of complex numbers where $u^p \pm v^q = 0$, where $(u, v) \in \mathbb{C}^2$, such that

¹⁷See the paper by Irvine for a complete proof of this [15], and their figure 3 for a geometric demonstration of this.

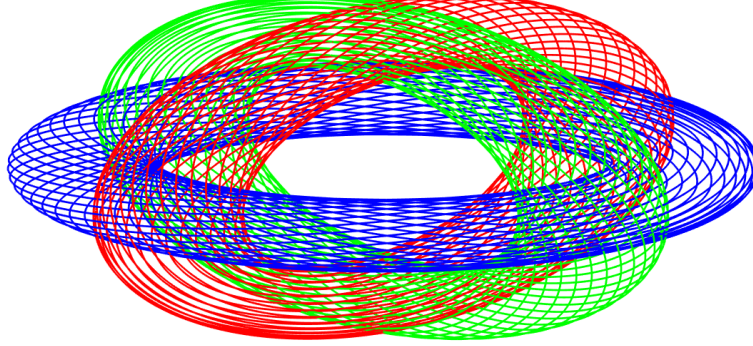


Figure 2.17: One latitude level of S^2 from the Hopf fibration projected into the electric, magnetic, and Poynting fields at time $t = 0$

$|u|^2 + |v|^2 = 1$, these numbers will produce a (p, q) -torus knot - when p and q are co-prime, and $(p, q) > 1$. Clearly, these sets of numbers are also coordinates on S^3 . Kedia, et al. used this theorem to select the input functions ($f(\alpha, \beta)$ and $g(\alpha, \beta)$) to apply to their specified α and β for the Hopf fibration and to be entered into the Riemann-Silberstein vector.

$$\begin{aligned} \alpha &= \frac{k^2 r^2 - k^2 c^2 t^2 - 1 + 2i k z}{k^2 r^2 - (k c t - i)^2}, & \beta &= \frac{2(kx - iy)}{k^2 r^2 - (k c t - i)^2}, \\ f(\alpha, \beta) &= \alpha^p, & g(\alpha, \beta) &= \beta^q. \end{aligned} \quad (2.75)$$

These input functions are put into equations 2.33 and 2.34 to check viability for use within the Riemann-Silberstein vector and, therefore, Maxwell's equations:

$$\begin{aligned} (\nabla\alpha)^2 - \left(\frac{\partial\alpha}{\partial t}\right)^2 &= 0, \\ (\nabla\beta)^2 - \left(\frac{\partial\beta}{\partial t}\right)^2 &= 0, \\ \nabla\alpha \cdot \nabla\beta - \frac{\partial\alpha}{\partial t} \frac{\partial\beta}{\partial t} &= 0, \end{aligned} \quad (2.76)$$

$$\nabla\alpha \times \nabla\beta = \frac{i}{c} \left(\frac{\partial\alpha}{\partial t} \nabla\beta - \frac{\partial\beta}{\partial t} \nabla\alpha \right). \quad (2.77)$$

To prove that they are, indeed, coordinates sat on S^3 ,

$$|\alpha|^2 + |\beta|^2 = 1. \quad (2.78)$$

The choices of α and β conform to the initial conditions and, therefore, so too do $f(\alpha, \beta)$ and $g(\alpha, \beta)$. This is now inserted into the Riemann-Silberstein vector,

$$\begin{aligned} \mathbf{R} &= E_0 \nabla\alpha^p \times \nabla\beta^q \\ &= E_0 p q \alpha^{p-1} \beta^{q-1} (\nabla\alpha \times \nabla\beta), \end{aligned} \quad (2.79)$$

where,

$$h(\alpha, \beta) = pq\alpha^{p-1}\beta^{q-1}. \quad (2.80)$$

It becomes transparent that the Hopfion solution is a limiting case of this torus-knotted set-up where if $p = 1$ and $q = 1$, this equation returns the Hopf fibration within the fields - in the same manner as in section 2.2.4. Any value can be assigned to p and q , but only those that are co-prime will return torus knots within the fields. All other number combinations return torus links.

2.2.6 Visualisation of the Electromagnetic Fields

To gain a complete picture of what the mathematics describes, it is useful to find a geometric method of visualising what these fields look like. This section aims to address this, while expanding upon recently published work on zilches, authored by Smith and Strange (see Chapter 3) [38][39]. The method broached was originally discussed by Kedia, et al. [16] and availed further by Hoyos, et al. [40]. It defines a scalar field that can be used to create the electric and magnetic fields to study their topology. In order to make it applicable to Chapter 3 of this thesis, it needs generalising. Defining,

$$\phi = \alpha\beta = \phi_1 + i\phi_2, \quad (2.81)$$

it can be shown that if $\mathbf{R} = \nabla\alpha \times \nabla\beta$, then,

$$\mathbf{R} \cdot \nabla\phi = 0. \quad (2.82)$$

If one takes the real and imaginary parts of this relation,

$$\begin{aligned} \mathbf{E} \cdot \nabla\phi_1 - \mathbf{B} \cdot \nabla\phi_2 &= 0, \\ \mathbf{B} \cdot \nabla\phi_1 + \mathbf{E} \cdot \nabla\phi_2 &= 0. \end{aligned} \quad (2.83)$$

These equations will always be satisfied. There are a number of outcomes that arise from these equations which allow the scalar functions $\phi_{1(2)}$ to be fully characterised. If, for example, the first of the two equations is satisfied because the scalar products are both zero, then ϕ_1 and ϕ_2 represent the electric and magnetic fields, respectively. Or, if the second of the two equations is satisfied because, again, each scalar product is zero, then it can be said that ϕ_1 and ϕ_2 represent the magnetic and electric fields, respectively. There is also the usual case, where the two equations are satisfied because the scalar products cancel out. In this situation, both ϕ_1 and ϕ_2 are needed to describe the total electromagnetic field, but do not describe the electric and magnetic fields separately. Therefore, ϕ is a complex scalar field that we can use to examine

the topology of the electromagnetic fields, where at each point in space there is a real and imaginary component. In the set-up of the knotted electromagnetic fields the second of the two equations is satisfied for the above reason and, therefore, ϕ_1 and ϕ_2 represent the magnetic and electric fields, respectively.

This is a productive way of viewing each of the fields, as the topology of the field lines is preserved on the scalar surfaces. The surfaces do not appear, as one may imagine, for imaging surfaces of the Hopf fibration or the torus knots - as they appear within the fields. Take the Hopf-knotted electromagnetic fields, for example. If one considers multiple points from a choice of latitude levels of S^2 , the pre-image stereographically projected into the magnetic (electric) field lines take on the form of figure 2.18. Take, for instance, a single latitude level of S^2 - the projected field lines would map out a perfectly symmetric torus (see figure 2.15). In the vector field plots, the field lines for both the electric and magnetic fields are each linked once through their mutual centre, with the separate fields sat orthogonal to each other. This means that, if one considered one latitude level of S^2 , the results would be two single torus surfaces sat at 90° to each other - with the holes of both tori coinciding (see figure 2.17). As figure 2.19 demonstrates, the scalar surfaces link through the tori holes and are deformed.

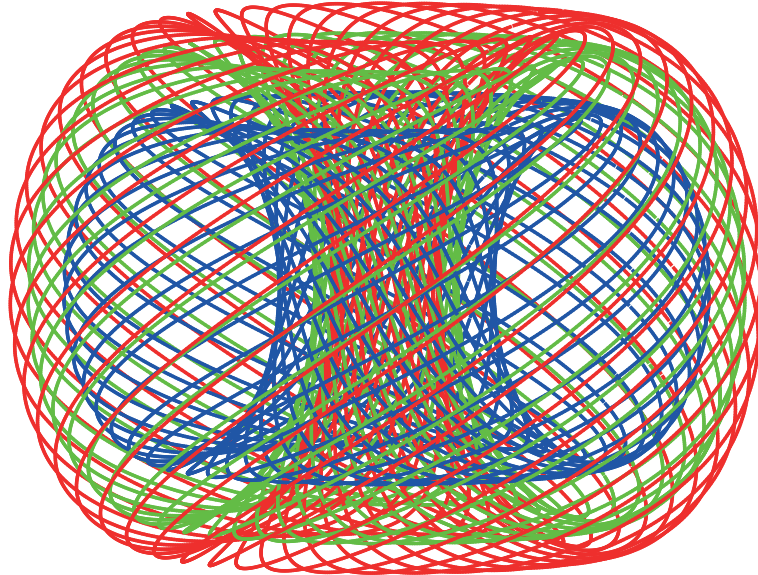


Figure 2.18: The three levels of S^3 from the Hopf fibration projected into R^3

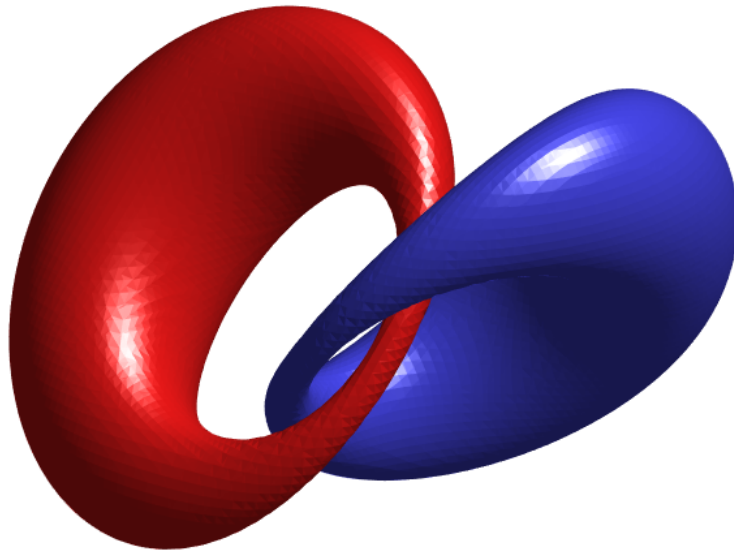


Figure 2.19: One magnitude level of the electric and magnetic scalar fields

To explain the reasons for this *seemingly* abnormal appearance within the scalar fields, one must consider the equation used to create the gradient field. The equations below demonstrate that, for the magnetic field, there is an orthogonal vector field, divergence with the magnetic field of which is zero. This can be seen as a rotation of the magnetic field by $\frac{\pi}{2}$.

Before advancing on this discussion in more detail, it is necessary to consider the method to turn a torus ‘inside-out’. It is possible, within topology, to puncture a torus and peel it over itself to create an orthogonal torus, the axis of which has been flipped, before resealing the original hole (see figure 2.20). This means that a circle on the original torus surface, that was mapped out in the toroidal direction, will appear in the poloidal direction on the surface of the inside-out torus. Most simply, circles on the original torus become bands on the inside-out torus. The hole through the original torus becomes the inside of the inverted torus.

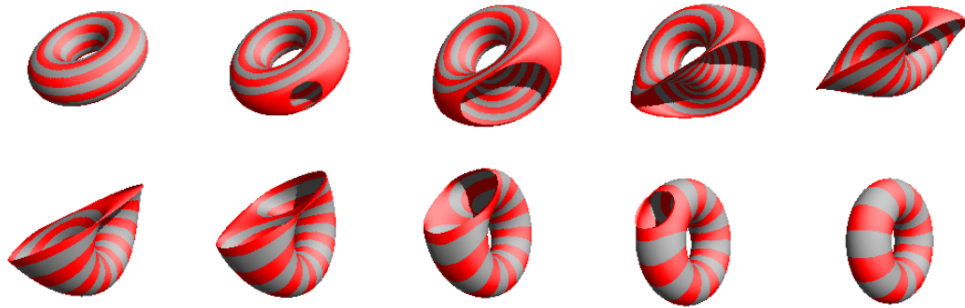


Figure 2.20: The puncturing and turning inside-out of the torus to form an orthogonal torus¹⁸

Within the vector field, the field lines take on the usual characteristics, where a higher density of field lines produces a stronger magnitude, and a lower density of field lines produces a weaker magnitude. Contemplate the Hopf fibration projected into one field - the magnetic field (figure 2.18). The field lines are the closest together as they pass through the middle of the torus and denote the region of highest magnitude. The field lines are furthest apart on the largest circumference of the torus and represent the region of lowest magnitude. The circles and bands can be represented by the regions of high or low magnitude of the vector field, when considering a single latitude level of S^2 - (figure 2.21). The magnitude of the inside-out torus is now contained as bands that wrap around the poloidal direction of the torus, as opposed to the toroidal direction demonstrated by the initial torus.

¹⁸Image sourced at [41].

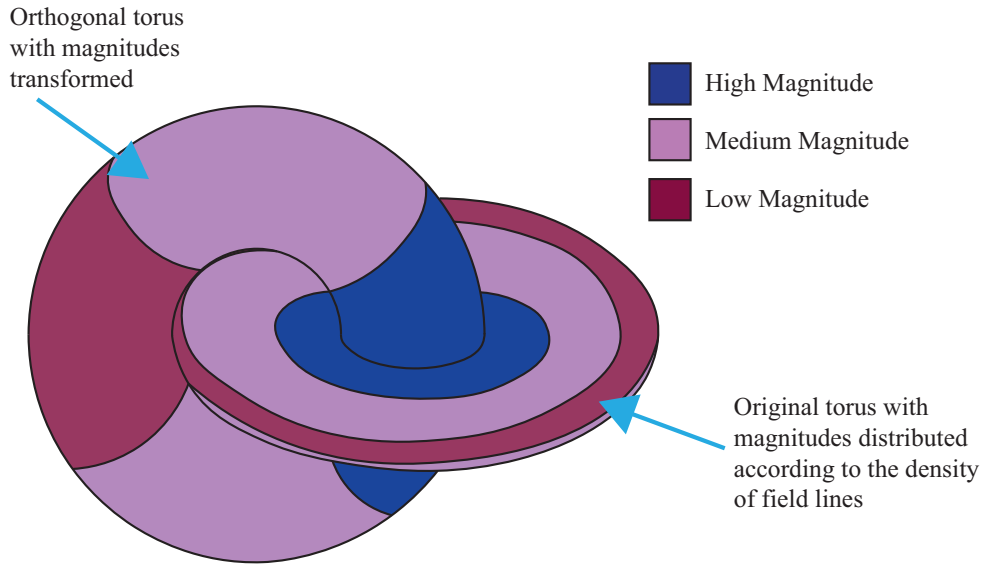


Figure 2.21: The magnitudes of both the original and inside-out torus

This new inside-out torus can represent our orthogonal scalar gradient field, $\nabla\phi_1$. But the scalar fields underlying this vector field are deformed, as shown in figure 2.22.

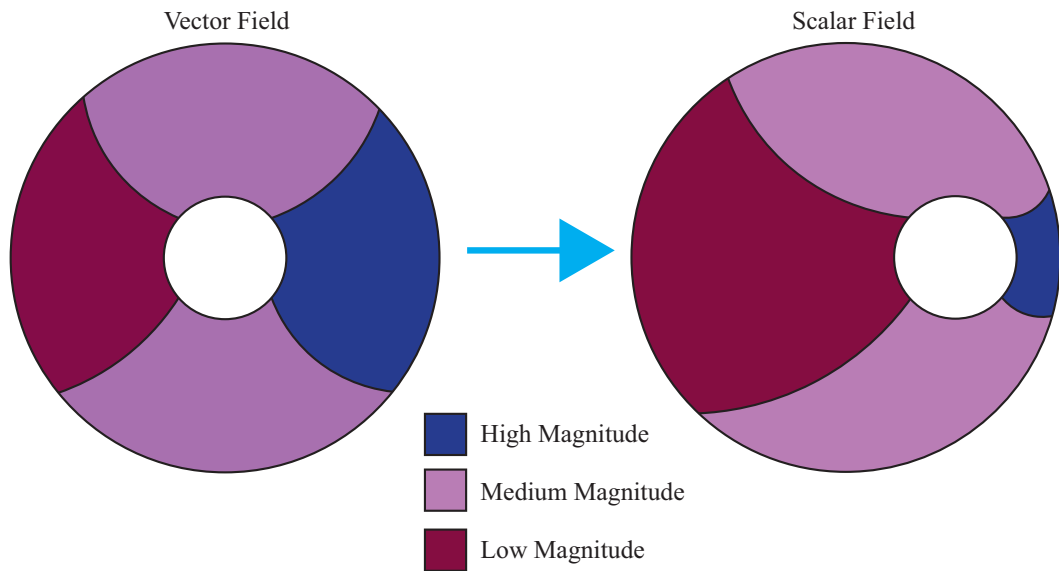


Figure 2.22: The deformation of the scalar torus

The problem of thinking about peeling the torus inside-out is that it would be applied to the projection from the pre-image of the Hopf-map and, therefore, cannot produce the same deformed fields. Another way to achieve this is through rotations within S^3 ,

rather than in \mathbb{R}^3 . If a torus is rotated in the three-sphere, it can be deformed and turned completely inside-out through a rotation - without the need to puncture it. The stereographic projection of a smaller rotation will look the same as the deformed scalar plots in figure 2.19.¹⁹ Therefore, one way to reflect on the orthogonal gradient field - the dot product with the magnetic (electric) field of which is zero - is a rotation of the magnetic (electric) field within the three sphere. The stereographic projection of this reveals a deformed torus the core of which is the inside of the orthogonal field and is shown to be knotted around the electric (magnetic) field. Tori deformed in this way are called Dupin cyclides [43].

This explains the deformed nature of each of the scalar fields. However, that, alone, does not account for the illumination of the knottedness of the fields. That comes from an understanding of what exactly is being knotted *within* the fields - the holes through the middle of the initial torus. The hole through the middle of the initial torus became the inside of the orthogonal torus that lead to the scalar field depiction. Therefore, the scalar field plots demonstrate precisely how the cores of the electric and magnetic field tori are knotting around each other. Their deformed shape is accounted for by the mathematics of rotations within the three-sphere.

Now that a method for visualising the different knots geometrically has been established, examples of knots projected into the electric and magnetic fields are required.

¹⁹Banchoff has created animations demonstrating this [42]

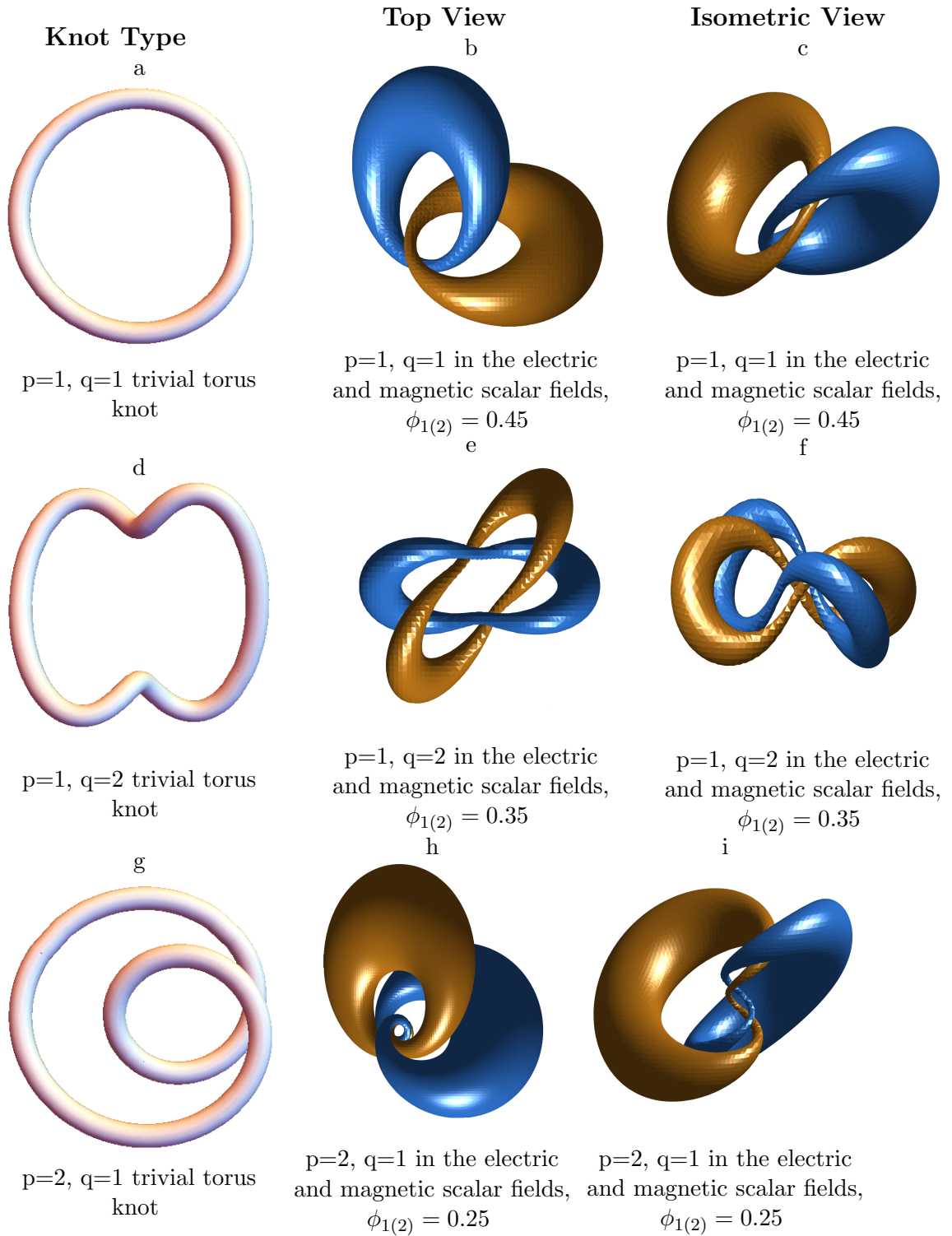


Figure 2.23: Scalar plots of the electric and magnetic fields with differing trivial (p, q) -knots, projected at different magnitudes of $\phi_{1(2)}$

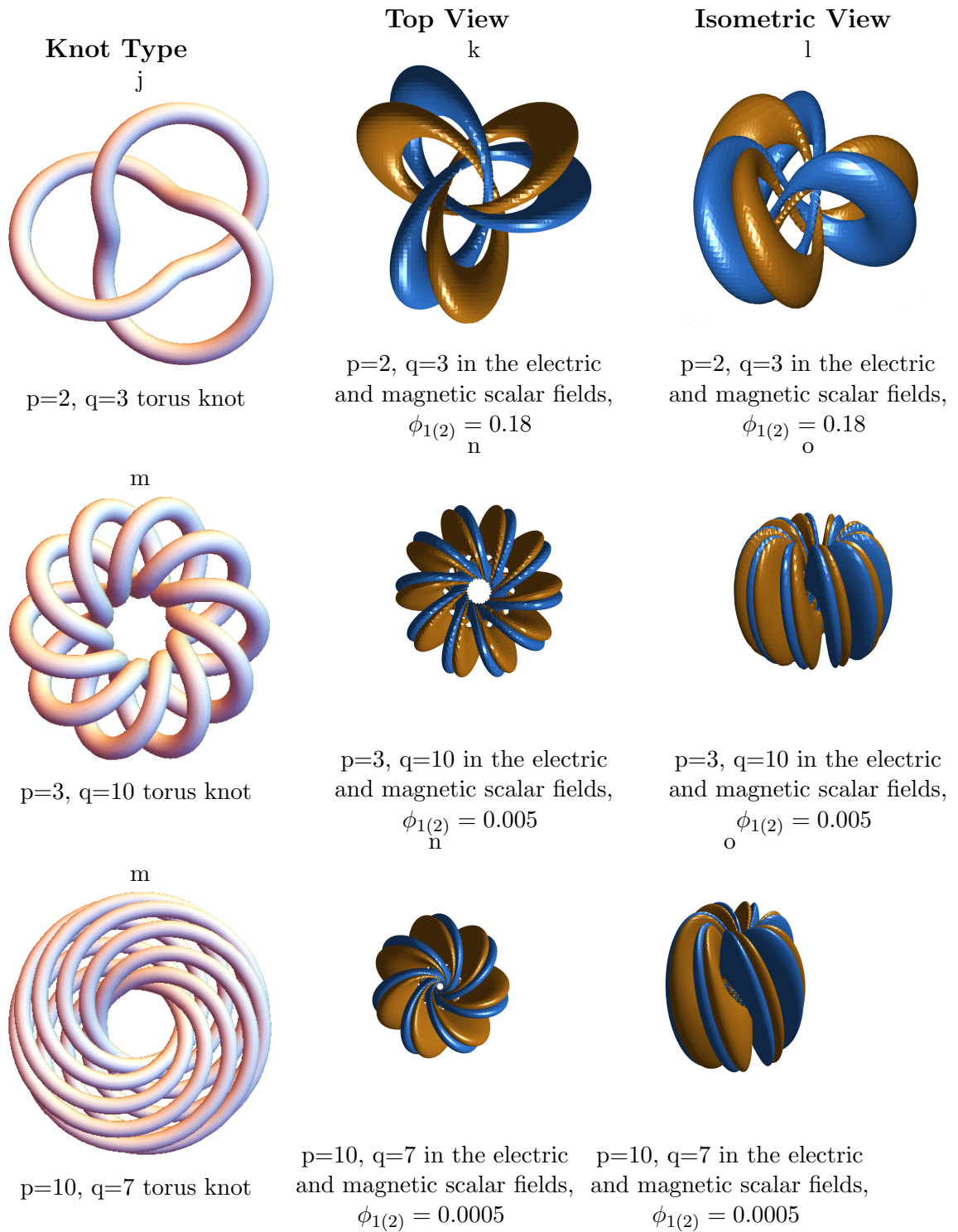


Figure 2.24: Scalar plots of the electric and magnetic fields with differing (p, q) -knots projected at different magnitudes of $\phi_{1(2)}$

It can be seen that, in the scalar fields, both the electric and magnetic fields take on the shape of the corresponding torus knots - and are both linked with each other. This is to be expected, as the scalar fields show the cores of the vector fields knotting around each other. These plots are all for $t = 0$. The electric and magnetic fields warp with the flow of time. This is demonstrated in figure 2.25 for a couple of knot types. With time, the fields warp, whilst expanding outward in the $x - y$ plane and translating along the z -axis at the speed of light. The warping is related to the need to remain orthogonal to the velocity field (normalised Poynting field), which remains constant with time. Although the fields warp, the topology in the field lines is preserved.

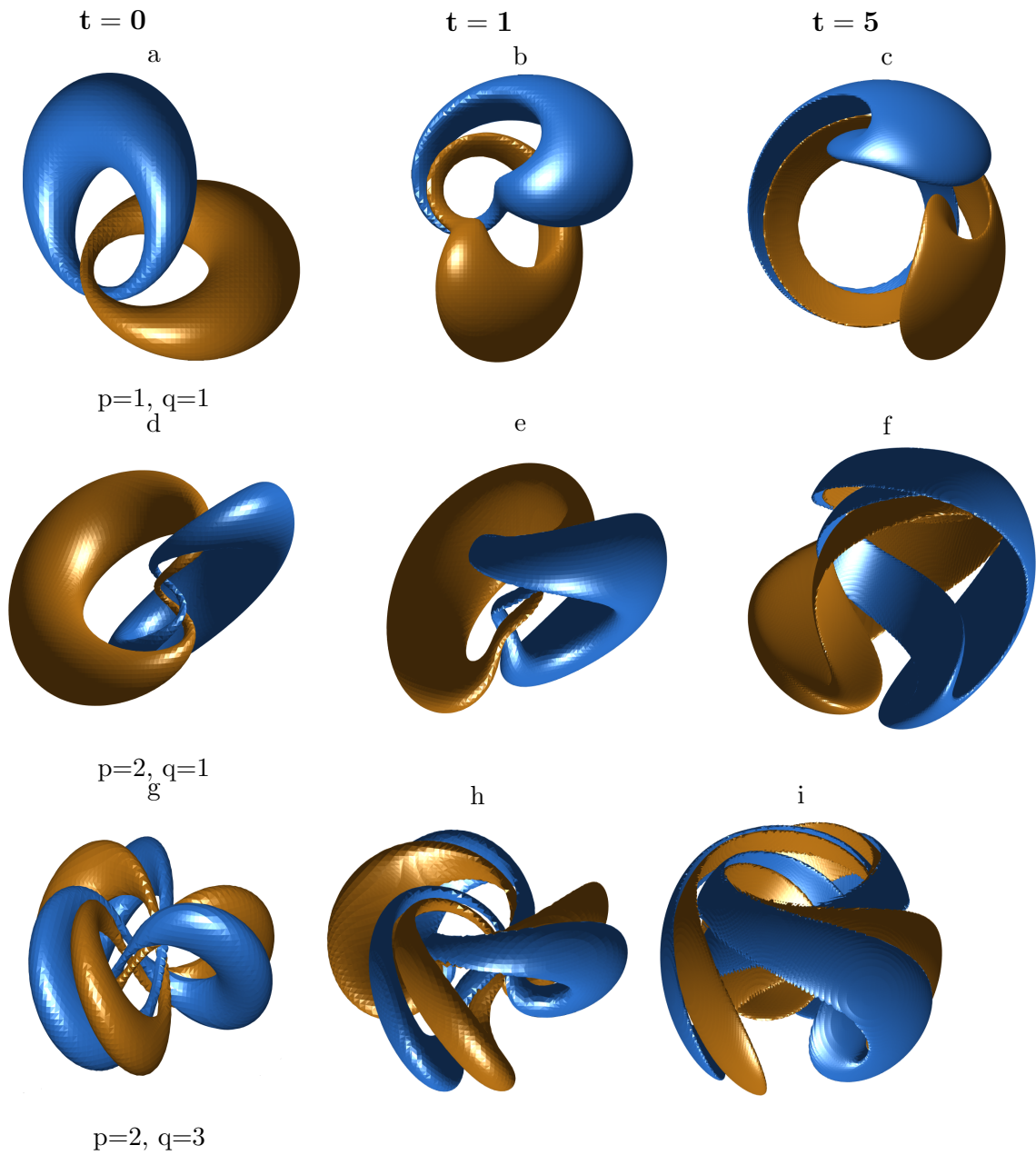


Figure 2.25: Time evolution for three different knots projected into the electric and magnetic field lines

2.2.7 Known Properties of Knotted Solutions to Maxwell's Equations

Now that the Hopf and torus-knotted fields have been demonstrated, some of the properties of the fields will be reviewed in order to obtain a greater comprehension of the area on which this thesis focuses. A list of a selection of conserved quantities within the Hopf-knotted and torus-knotted fields are known [16][40]. The densities of known, conserved quantities within the electromagnetic fields are shown below in table 2.1. The final values of the conserved quantities are given, once integrated over all three dimensional real space, \mathbb{R}^3 - where; \mathbf{E} , \mathbf{B} , are the electric and magnetic field vectors and \mathbf{A} , \mathbf{C} are the magnetic vector potential and the electric equivalent (where $\mathbf{E} = \nabla \times \mathbf{C}$).

Quantity	Expression
Energy Density:	$\xi = \frac{1}{2}(\mathbf{E}^2 + \mathbf{B}^2),$
Momentum Density:	$\mathbf{p} = (\mathbf{E} \times \mathbf{B}),$
Angular Momentum Density:	$\mathbf{l} = (\mathbf{p} \times \mathbf{x}),$
Magnetic Helicity Density:	$h_{mm} = \mathbf{A} \cdot \mathbf{B},$
Electric Helicity Density:	$h_{ee} = \mathbf{C} \cdot \mathbf{E},$

Table 2.1: Table displaying the densities of known, conserved quantities

The helicities of each field are topological constants which indicate the linking number of the field. Each density has been integrated over all space to confirm the previous results, by employing a combination of algebraic and numerical mathematics in *Maple* and *Matlab*. The results for all (p, q) -knotted solutions are all related to the total energy of the field given by,

$$E_{p,q} = \frac{2(p+q)pq\pi^2 p!q! \epsilon_0 E_0^2}{(p+q)!} k. \quad (2.84)$$

This can be written in terms of the total energy of the Hopfion solution,

$$E_{1,1} = 2\pi^2 k \epsilon_0 E_0^2, \quad (2.85)$$

giving,

$$E_{p,q} = \frac{pq p!q!}{(p+q-1)!} E_{1,1}, \quad (2.86)$$

where E_0 is an arbitrary constant, with units of electric field times distance squared, k is a scaling factor with units of inverse distance, and ϵ_0 is the usual permittivity of free space - all of which are set to unity. A beneficial way of viewing this family of knotted solutions to Maxwell's equations is not necessarily as independent fields, but

of excitations of a single field - the Hopf-knotted field. The conserved quantities for the knotted fields in terms of the total energy of the field are therefore,

Quantity	Expression
Momentum:	$\mathbf{P}_{p,q} = (0, 0, -\frac{p}{p+q} E_{p,q}),$
Angular Momentum:	$\mathbf{L}_{p,q} = (0, 0, -\frac{q}{p+q} E_{p,q}),$
Magnetic Helicity:	$H_{p,q}^m = \frac{1}{p+q} E_{p,q},$
Electric Helicity:	$H_{p,q}^e = \frac{1}{p+q} E_{p,q}.$

Table 2.2: Table displaying the conserved quantities in terms of the winding numbers of the fields, (p, q) , and the total energy of the fields, $E_{p,q}$

2.3 Summary

This chapter aimed to provide a theoretical and mathematical framework for the research presented in this thesis. The subsequent chapters draw from this foundation knowledge. This chapter has provided an historical review of the most relevant literature and permits an understanding of the position of this study within the context of previous research.

This research examines properties of knotted electromagnetic fields. Therefore, the essentials of knot theory were central to this chapter - including detailed descriptions of the Hopf fibration, torus knots and other knot invariants. The method by which one can view the Hopf fibration (the mapping $S^3 \rightarrow S^2$) - stereographic projection - was discussed in order to facilitate further deliberation on: the mathematical approach to this research; and why and how the Hopf fibration is projected into electromagnetic fields. An extension to this was demonstrated, producing an infinite family of solutions - torus knots.

In order to provide a basis for understanding Chapter 3 and 4, an exploration of how the Hopf fibration, and family of torus knots, could be projected into the field lines of charge-free solutions to Maxwell's equations was provided, demonstrating an important method: Bateman's construction. This construction preserves the topology of the fields for all time.

A novel method for visualising knotting and linking of the cores of the electromagnetic fields was exhibited via the scalar fields. It was shown that, via a rotation of the

three-sphere, the tori that make up the projection of the Hopf fibration were turned inside-out. When viewed through the scalar fields, they produced Dupin cyclides. This method of visualisation allows one to observe a deep topological connection with zilches (see Chapter 3).

Finally, the known properties of the Hopf-knotted and torus-knotted fields were shown to be related to the total energy of the field. In addition, an interpretation - which allows the properties to be written in terms of the total energy of the Hopfion solution - was outlined. The known, conserved quantities of the fields are shown to be related to zilches in Chapter 3.

ZILCHES OF KNOTTED ELECTROMAGNETIC FIELDS

In 1964, Lipkin discovered a set of ten conserved quantities within electromagnetism, represented by a third-rank tensor which he collectively named, the ‘zilch’ [44]. The zilches were shown to have units of force - but Lipkin felt that they might be linked, in some way, to the helicity of fields of light. They demonstrated changes of direction of flow, when examined in the context of the handedness of circularly polarised plane-waves (with respect to the propagation direction). However, they could not be linked with units of angular momentum. Further, the flow of zilch could not be found for linearly polarised plane-waves - lending additional weight to Lipkin’s conjecture. Lipkin suggested they were independent of the electromagnetic stress energy tensor, as they could not be linked to its derivatives. Since their introduction, the zilches have been heavily investigated and explored in numerous papers. They are understood mathematically, but their *physical nature* is still debated.

In the subsequent year, the questions initially posed by Lipkin attracted various responses. Candlin [45], followed by Morgan [46], O’Connell and Tompkins [47] and Kibble [48], all managed to show that, for any free field, one can find an infinite number of conserved quantities, with densities that are bilinear functions of the charge-free electromagnetic fields. Candlin specifically related these extensions to optical helicity. Kibble demonstrated how the zilches were related to usual quantities in electromagnetism: the electromagnetic field tensor; and the Maxwell stress-energy tensor. Each author made the inference that it was unlikely any *physical* significance would be found from further examination of the zilches.

In 1918, Noether expounded a remarkable theorem which showed that a conservation law would imply a symmetry of the Lagrangian [49]. For the zilches (conserved quantities), this symmetry remained a mystery until recently. Their conservation has been shown to be a symmetry involving the second derivative of both the magnetic and electric vector potential [50] - and of the magnetic vector potential [51]. Previously, this symmetry has also been suggested for the individual zilches [52][53].

In the attempt to find a physical interpretation of the zilches, the literature has mainly been restricted to the Z^{000} zilch. Z^{000} has been thought of as a measure of optical chirality and has been used in this capacity to successfully predict and interpret experiments [54][55]. For monochromatic light, Z^{000} has been shown to be proportional to the helicity of the field and the Z^{0j0} -zilches have been proved proportional to the components of spin of the fields [56][57][58]. As emphasised by Cameron and Barnett [50], there are no such proportionalities in a polychromatic field. Beyond Z^{000} , virtually nothing has been said about the physical interpretation of the zilches. Hence, the full meaning of these conserved quantities has remained a mystery throughout the 55 years since their discovery. Any new contribution to the understanding of the zilches is, therefore, of fundamental import.

This chapter explores the properties of the zilches using topologically unusual electromagnetic fields. It will demonstrate a profound connection between the topology of three different electromagnetic fields and their zilches. Connections to the Maxwell stress energy and angular momentum tensors are also demonstrated, through an interpretation that allows the zilches to be written in terms of the other conserved properties of the fields.

3.1 Lipkin's Zilches

Lipkin's original work [44] started with the unveiling of a new conservation law in vacuum electrodynamics. This led to the creation of a tensor formulation, the parts of which, he conjectured, may be new physical quantities. He found that the tensor form had symmetry properties,

$$\mathcal{Z}^{\nu\mu\gamma} = \mathcal{Z}^{\mu\nu\gamma}, \quad (3.1)$$

which also satisfy the divergence equation,²⁰

$$\partial_\gamma \mathcal{Z}^{\nu\mu\gamma} = 0. \quad (3.2)$$

These symmetries limited the total number of independent equations to ten. Lipkin suggested that the components in $\mathcal{Z}^{\nu\mu 0}$ should be interpreted as the spatial densities of the conserved quantities. The components $\mathcal{Z}^{\nu\mu i}$ should be interpreted as the fluxes of the conserved quantities. The conserved quantities can be written concisely by using only the first two indices of the original tensor. The spatial density components of zilch can be found in vacuum, with an input of the electric field vector, \mathbf{E} , and magnetic field vector, \mathbf{B} . This is given by,

$$\mathcal{Z}^{000} = \frac{\epsilon_0}{2} (\mathbf{E} \cdot (\nabla \times \mathbf{E}) + c^2 \mathbf{B} \cdot (\nabla \times \mathbf{B})), \quad (3.3)$$

$$\mathcal{Z}^{0i0} = \frac{\epsilon_0 c}{2} (\mathbf{E} \times (\nabla \times \mathbf{B}) - \mathbf{B} \times (\nabla \times \mathbf{E}))_i, \quad (3.4)$$

$$\mathcal{Z}^{ij0} = \delta_{ij} \mathcal{Z}^{000} - \frac{\epsilon_0}{2} (E_i (\nabla \times \mathbf{E})_j + E_j (\nabla \times \mathbf{E})_i + c^2 B_i (\nabla \times \mathbf{B})_j + c^2 B_j (\nabla \times \mathbf{B})_i). \quad (3.5)$$

The flux density components of zilch are given by,

$$\mathcal{Z}^{ijk} = \delta_{ij} \mathcal{Z}^{00k} + \frac{\epsilon_0 c}{2} \left(B_i \frac{\partial E_j}{\partial x_k} + B_j \frac{\partial E_i}{\partial x_k} - E_i \frac{\partial B_j}{\partial x_k} - E_j \frac{\partial B_i}{\partial x_k} \right). \quad (3.6)$$

Finally, other symmetry relationships are that,

$$\mathcal{Z}^{00i} = \mathcal{Z}^{0i0}, \quad \mathcal{Z}^{0ij} = \mathcal{Z}^{ij0}. \quad (3.7)$$

Consider a surface, X , bounding a region of space in vacuum. If the densities are integrated over a defined volume within X , they give the total conserved quantities

²⁰Where Greek letters are used in the superscripts, they represent 1 dimension of time and the 3 dimensions of space. Where Latin letters are used, they represent the 3 dimensions of space *only*.

within that region,²¹

$$Z^{\nu\mu} = \int \mathcal{Z}^{\nu\mu 0} d^3\mathbf{r}. \quad (3.8)$$

Lipkin concluded that these newly discovered, conserved quantities might possibly be found in other areas of physics and, therefore, would need a defining name - zilch.²² Considering the remaining components of the zilch tensor and integrating over the surface, X_i , of the defined volume,

$$S^{\nu\mu} = \int \mathcal{Z}^{\nu\mu i} dX_i. \quad (3.9)$$

$S^{\nu\mu}$, therefore, represents the rate of flow of zilch out of the volume. Thus, the integral form of the conservation law is expressed, as stated in Lipkin's paper, as,

$$\frac{d}{dt} Z^{\nu\mu} = -S^{\nu\mu}. \quad (3.10)$$

All ten components of the total zilch for a given volume, as defined in equation 3.8, have units of force. As Lipkin suggested, if multiplied by a factor that has dimensions of the speed of light, it will give units of power. This implies that the zilches are a dynamical quantity. To give further strength to Lipkin's conjecture, the zilches do not appear in static fields. Finally, Lipkin discussed the propagation of zilch in the charge-free electromagnetic fields. Zilch is not transported by linearly polarised fields. The zilch will flow in circularly polarised fields, in the same - or opposite - direction as the energy and momentum of the field. The direction of the flow is distinctly connected to the handedness of the circular polarisation. In addition, Lipkin highlighted the linear connection between the rate of flow of zilch and the frequency of oscillation of the field.

In this chapter, the fields employed to explore the zilches are completely distinct from their plane-wave counterparts - those which have been used in past examinations. The relationship between the zilch and the twisting of the fields will become apparent, as they are linked to the fields' topology. The computation of the zilches is straightforward once the electric and magnetic field vectors are known. The calculations have been carried out using the algebraic mathematics program, *Maple*, as well as numerically, using *Matlab*. A number of sets of unusual electromagnetic fields

²¹For this chapter, densities will be shown via calligraphic letters, while for total, integrated quantities, Latin letters will be used.

²²Lipkin did not elaborate on his choice of name unfortunately.

will be used to examine the role of zilches within electromagnetism, starting with the knotted solutions to Maxwell's equations. There are two specific areas on which this analysis is focused: relationship of the zilches to known physical quantities of the fields; and the relationship of the zilches to the topological properties of the fields.

3.2 Zilches in Knotted Electromagnetic Fields

Chapter Two gave a detailed description of the construction of knotted solutions to Maxwell's equations. Here, the results of calculating the zilches from these knotted solutions will be presented. To be specific, the α and β used are those from equation 2.75, the powers of which, p and q , are the winding numbers - dictating which type of torus knot or link will be projected into the field lines.

The known properties of the knotted fields are calculated to check the validity of equations given in the literature (see section 2.2.7) [40][16]. Alongside this, the zilches are also calculated by inserting the components of the electric and magnetic fields into equations 3.3-3.6. Initial analysis demonstrates that the zilches are not all independent for knotted electromagnetic fields, as,

$$Z_{p,q}^{000} = Z_{p,q}^{110} + Z_{p,q}^{220} + Z_{p,q}^{330}. \quad (3.11)$$

As the zilches are conserved quantities within the electromagnetic fields, it is necessary to put them in a form for comparison with the known conserved quantities: energy, momentum, angular momentum etc. In order to do this, the total zilch is divided by the total energy of the field for each component. The known conserved quantities have already been shown, in Chapter Two, to be summarised in terms of *only* the winding numbers of the fields (in this set of units - with $c = k = 1$). Upon examination of the zilches, patterns started emerging for all calculated combinations of knotted field - in the form of rational numbers (see table 3.1).

This warranted further exploration - to ascertain if the zilches could be written in terms of the winding numbers *and* in terms of the total energy of the fields - as concisely as the other conserved quantities. A standardised method is required, in order to be consistent across all results. To achieve this, an ansatz was made of the possible form that the combination of winding numbers could take. Once multiplied by the total energy of the field, this would reveal the zilch being analysed. The initial

3.2. ZILCHES IN KNOTTED ELECTROMAGNETIC FIELDS

Winding Number (p,q)	$Z^{000}/E_{p,q}$	$Z^{030}/E_{p,q}$	$Z^{011}/E_{p,q}$	$Z^{022}/E_{p,q}$	$Z^{033}/E_{p,q}$
(1, 1)	$\frac{5}{2}$	$-\frac{5}{4}$	$\frac{3}{4}$	$\frac{3}{4}$	$\frac{4}{4}$
(1, 2)	$\frac{7}{2}$	$-\frac{7}{6}$	$\frac{8}{6}$	$\frac{8}{6}$	$\frac{5}{6}$
(1, 3)	$\frac{9}{2}$	$-\frac{9}{8}$	$\frac{15}{8}$	$\frac{15}{8}$	$\frac{6}{8}$
(1, 4)	$\frac{11}{2}$	$-\frac{11}{10}$	$\frac{24}{10}$	$\frac{24}{10}$	$\frac{7}{10}$
(1, 5)	$\frac{13}{2}$	$-\frac{13}{12}$	$\frac{35}{12}$	$\frac{35}{12}$	$\frac{8}{12}$
(1, 6)	$\frac{15}{2}$	$-\frac{15}{14}$	$\frac{48}{14}$	$\frac{48}{14}$	$\frac{9}{14}$
(2, 1)	$\frac{8}{2}$	$-\frac{17}{6}$	$\frac{5}{6}$	$\frac{5}{6}$	$\frac{14}{6}$
(2, 2)	$\frac{10}{2}$	$-\frac{22}{8}$	$\frac{12}{8}$	$\frac{12}{8}$	$\frac{16}{8}$
(3, 1)	$\frac{11}{2}$	$-\frac{27}{8}$	$\frac{7}{8}$	$\frac{7}{8}$	$\frac{30}{8}$
(3, 2)	$\frac{13}{2}$	$-\frac{43}{10}$	$\frac{16}{10}$	$\frac{16}{10}$	$\frac{33}{10}$
(4, 1)	$\frac{14}{2}$	$-\frac{59}{10}$	$\frac{9}{10}$	$\frac{9}{10}$	$\frac{52}{10}$
(5, 1)	$\frac{17}{2}$	$-\frac{89}{12}$	$\frac{11}{12}$	$\frac{11}{12}$	$\frac{80}{12}$
(6, 1)	$\frac{20}{2}$	$-\frac{125}{14}$	$\frac{13}{14}$	$\frac{13}{14}$	$\frac{114}{14}$

Table 3.1: Table displaying the numerical components of zilch for a variety of the winding numbers of the fields, (p, q)

estimate was that the combinations of (p, q) -winding numbers are either linear or quadratic in nature. For example,

$$Z_{p,q}^{000} = (A p^2 + B q^2 + C p q + D p + E q + F) E_{p,q}. \quad (3.12)$$

This leaves a set of six coefficients, A-F, to be found, in order to confirm this assumption. To obtain the coefficients, six simultaneous equations needed to be solved, where the form of the zilch is calculated for a variety of (p, q) -winding numbers. The elimination method was used in *Maple* to obtain algebraic forms of each of the coefficients, in terms of the possible zilch values, for the associated inputs of p and q . For example, taking the value for zilch in terms of the total energy of the field for a combination of winding numbers gives,

$$\begin{aligned} \frac{Z_{1,1}^{000}}{E_{1,1}} &= (A + B + C + D + E + F) &= \frac{5}{2}, \\ \frac{Z_{1,2}^{000}}{E_{1,2}} &= (A + 4B + 2C + D + 2E + F) &= \frac{7}{2}, \\ \frac{Z_{2,1}^{000}}{E_{2,1}} &= (4A + B + 2C + 2D + E + F) &= \frac{8}{2}. \end{aligned} \quad (3.13)$$

Once the elimination method has been applied, the coefficients are found for each

zilch. For $Z_{p,q}^{000}$,

$$\frac{Z_{p,q}^{000}}{E_{p,q}} = \frac{3p + 2q}{2}. \quad (3.14)$$

This method is applied to all the zilches, giving the results in the table below. The results are then checked against a number of p, q -torus knots to test for validity (see table 3.2).

Quantity	Expression
$Z_{p,q}^{000} / E_{p,q} :$	$\frac{3p+2q}{2}$
$Z_{p,q}^{030} / E_{p,q} :$	$\frac{(q-3p(p+q))}{2(p+q)}$
$Z_{p,q}^{110} / E_{p,q} = Z_{p,q}^{220} / E_{p,q} :$	$\frac{(q^2+2pq)}{2(p+q)}$
$Z_{p,q}^{330} / E_{p,q} :$	$\frac{(3p^2+pq)}{2(p+q)}$

Table 3.2: The zilches in terms of the total energy of the field are completely related to the winding numbers of the field

The results have been confirmed for all combinations of winding numbers up to $p + q = 15$. The forms of the zilches given here allow them to be written entirely in terms of the other conserved quantities: momentum, angular momentum and energy (see table 3.3).

Quantity	Expression
$Z_{p,q}^{000} :$	$-\frac{(p+q)kc}{2}(3P_{p,q}^z + 2kL_{p,q}^z)$
$Z_{p,q}^{030} :$	$-\frac{3(p+q)kc^2P_{p,q}^z}{2E_{p,q}}(P_{p,q}^z + kL_{p,q}^z) - \frac{k^2c}{2}L_{p,q}^z$
$Z_{p,q}^{110} = Z_{p,q}^{220} :$	$\frac{(p+q)k^2c^2L_{p,q}^z}{2E_{p,q}}(kL_{p,q}^z + 2P_{p,q}^z)$
$Z_{p,q}^{330} :$	$\frac{(p+q)kc^2P_{p,q}^z}{2E_{p,q}}(3P_{p,q}^z + kL_{p,q}^z)$

Table 3.3: The zilches in terms of known conserved quantities of the knotted fields

As the zilches can be shown to be comprised of these conserved quantities, one can state that the zilches are conserved. These results also allow the zilches to be used as a gauge of other dynamical quantities within the knotted fields - although how useful

this might be is open to interpretation.

3.2.1 Linking the Zilches to Topological Properties of the Fields

This section will probe previously unseen connections between the zilches and the properties of the fields. The topological constants for torus knots and links will be shown to be embedded in the zilches and therefore show a strong topological connection to the fields. In a particular set of units, the zilches reveal even more about their structure. The units employed were selected as they are the lowest that give all the zilches as dimensionless integers. To obtain them, the non-zero zilches are all divided by $\frac{1}{4^{(p+q)}} E_{p,q} = p q \pi^2 p! q! \epsilon_0 E_0^2 k^2 / (2(p+q)!)$. The following figures (3.1-3.5) will display a selection of seperate combinations of winding number used - and therefore torus knots and links explored. The numerical results for the non-zero zilches are then specified. They will assist in the explanation of the methods used to establish the algebraic results.

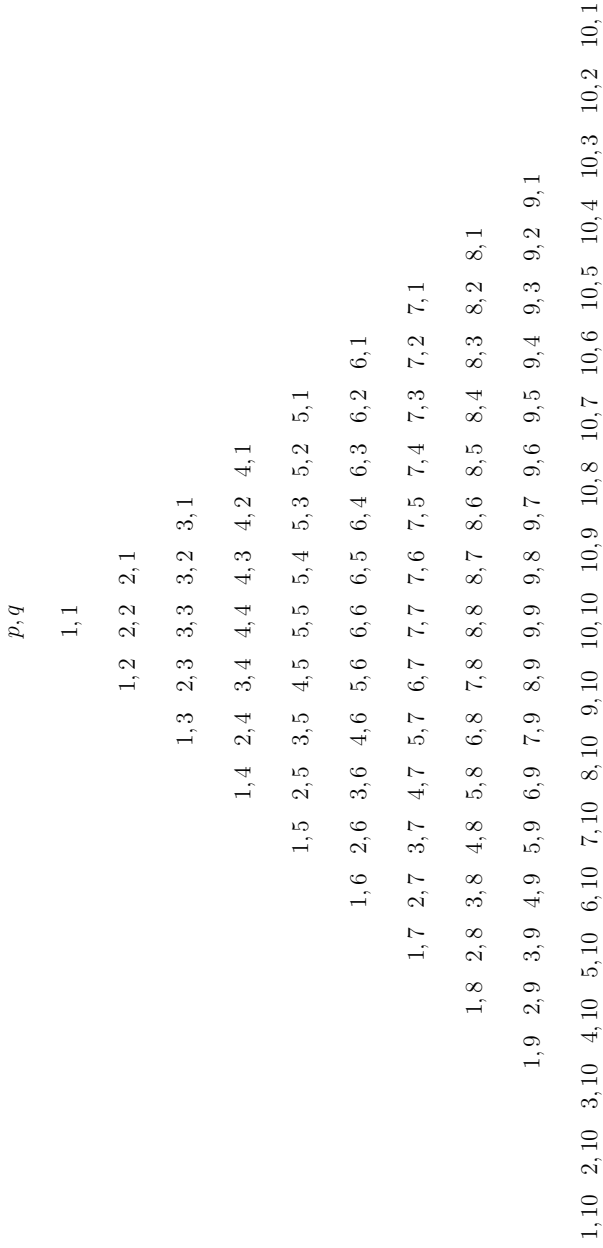


Figure 3.1: The p - q winding number tree showing the various combinations possible for $p = 1 - 10$ and $q = 1 - 10$.

$Z_{p,q}^{000}$	
10	
21 40 24	
36 60 90 65 44	
55 84 119 160 126 96 70	
78 112 152 198 250 207 168 133 102	
105 144 189 240 297 360 308 260 216 176 140	
136 180 230 286 348 416 490 429 372 319 270 225 184	
171 220 275 336 403 476 555 640 570 504 442 384 330 280 234	
210 264 324 390 462 540 624 714 810 731 656 585 518 455 396 341 290	
253 312 377 448 525 608 697 792 893 1000 912 828 748 672 600 532 468 408 352	

Figure 3.2: The results for Z^{000} when put in units per $\frac{1}{4(p+q)}E_{p,q} = p q \pi^2 p! q! \epsilon_0 E_0^2 k^2 / (2(p+q)!)$

$Z_{p,q}^{030}$	-5
-7 - 22 - 17	
-9 - 27 - 51 - 43 - 35	
-11 - 32 - 59 - 92 - 81 - 70 - 59	
-13 - 37 - 67 - 103 - 145 - 131 - 117 - 103 - 89	
-15 - 42 - 75 - 114 - 159 - 210 - 193 - 176 - 159 - 142 - 125	
-17 - 47 - 83 - 125 - 173 - 227 - 287 - 267 - 247 - 227 - 207 - 187 - 167	
-19 - 52 - 91 - 136 - 187 - 244 - 307 - 376 - 353 - 330 - 307 - 284 - 261 - 238 - 215	
-21 - 57 - 99 - 147 - 201 - 261 - 327 - 399 - 477 - 451 - 425 - 399 - 373 - 347 - 321 - 295 - 269	
-23 - 62 - 107 - 158 - 215 - 278 - 347 - 422 - 503 - 590 - 561 - 532 - 503 - 474 - 445 - 416 - 387 - 358 - 329	

Figure 3.3: The results for Z^{030} when put in units per $\frac{1}{4(p+q)}E_{p,q} = p q \pi^2 p! q! \epsilon_0 E_0^2 k^2 / (2(p+q)!)$

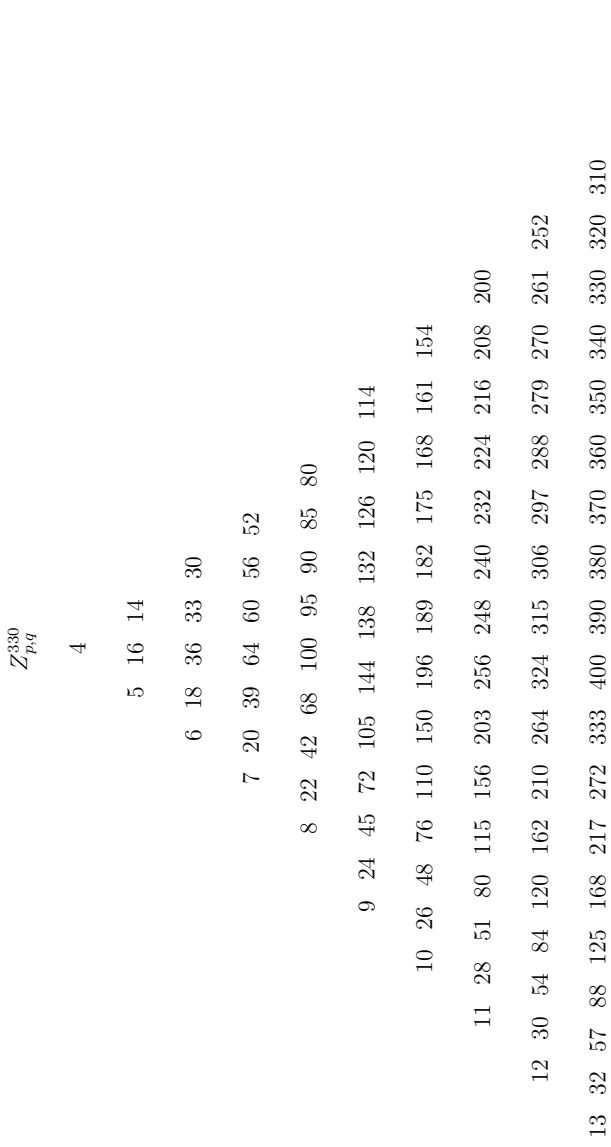


Figure 3.5: The results for Z^{330} when put in units per $\frac{1}{4^{(p+q)}} E_{p,q} = p q \pi^2 p! q! \epsilon_0 E_0^2 k^2 / (2(p+q)!)$

This thesis introduces now a prescription to obtain the number of pieces of surface of the torus knots and links via the zilches:

1. Evaluate $Z_{p,q}^{000}$, $Z_{p,q}^{030}$, $Z_{p,q}^{110}$ and $Z_{p,q}^{330}$.
2. Evaluate $Z_{q,p}^{000}$, $Z_{q,p}^{030}$, $Z_{q,p}^{110}$ and $Z_{q,p}^{330}$.
3. Evaluate $Y_{p,q} = \gcd(Z_{p,q}^{000}, Z_{p,q}^{030}, Z_{p,q}^{110}, Z_{p,q}^{330})$ and $Y_{q,p} = \gcd(Z_{q,p}^{000}, Z_{q,p}^{030}, Z_{q,p}^{110}, Z_{q,p}^{330})$.
4. Evaluate $N_{p,q}^s = \gcd(Y_{p,q}, Y_{q,p})$.

The value given by $N_{p,q}$ is exactly the number of pieces of surface associated with the scalar knotted fields for every (p,q) and (q,p) torus knot and link examined. The scalar knotted fields are those demonstrated in Chapter Two, revealing the underlying topology. The number of pieces of surface are easily calculated for (p,q)-torus knots and links - calculated as the greatest common divisor (gcd) of both p and q - and can be seen in the scalar field plots. This prescription demonstrates that this topological information is also encoded in the zilches. To better demonstrate this prescription, an example will be exhibited. Below is a table giving the values of the zilches within the previously stated units.

(p, q)	(1, 5)	(2, 4)	(3, 3)	(4, 2)	(5, 1)
$Z_{p,q}^{000}$	78	84	90	96	102
$Z_{p,q}^{030}$	-13	-32	-51	-70	-89
$Z_{p,q}^{110} = Z_{p,q}^{220}$	35	32	27	20	11
$Z_{p,q}^{330}$	8	20	36	56	80
$Y_{p,q}$	1	4	3	2	1
$N_{p,q}$	1	2	3	2	1

Table 3.4: The values of the zilches for the various $p + q = 6$ knot-types and the results for calculating the number of pieces of surface, $N_{p,q}$

Consider now the zilches with $p = 2$ and $q = 4$, and $p = 4$ and $q = 2$. The $\gcd(2, 4) = \gcd(4, 2) = 2$, meaning that these particular torus-links have two distinct pieces. If one now considers the values of the zilches from the table for $p = 2$ and $q = 4$: $Z_{2,4}^{000} = 84$, $Z_{2,4}^{030} = -32$, $Z_{2,4}^{110} = 32$ and $Z_{2,4}^{330} = 20$. The gcd of all four of these

zilches is given by, $Y_{2,4} = \gcd(84, -32, 32, 20) = 4$. Now considering for $p = 4$ and $q = 2$: $Z_{4,2}^{000} = 96$, $Z_{4,2}^{030} = -70$, $Z_{4,2}^{110} = 20$ and $Z_{4,2}^{330} = 56$. The gcd of all four of these zilches is given by, $Y_{4,2} = \gcd(96, -70, 20, 56) = 2$. To find the number of pieces of surfaces, $N_{2,4}^s = \gcd(Y_{2,4}, Y_{4,2}) = 2$. This corroborates the number of pieces of surface for the torus-link. Furthermore, this has been confirmed for all combinations of p and q , up to $p + q = 15$.

There are also a number of other topological constants that can be found from the zilches. In Chapter Two, various invariants were discussed, such as crossing number, $c(K)$, and unknotting number, $u(K)$. For the torus-knotted fields, these were shown to be calculated from the winding numbers, as follows:

$$c(T(p, q)) = \min(p(q - 1), q(p - 1)), \quad (3.15)$$

$$u(T(p, q)) = \frac{1}{2}(p - 1)(q - 1), \quad (3.16)$$

for $p, q > 1$ and $p \neq q$. The crossing number can be determined from the zilches via Z^{110} when they are put in the same units, for $p, q > 1$ and $p \neq q$. For $p + q$ odd,

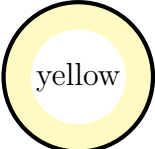

$$\begin{aligned} c(T(p, q)) &= Z_{(q-p+1)/2, p-1}^{110}, \quad q > p, \\ &= Z_{(p-q+1)/2, q-1}^{110}, \quad q < p. \end{aligned} \quad (3.17)$$

While for $p + q$ even,

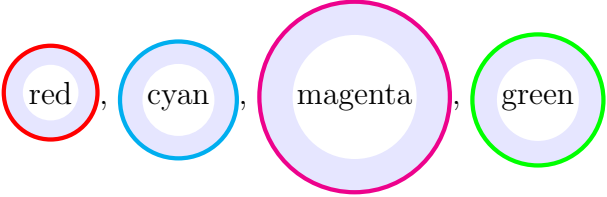
$$\begin{aligned} c(T(p, q)) &= \frac{1}{2}(Z_{(q-p)/2, p-1}^{110} + Z_{(q-p+2)/2, p-1}^{110}), \quad q > p, \\ &= \frac{1}{2}(Z_{(p-q)/2, q-1}^{110} + Z_{(p-q+2)/2, q-1}^{110}), \quad q < p. \end{aligned} \quad (3.18)$$

Perhaps strangely, when one inputs the winding numbers, the zilch that gives the corresponding result originates from a field with a different set of winding numbers. To demonstrate that these numbers are, indeed, appearing in the zilches, the following figures (3.6-3.7) give a visual representation of the results. Here, figure 3.6 for $Z_{p,q}^{110}$ has been reproduced for the sake of comparison. One will notice multiple colours and circles around the numbers. The colours and circles are split broadly into two categories for the crossing numbers, $c(Tp, q)$: coloured numbers, **red**, **orange**, **blue**,

refer to the crossing numbers that appear when $p+q = \text{odd}$; coloured circles, **blue**,

 , denote the pairs of $Z_{p,q}^{110}$ needed to obtain $c(Tp, q)$ for $p + q =$

even. Their specific colour shows the column in which they appear in $c(Tp, q)$, figure

3.7. Additional colours,  , are used in the

outlines of the circles to emphasise which pairs of numbers are used in $Z_{p,q}^{110}$. Finally, there are a number of circles that have no colour to them. These circles have been highlighted to show that they are results but, as the pairs of numbers producing them overlap with numbers from other columns, they have not been highlighted in figure 3.6 of $Z_{p,q}^{110}$. To help clarify this system, consider this example. For $p = 2, q = 5$:

$p + q = 7 = \text{odd}$ and $q > p$

$$\begin{aligned} c(T(2, 5)) &= Z_{(5-2+1)/2, 2-1}^{110} \\ &= Z_{2,1}^{110} \\ &= 5. \end{aligned} \tag{3.19}$$

Quite simply, checking the positions on both pages confirms this to be true, whilst showing the number highlighted in orange. Consider another example. For $p = 10, q = 12$:

$p + q = 22 = \text{even}$ and $q > p$

$$\begin{aligned} c(T(10, 12)) &= \frac{1}{2}(Z_{(12-10)/2, 10-1}^{110} + Z_{(12-10+2)/2, 10-1}^{110}) \\ &= \frac{1}{2}(Z_{1,9}^{110} + Z_{2,9}^{110}) \\ &= \frac{1}{2} \left(\textcircled{99} + \textcircled{117} \right) \\ &= \textcircled{108}. \end{aligned} \tag{3.20}$$

Repeated results are shown also for the swapping of p and q , as there is a line of symmetry (figure 3.7) through the values with $p = q$.

The unknotting number can also be written in terms of Z^{110} for $p, q > 2$ and $p \neq q$. The results for the unknotting number are, again, explained graphically in the following figures (3.6-3.8), using the same colour and circle referencing system, but with $p + q = \text{odd}$ and $p + q = \text{even}$ exchanged. Algebraically, for $p + q$ even,

$$\begin{aligned} u(T(p, q)) &= \frac{1}{2} Z_{(q-p)/2, p-1}^{110}, \quad q > p, \\ &= \frac{1}{2} Z_{(p-q)/2, q-1}^{110}, \quad q < p. \end{aligned} \tag{3.21}$$

While for $p + q$ odd,

$$\begin{aligned}
 u(T(p, q)) &= \frac{1}{4}(Z_{(q-p-1)/2, p-1}^{110} + Z_{(q-p+1)/2, p-1}^{110}), \quad q > p, \\
 &= \frac{1}{4}(Z_{(p-q-1)/2, q-1}^{110} + Z_{(p-q+1)/2, q-1}^{110}), \quad q < p.
 \end{aligned}
 \tag{3.22}$$

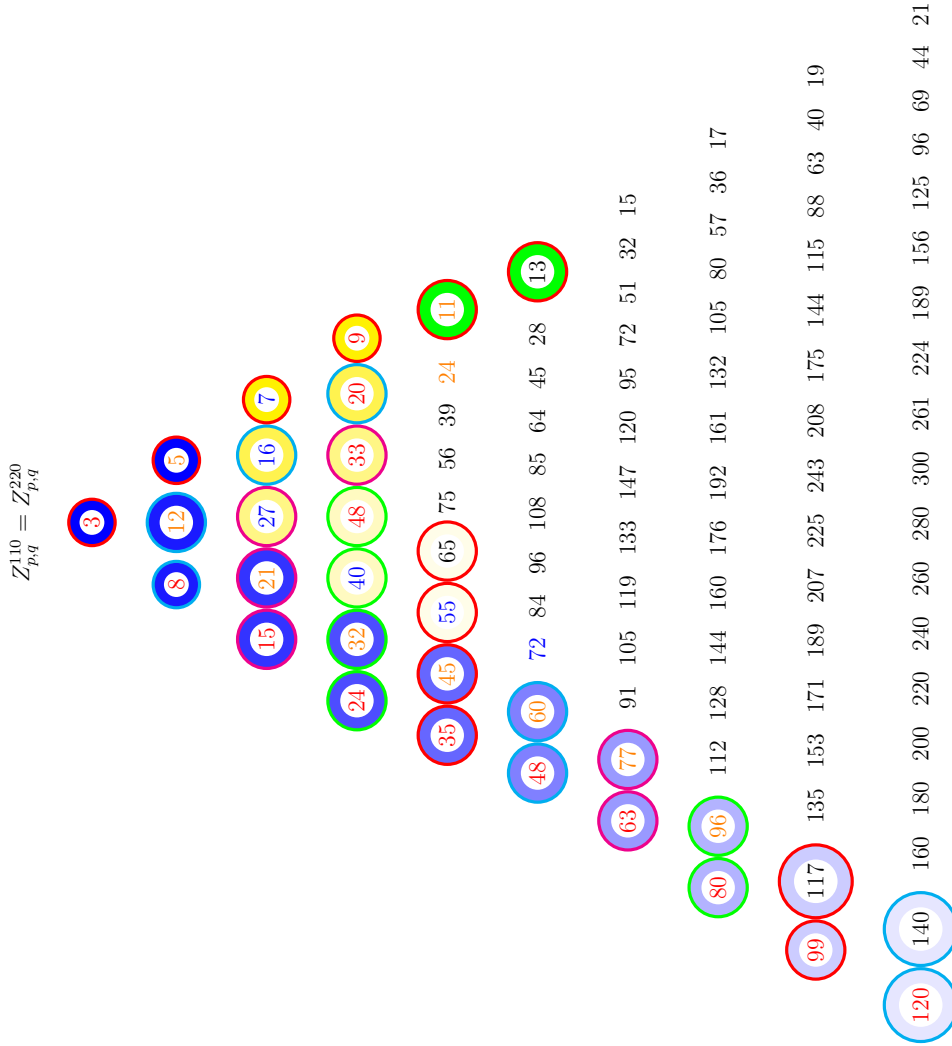


Figure 3.6: The results for Z^{110} with the components highlighted using the colour coding system described in the text body that are used for calculating the crossing and unknotting numbers for torus knots

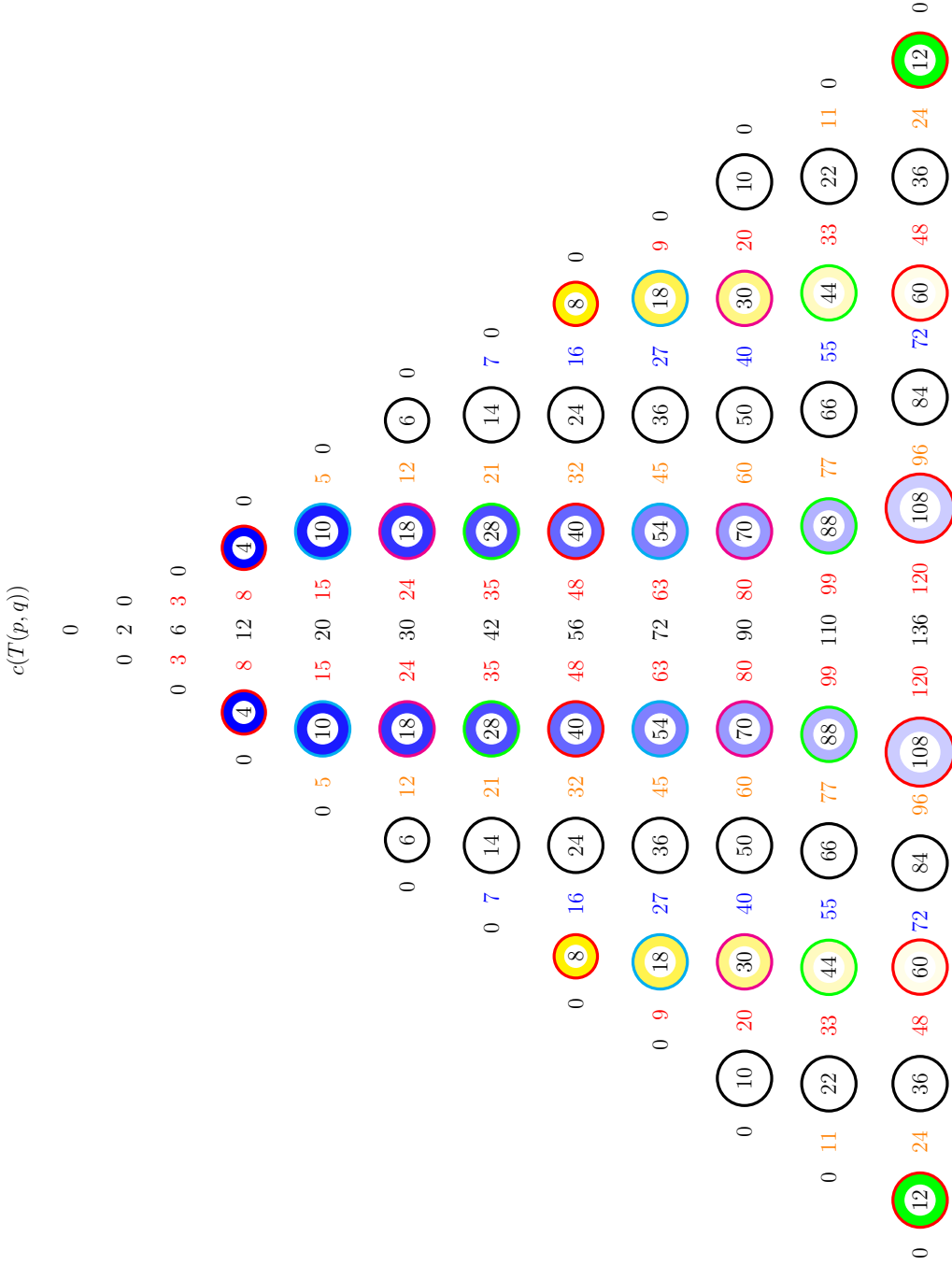


Figure 3.7: The results for $c(T(p, q))$ with the components highlighted using the colour coding system described in the text body that are used for calculating the crossing and unknotting numbers for torus knots

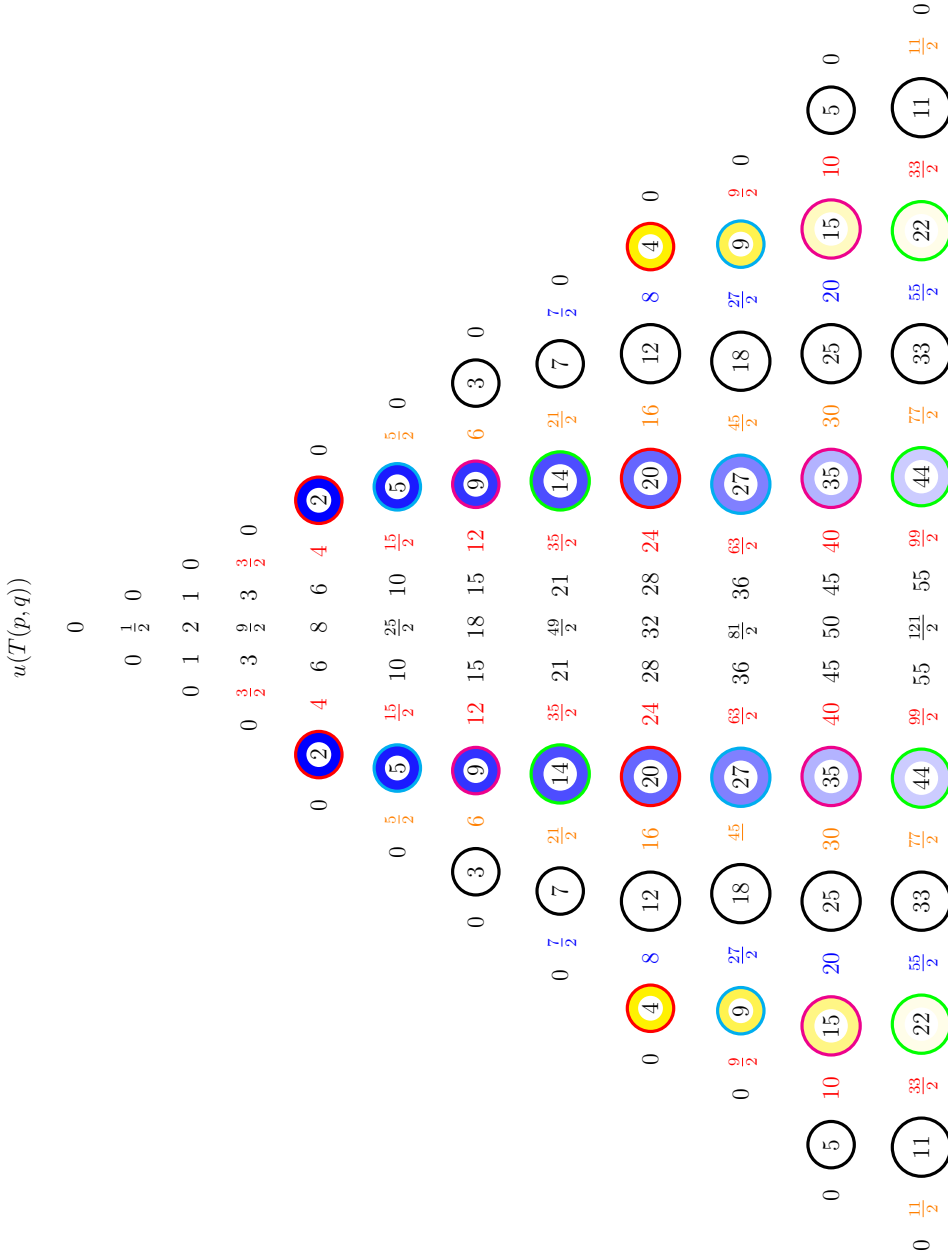


Figure 3.8: The results for $u(T(p, q))$ with the components highlighted using the colour coding system described in the text body that are used for calculating the crossing and unknotting numbers for torus knots

Finally, a supplementary surface property can be demonstrated in the zilches. If one considers a knotted surface, with $q = 1$, a helix will be observed. The number of turns of the helix within this surface can be extracted from the zilches via,

$$N_t(T(p, 1)) = \frac{1}{2}(Z_{p,1}^{110} - 3). \quad (3.23)$$

This section has shown that, in the arena of knotted electromagnetic fields, the zilches can be written in terms of the other conserved quantities, whose physicality is *known*. It has also demonstrated that there is an integral relationship between the zilches and the topology of the knotted fields that has not before been seen. This could explain the connection to the change in direction of the flow of zilch, when considering the different handed circularly polarised light.

The following sections will demonstrate that these properties are also true for other families of solutions to Maxwell's equations. It is essential to demonstrate that these results can be reproduced in other fields and, therefore, verify that zilches do, indeed, have an intrinsic topological connection - and that this is the case across multiple examples.

3.3 Zilches in Segmented Electromagnetic Fields

It is possible to generate new solutions to Maxwell's equations by taking known solutions and applying transformations. As long as the new equations adhere to the criteria given in equations 2.34, they will provide solutions to Maxwell's equations, via Bateman's construction. One possible transformation that can be conducted is called a *special conformal transformation* (SCT). A SCT, applied to the coordinates of the knotted solutions to Maxwell's equations, gives new expressions:

$$\alpha = \frac{2ik(z-ct)-1}{A+4ikt}, \quad \beta = \frac{2k(x-iy)}{A+4ikt}, \quad (3.24)$$

where, $A = 1 + 4k^2(x^2 + y^2z^2 - c^2t^2)$. Again, the functions $f(\alpha, \beta) = \alpha^p$ and $g(\alpha, \beta) = \beta^q$ are used to generate a whole family of solutions. As α and β satisfy equations 2.34, then so too do $f(\alpha, \beta)$ and $g(\alpha, \beta)$. These solutions give completely different scalar surfaces to those of the knotted solutions to Maxwell's equations (see figure 3.9). Again, the scalar fields are used to illuminate the underlying topology of the fields. Quite clearly, the common features are that there are specific numbers of pieces of closed surface appearing - some of which are twisting around each other. These examples, differ from the plane-wave solutions that are typically examined

when discussing zilches, in that the scalar surfaces are all closed. This could be the key to understanding *why* such results have remained obscured.

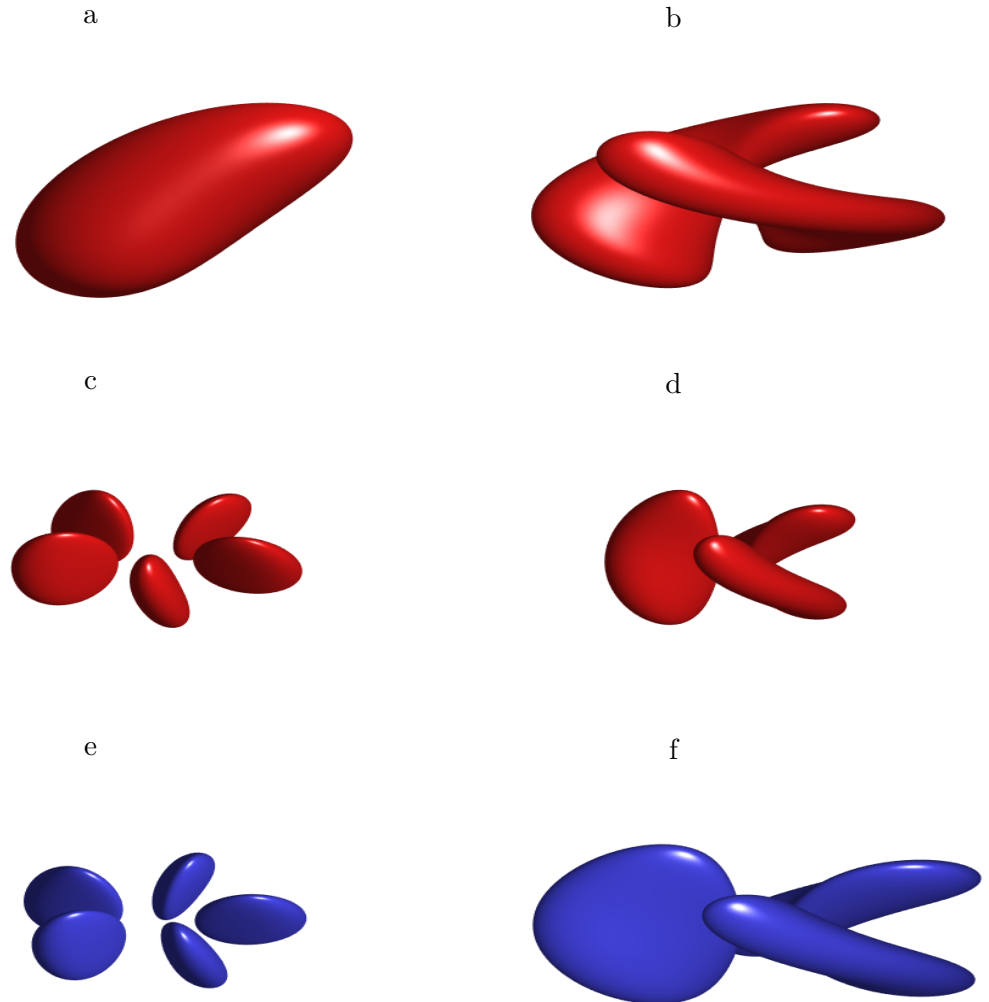


Figure 3.9: Segmented surfaces for: a. $(p, q) = (1, 1)$, $\phi_2 = 0.20$, giving one surface; b. $(p, q) = (4, 2)$, $\phi_2 = 0.005$, giving two surfaces; c. $(p, q) = (1, 5)$, $\phi_2 = 0.005$, giving five surfaces; d. $(p, q) = (3, 3)$, $\phi_2 = 0.005$, giving three surfaces; e. $(p, q) = (1, 5)$, $\phi_1 = 0.005$, giving five surfaces; f. $(p, q) = (3, 3)$, $\phi_1 = 0.005$, giving three surfaces

As with the knotted electromagnetic fields, the momentum and angular momentum are both in the z -direction. The number of pieces of surface can easily be counted and, in every case tested, is shown to be equal to q - where p appears to give a measure of to what extent the potential surfaces wrap around themselves. The relationship between the zilches and the field properties are straightforward. The units are the minimum necessary for the conserved quantities to take on integer values. To achieve this, all the values are calculated from the initial equations (3.24) and then divided by, $p q p! q! \pi^2 \epsilon_0 E_0^2 / 2^{2(p+q)-1} (p+q)!$ - with $c = k = 1$. Once in this form, the conserved quantities (including the zilches) can be calculated by inserting the electric and magnetic fields in the same way as in section 3.2.1. From these results, the following relations are obtained:

$$\begin{aligned}
 E_{p,q} &= \frac{Z_{p,q}^{000}}{((2p+2q+1)k)}, \\
 P_{p,q}^z &= \frac{Z_{p,q}^{030}}{((2p+2q+1)k)}, \\
 L_{p,q}^z &= \frac{Z_{p,q}^{110}}{((4p+2q)k^2)}, \\
 H_{p,q}^e = H_{p,q}^m &= -\frac{Z_{p,q}^{030}}{(2pk^3(2p+2q+1))} = \frac{Z_{p,q}^{000}}{(2k^3(2(p+q)^2+p+q))}.
 \end{aligned} \tag{3.25}$$

The number of pieces of surface, $N_{p,q}^s$, is quite simply related to the zilches and other conserved quantities, too.

$$N_{p,q}^s = \frac{2(p+q)^2 + p + q}{2p+q} \frac{Z_{p,q}^{110}}{Z_{p,q}^{000}} = -\frac{2p^2 + 2pq + p}{2p+q} \frac{Z_{p,q}^{110}}{Z_{p,q}^{030}} = -\frac{L_{p,q}^z}{k H_{p,q}^e}. \tag{3.26}$$

These relations can all be verified with a simple example. The results for the conserved quantities and number of pieces of surface of the $(p, q) = (2, 3)$ segmented field are shown in the table below.

(p, q)	$E_{p,q}$	$P_{p,q}^z$	$L_{p,q}^z$	$H_{p,q}^e$	$Z_{p,q}^{000}$	$Z_{p,q}^{030}$	$Z_{p,q}^{110}$	$Z_{p,q}^{330}$	$N_{p,q}^s$
$(2, 3)$	60	-24	-18	6	660	-264	252	156	3

Table 3.5: Conserved field properties and number of pieces of surface for the $(p, q) = (2, 3)$ segmented field

These results demonstrate, for another type of field, that the zilches can be related to the conserved properties of the field, and are related to the number of pieces of surface. Although these fields are different to the knotted fields, they have been created through a transformation of the original inputs. To show that the same results can be found outside of the knotted solutions and transformations, another distinct example will be issued.

3.4 Zilches in ‘Dripping’ Electromagnetic Fields

The final example is of a disparate family of fields that are solutions to Maxwell’s equations in a vacuum (see figure 3.10). These are now termed the ‘Dripping’ electromagnetic fields - named for their appearance and time evolution within the scalar fields. One can see, when propagating the fields with time, that each piece moves towards the lowest piece of surface and starts flattening out, like drops of water. The Dripping fields are given by the following forms for α and β ,

$$\alpha = \frac{1}{2} - \frac{i(-i + kct + ikx + ky - kz)}{2A + 2ikct}, \quad \beta = \frac{1}{2} - \frac{i(kct - i - kz)}{2A + 2ikct}, \quad (3.27)$$

where, $A = \frac{1}{2}(k^2 x^2 + k^2 y^2 + k^2 z^2 - k^2 c^2 t^2 + 1)$. Again, the functions $f(\alpha, \beta) = \alpha^p$ and $g(\alpha, \beta) = \beta^q$ are used. As α and β satisfy equations 2.34, so to do $f(\alpha, \beta)$ and $g(\alpha, \beta)$. The Dripping fields produce motion in the y -direction. The implications of this are that $P_{p,q}^y$, $L_{p,q}^y$ and $Z_{p,q}^{020}$ are non-zero, and $Z_{p,q}^{110} \neq Z_{p,q}^{220}$.

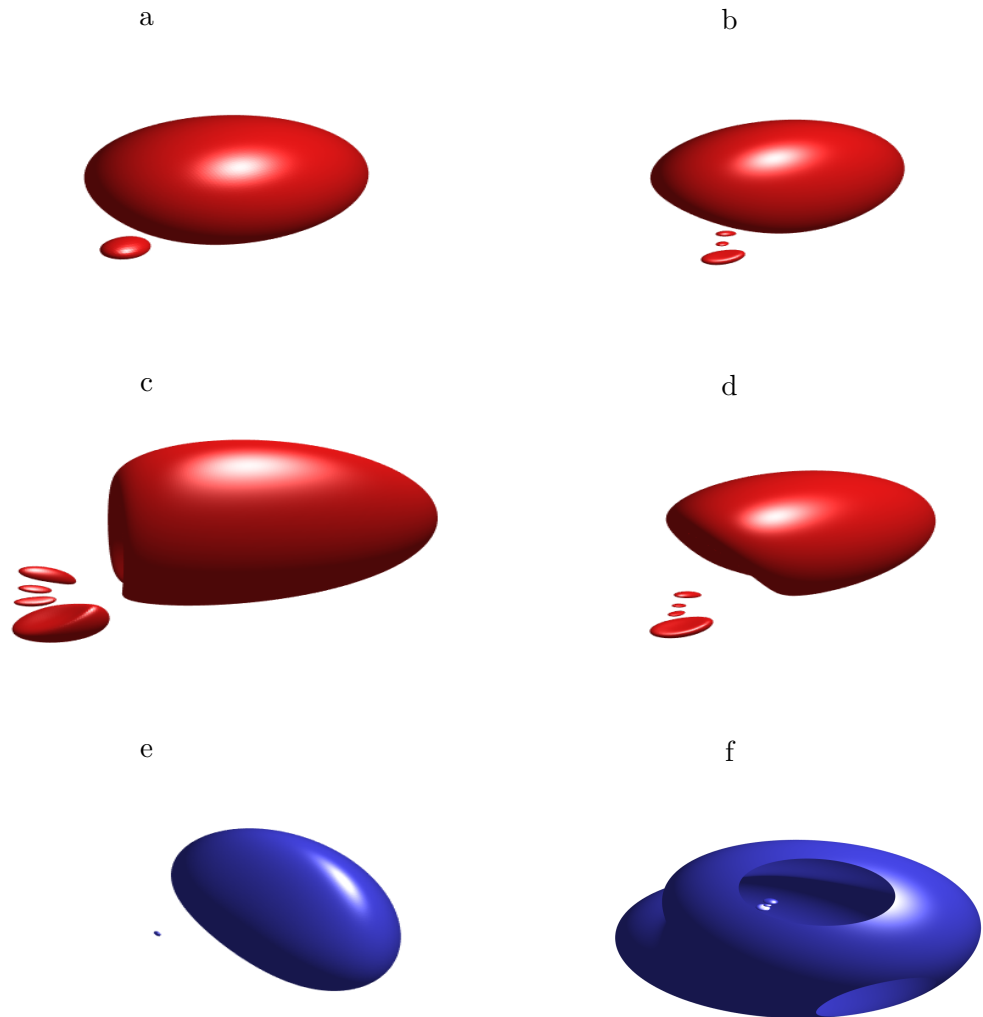


Figure 3.10: Dripping surfaces for: a. $(p, q) = (1, 1)$, $\phi_2 = 0.20$, giving two surfaces; b. $(p, q) = (1, 3)$, $\phi_2 = 0.05$, giving four surfaces; c. $(p, q) = (4, 1)$, $\phi_2 = 0.04$, giving five surfaces; d. $(p, q) = (2, 3)$, $\phi_2 = 0.03$, giving five surfaces; e. $(p, q) = (1, 1)$, $\phi_1 = 0.29$, giving two surfaces; f. $(p, q) = (1, 3)$, $\phi_1 = 0.05$, giving four surfaces (the plotting grid has been chosen here to cut holes in the outer surface so as to view the inner surfaces, in reality this surface is closed)

As with the last two sections of this chapter, the conserved quantities of the fields are calculated - but this time divided by $u = \frac{pq p! q! \pi^2 \epsilon_0 E_0^2 k^2}{2^{2(p+q)}(p+q)!}$ - to be put in a dimensionless set of units, where all values are integers. These conserved quantities of the fields can then be compared to the zilches. For example,

$$Z_{p,q}^{000} = -k(p+q) \left(\frac{3}{2} P_{p,q}^z + k L_{p,q}^y \right). \quad (3.28)$$

Also, the motion in the y -direction is encoded in the zilches,

$$P_{p,q}^y = -k L_{p,q}^y = \frac{2}{(3(p+q)+1)k} Z_{p,q}^{020}. \quad (3.29)$$

The number of pieces of surface can also be calculated via,

$$N_{p,q}^s = gcd(Z_{p,q}^{000}) = gcd \left(Z_{p,q}^{110} + Z_{p,q}^{220} + Z_{p,q}^{330} \right) \quad \forall p+q = \text{constant}. \quad (3.30)$$

Examples to demonstrate the number of pieces of surface for $p+q=5$ are shown in the subsequent table. To be clear, the $Z_{p,q}^{000}$ needs to be calculated for *all* combinations of $p+q = \text{constant}$. Then the gcd of the results is equal to the number of pieces of surface that appear in each of the fields for which $Z_{p,q}^{000}$ has been calculated.

(p, q)	(1, 4)	(2, 3)	(3, 2)	(4, 1)
$Z_{p,q}^{000}$	70	245	530	500

Table 3.6: Examples to demonstrate the number of pieces of surface for $p+q=5$

Considering the results, it is apparent that the $gcd = 5$, and that it is also the number of pieces of surface that appear in the Dripping fields. ²³

This section has established a further example of a family of electromagnetic fields the zilches of which, when put in units that make them integers, are related to the conserved properties and the topology of the fields. Again, the type of field being considered gives closed surfaces within the scalar field plots, making them different to the plane-wave solutions previously considered.

²³Two of the examples listed in the above table are also displayed in figure 3.10.

3.5 Summary

The aim of this chapter was to consider Lipkin's zilches within a previously unconsidered set of solutions to Maxwell's equations - to uncover anything new pertaining to them. Three sets of solutions were selected, ranging from the knotted solutions to Maxwell's equations, to the dripping field solutions.

The similarities between solutions studied were that they all produced converging values, when their densities were integrated over all space. They all gave closed surfaces, when considering their scalar field plots - for constant magnitude, $\phi_{1,2}$. The results produced can be positioned into two categories. Firstly, because analytic expressions for the components of the zilch have been produced, it has been demonstrated that they can be written entirely in terms of the known conserved quantities of the field: energy, momentum, angular momentum and helicity. Secondly, the zilches, quite clearly, contain information about the topology of the fields - the most evident being the number of pieces of closed surface. Even more specific properties of the fields' topology were determined for the knotted fields, in finding the crossing and unknotting numbers in terms of the $Z_{p,q}^{110}$. All these quantities can be determined from the number of theoretic properties of the zilches. There also appears to be an unquantified correlation between the zilches and the degree of chirality in the field. This chapter conjectures that the results shown will always be the case for this class of fields.

Exploration of electromagnetic fields, of which the field energy does not converge (such as plane-waves or constant fields), have not been found to give the same relationship between the components of the zilch and other properties of the field. The obvious difference between the aforementioned fields, and the ones produced in this chapter, is that, when plotting the scalar fields, the surfaces generated are neither finite, nor closed. This further supports the hypothesis of this chapter - that the components of the zilch describe the topology of the fields when their properties are convergent, and that the converse can be said when the field properties become divergent.

THE GENERALIZED, MULTIPOLAR EXPANSION OF KNOTTED ELECTROMAGNETIC FIELDS

In 2008, Irvine and Bouwmeester published an exciting paper, suggesting a possible route to the experimental verification of the Hopf-knotted solutions to Maxwell's equations [18]. They conducted a multipole expansion on the Vector Spherical Harmonics (VSH) of the knotted fields, using a method given in the book, *Classical Electrodynamics*, by Jackson [2]. Irvine and Bouwmeester utilised this expansion to ascertain the magnetic vector potential, in a form known as the Chandrasekar-Kendal eigenstates [59]. From this, they suggested a way of generating approximate knotted solutions, using condensed circularly polarised laser beams. In a following paper [15], Irvine went on to use this method to make a suggestion for an extension to all knot types for a particular case.²⁴

The aim of this chapter is to assess the published literature [18][15], working through the derivations of the methods in order to argue that they are not ideally suited for conducting a multipole expansion on the Hopf-knotted and torus-knotted solutions to Maxwell's equations. It will start by considering the first paper by Irvine and Bouwmeester - focussing on the Hopf-Knotted solutions, before then moving on to the second paper, by Irvine, which provides an extension to torus-knotted solutions - giving an equation that generalises to all knot-types [15]. The latter paper's extension will be produced and show differing results to those published. This chapter goes on to discuss a prescription for the multipole emerging coefficients, as well as the potential for patterns occurring between them. This will be followed by a new, more

²⁴This example is of a knotted non-null field with conserved magnetic helicity. Irvine suggests its construction is via the same method described in this chapter. Section 4.1.1 will contest this.

widely applicable and more accurate method for conducting a multipole expansion on the VSH for the Hopf-knotted and torus-knotted fields. The results will be compared with those from the body of work led by Irvine.

This chapter will conclude with an analysis of the patterns which emerge between the multipole coefficients. A set of 18 equations is demonstrated, that produces the first 3,680 multipole coefficients which appear for the first 49 different knot configurations - in terms of only the radius, r , the winding numbers, p and q , the dimensionless constant, k , and the angular momentum numbers, l and m .

4.1 Multipolar Expansion of the Vector Spherical Harmonics for the Hopf-Knotted Fields

This section is specifically concerned with Irvine and Bouwmeester's 2008 paper. It will dissect their method - reproducing critical parts of that method, discuss their assumptions and analyse their final results.²⁵ Scrutiny of this paper allows for a comparison with the fresh results presented in this thesis.

Chapter Two discussed how multipole expansions are usually used to determine the size of the fields generated by a set of charges, the shape of the field lines, and how quickly the magnitude falls off with distance from the origin. A multipole expansion could be conducted on any one of the fields that are present, but the most common, and obvious, is via the magnetic vector potential. This was one of the core aims of Irvine and Bouwmeester. As the solutions are comprised of complex vector fields, this could only be conducted through the VSH. In Jackson's book [2], there is a brief analysis for obtaining the multipole coefficient equations (This method is fully derived in the section 4.1.2.). Jackson derives the equations for the magnetic vector potential in terms of multipolar coefficients, with the assumption of an exponential time-dependence - as is common in plane wave solutions to Maxwell's equations. The equations he arrives at (for the magnetic vector potential - P746-747, eq:16.46 & 16.47) are also the starting point for the work by Irvine and Bouwmeester:

$$\mathbf{A}(\mathbf{r}, t) = \int dk \sum_{l=1}^{\infty} \sum_{m=-l}^l [\alpha_{lm}^{TM}(k) \mathbf{A}_{lm}^{TM}(k, \mathbf{r}) + \alpha_{lm}^{TE}(k) \mathbf{A}_{lm}^{TE}(k, \mathbf{r})] e^{-i\omega t} + c.c., \quad (4.1)$$

²⁵The method derived in this chapter focusses primarily on the multipole expansion given in the 'supplementary methods' section of Irvine and Bouwmeester's work.

4.1. MULTIPOLAR EXPANSION OF THE VECTOR SPHERICAL
HARMONICS FOR THE HOPF-KNOTTED FIELDS

where,

$$\mathbf{A}_{lm}^{TE}(k, \mathbf{r}) = \frac{1}{i\omega} f_l(kr) \mathbf{L}Y_{lm}(\theta, \phi), \quad (4.2)$$

$$\mathbf{A}_{lm}^{TM}(k, \mathbf{r}) = \frac{1}{k^2} \nabla \times [f_l(kr) \mathbf{L}Y_{lm}(\theta, \phi)], \quad (4.3)$$

are the contributions from the transverse electric (TE) and transverse magnetic (TM) parts of the field.²⁶ The operator,

$$\mathbf{L} = -i\mathbf{r} \times \nabla, \quad (4.4)$$

and in free-space the function,

$$f_l(kr) = \frac{j_l(kr)}{\sqrt{l(l+1)}}, \quad (4.5)$$

with the spherical Bessel functions, $j_l(kr)$, taking on their usual form. The spherical harmonics:

$$Y_{lm}(\theta, \phi) = \sqrt{\frac{1+2l}{2\pi}} \sqrt{\frac{(l-m)!}{(l+m)!}} L_l^m(\cos(\theta)) e^{im\phi}, \quad (4.6)$$

where L_l^m are the usual associated Legendre polynomials. Finally, the multipolar coefficients are given by:

$$\alpha_{lm}^{TE}(k) j_l(kr) = \frac{k}{\sqrt{l(l+1)}} \int d\Omega Y_{lm}^* \mathbf{B} \cdot \mathbf{r}, \quad (4.7)$$

$$\alpha_{lm}^{TM}(k) j_l(kr) = -\frac{k}{\sqrt{l(l+1)}} \int d\Omega Y_{lm}^* \mathbf{E} \cdot \mathbf{r}, \quad (4.8)$$

where $j_l(kr)$ are, again, the spherical Bessel functions, and l and m are the angular momentum numbers. The multipole coefficients are the equations that will determine the type of fields investigated - demonstrating whether they are completely pure fields (such as a dipole or quadrupole field), or comprised of combinations of fields (as only certain angular momentum numbers give finite values for the coefficients). Their solution makes them the most important to understanding how the Hopf-knotted electromagnetic fields fall off with distance. The key limit of Irvine and Bouwmeester's method is the inclusion of an exponential time dependency, whilst simultaneously excluding it by putting it to unity through $t = 0$. In the equations, initially employed by Jackson to derive equation 4.7 and 4.8, the same occurs. This is not compatible with

²⁶Transverse magnetic refers to those components that are perpendicular to the radius vector of the magnetic multipole - in other words, the electric field. Transverse electric (TE) refers to those components that are perpendicular to the radius vector of the electric multipole - in other words, the magnetic field - which is explained in more detail in section 4.1.2

the Hopf-knotted and torus-knotted fields: firstly, the knotted fields do not have any exponential time dependency and, therefore, it seems inappropriate to include it to fit a method; secondly, without an exponential time dependency, the *final* equations for the multipole coefficients (4.7 and 4.8) cannot be obtained.²⁷ In order to demonstrate the limitations of Irvine and Bouwmeester's work, this chapter will, now, fully derive their method and that of Jackson [2].

4.1.1 Irvine and Bouwmeester's Multipole Expansion Method

The following method will start with field components that are slightly different to those given by Irvine and Bouwmeester, due to the use of differing units and derivation methods - as outlined in Chapter Two.²⁸ For the units to make sense, x , y , and z are scaled with a constant of which the units are inverse distance, set to 1 - to make them dimensionless. \mathbf{k} is already dimensionless, and E_0 is set to unity and has units of electric field - in accordance with equations 2.74.

$$\mathbf{B}(\mathbf{r}, t = 0) = \frac{4}{(r^2 + 1)^3} (2(xy - z), 1 - x^2 + y^2 - z^2, 2(yz + x)), \quad (4.9)$$

$$\mathbf{E}(\mathbf{r}, t = 0) = -\frac{4}{(r^2 + 1)^3} (1 + x^2 - y^2 - z^2, 2(xy + z), 2(xz - y)). \quad (4.10)$$

From here, Irvine and Bouwmeester applied a Fourier transform, followed by an inverse Fourier transform to the fields.²⁹ The Fourier inversion method was employed purely to obtain the final forms of the multipolar coefficients in terms of spherical Bessel functions. These cancel with those that they are multiplied on the left-hand-side of equation 4.7 and 4.8, to give a more concise presentation.

The TM multipole coefficient, $\alpha_{lm}^{TM}(k)$ will be considered first. This will involve applying the Fourier transform to the electric field. Using the x -component of the electric field and applying the transform:

$$\tilde{\mathbf{E}}_x(k) = -\int \frac{4}{(r^2 + 1)^3} (1 + x^2 - y^2 - z^2) e^{-i\mathbf{k}\cdot\mathbf{x}} d\mathbf{x}. \quad (4.11)$$

²⁷See section 4.1.2 for an explicit derivation.

²⁸Despite different input equations, the results are shown to be the same within this section.

²⁹For the remainder of the thesis, a Fourier transform followed by an inverse Fourier transform will be referred to as a Fourier inversion.

4.1. MULTIPOLAR EXPANSION OF THE VECTOR SPHERICAL
HARMONICS FOR THE HOPF-KNOTTED FIELDS

The integral can be made simpler if one considers the form that the second derivative of the exponential would take, with respect to k_x :

$$\frac{\partial^2(e^{-i\mathbf{k}\cdot\mathbf{x}})}{\partial k_x^2} = -x^2 e^{-i\mathbf{k}\cdot\mathbf{x}}. \quad (4.12)$$

The above can be rearranged and substituted into equation 4.11. The same method can be applied for both the $-y^2$ and $-z^2$ parts of the x -component of the electric field. This means that the Fourier transform becomes:

$$\tilde{\mathbf{E}}(k)_x = - \left(1 - \frac{\partial^2}{\partial k_x^2} + \frac{\partial^2}{\partial k_y^2} + \frac{\partial^2}{\partial k_z^2} \right) \int \frac{e^{-i\mathbf{k}\cdot\mathbf{x}}}{\pi(r^2 + 1)^3} d\mathbf{x}. \quad (4.13)$$

This integral has a solution [18],

$$\int \frac{e^{\pm i\mathbf{k}\cdot\mathbf{x}}}{(a^2 + r^2 - d)^{n+1}} d^3x = \frac{\partial^n}{\partial d^n} \left(\frac{2\pi^2}{n!k} e^{-k(a^2-d)^{\frac{1}{2}}} \right) \Big|_{d=0}. \quad (4.14)$$

After inserting the appropriate variables, then applying the chain rule and quotient rule, the solution becomes,

$$\begin{aligned} \frac{1}{\pi} \int \frac{e^{-i\mathbf{k}\cdot\mathbf{x}}}{(r^2 + 1)^3} d^3x &= \frac{\pi}{k} \frac{\partial^2}{\partial d^2} \left(e^{-k(1-d)^{\frac{1}{2}}} \right) \Big|_{d=0} \\ &= \frac{\pi e^{-k}}{4} (k + 1). \end{aligned} \quad (4.15)$$

Substituting this back into the Fourier transform,

$$\tilde{\mathbf{E}}_x(k) = - \left(1 - \frac{\partial^2}{\partial k_x^2} + \frac{\partial^2}{\partial k_y^2} + \frac{\partial^2}{\partial k_z^2} \right) \frac{\pi e^{-k}}{4} (k + 1). \quad (4.16)$$

Calculating the second derivatives and solving gives the final form for the Fourier transform,

$$\tilde{\mathbf{E}}_x(k) = -\frac{\pi e^{-k}}{2k} (k_y^2 + k_z^2). \quad (4.17)$$

This method can be repeated for the remaining components of the electric field, as well as the components of the magnetic field within the TE multipole coefficient, $\alpha_{lm}^{TE}(k)$, to give,

$$\begin{aligned} \tilde{\mathbf{E}}(k) &= -\frac{\pi e^{-k}}{2k} (k_y^2 + k_z^2, ikk_z - k_x k_y, ikk_y - k_x k_z), \\ \tilde{\mathbf{B}}(k) &= \frac{\pi e^{-k}}{2k} (ikk_z - k_x k_y, k_x^2 + k_z^2, ikk_x - k_y k_z). \end{aligned} \quad (4.18)$$

It is at this point that Irvine and Bouwmeester apply the inverse Fourier transform to obtain a unique form for the fields. Again, continuing with the electric field,

4.1. MULTIPOLAR EXPANSION OF THE VECTOR SPHERICAL
HARMONICS FOR THE HOPF-KNOTTED FIELDS

eventually focussing on the x -component. The inverse Fourier transform takes the form,

$$\mathbf{E}(\mathbf{r}) = \int \tilde{\mathbf{E}}(k) e^{i\mathbf{k}\cdot\mathbf{x}} d^3k, \quad (4.19)$$

therefore becoming,

$$\mathbf{E}(\mathbf{r}) = - \int \frac{\pi e^{-k}}{2k} (k_y^2 + k_z^2, ikk_z - k_x k_y, ikk_y - k_x k_z) e^{i\mathbf{k}\cdot\mathbf{x}} d^3k. \quad (4.20)$$

Focussing now on the x -component by itself,

$$\mathbf{E}_x(\mathbf{r}) = - \int \frac{\pi e^{-k}}{2k} (k_y^2 + k_z^2) e^{i\mathbf{k}\cdot\mathbf{x}} dk_x. \quad (4.21)$$

As with the Fourier transform, the integral can be simplified by considering derivatives of the exponential component - but this time, with respect to y first. The second derivative is given by,

$$\frac{\partial^2 (e^{i\mathbf{k}\cdot\mathbf{x}})}{\partial y^2} = -k_y^2 e^{i\mathbf{k}\cdot\mathbf{x}}. \quad (4.22)$$

Which can be rearranged and substituted, along with the z -derivative, into equation 4.21 to give,

$$\mathbf{E}_x(\mathbf{r}) = - \int \frac{\pi e^{-k}}{2k} \left(-\frac{\partial^2}{\partial y^2} - \frac{\partial^2}{\partial z^2} \right) e^{i\mathbf{k}\cdot\mathbf{x}} dk_x. \quad (4.23)$$

There is, now, another integral solution that can be used [18],

$$\int f(k) e^{\pm i\mathbf{k}\cdot\mathbf{x}} d^3k = \frac{4\pi}{r} \int f(k) k \sin(kr) dk. \quad (4.24)$$

The field now becomes,

$$\mathbf{E}_x(\mathbf{r}) = -2\pi^2 \int e^{-k} \left(-\frac{\partial^2}{\partial y^2} - \frac{\partial^2}{\partial z^2} \right) \frac{\sin(kr)}{r} dk. \quad (4.25)$$

The above corroborates the results of Irvine and Bouwmeester, other than a factor of two. This process can easily be repeated for the x and y components of the electric field and gives the form,

$$\mathbf{E}(\mathbf{r}) = -2\pi^2 \int e^{-k} \left(-\frac{\partial^2}{\partial y^2} - \frac{\partial^2}{\partial z^2}, \frac{\partial}{\partial x} \frac{\partial}{\partial y} + k \frac{\partial}{\partial z}, \frac{\partial}{\partial x} \frac{\partial}{\partial z} - k \frac{\partial}{\partial y} \right) \frac{\sin(kr)}{r} dk. \quad (4.26)$$

Now the Fourier inversion is complete, it is important to check that this equation produces the original Hopf-knotted fields, by solving the differentials in their Cartesian coordinates. This has been checked using the program, *Maple*. The equation returns

4.1. MULTIPOLAR EXPANSION OF THE VECTOR SPHERICAL
HARMONICS FOR THE HOPF-KNOTTED FIELDS

the same form in each spatial direction as given by equation 4.10 when evaluated at $k = 0$, but with a factor of $(-2\pi^2)$. As this amounts to a scaling factor, and is constant, one can ignore it. The next step is to solve the differentials, before substituting into equation 4.8. Before the substitution takes place, the electric field is multiplied with the radius vector, \mathbf{r} , to form the dot product, and then converted into spherical polar coordinates. This gives,

$$\mathbf{E} \cdot \mathbf{r} = \frac{2e^{-k}}{r^2} (\sin(kr) - kr \cos(kr)) \sin(\theta) \cos(\phi). \quad (4.27)$$

This can now be substituted into equation 4.8,

$$\alpha_{lm}^{TM}(k) j_l(kr) = -\frac{2e^{-k} k^3 \sqrt{\pi}}{\sqrt{l(l+1)}} \left(\frac{\sin(kr)}{k^2 r^2} - \frac{\cos(kr)}{kr} \right) \int d\Omega Y_{lm}^* \sin(\theta) \cos(\phi). \quad (4.28)$$

The part of this equation in the larger set of brackets looks very similar to that of the spherical Bessel function with angular momentum number $l = 1$. If one solves this equation for a number of integers for l , one will see which angular momentum numbers may or may not contribute - and therefore which multipole coefficients are non-zero. Once the integral is solved for each value of l , only one solution appears. It correspondingly has its own spherical Bessel function which cancels out with that on the left-hand-side of the equation. Therefore, this leaves only one, elegant solution - with angular momentum numbers $l = m = 1$,

$$\alpha_{1,1}^{TM} = \sqrt{\frac{4\pi}{3}} k^3 e^{-k}. \quad (4.29)$$

The principle reason to use the Fourier inversion method is *because* these spherical Bessel functions appear and then cancel out at the specific integers of l . The result demonstrates that the field is that of a *pure dipole*, due to the contributions only coming from $l = 1$. This process can be repeated for the TE multipole coefficient as well - again, finding results with angular momentum numbers $l = m = 1$,

$$\alpha_{1,1}^{TE} = -i \sqrt{\frac{4\pi}{3}} k^3 e^{-k}. \quad (4.30)$$

Finally, this gives the equation for the magnetic vector potential as,

$$\mathbf{A}(\mathbf{r}, t) = \sqrt{\frac{4\pi}{3}} \int dk k^3 e^{-k} [\mathbf{A}_{1,1}^{TM}(k, \mathbf{r}) - i \mathbf{A}_{1,1}^{TE}(k, \mathbf{r})] e^{-i\omega t} + c.c. \quad (4.31)$$

This corroborates the work of Irvine and Bouwmeester. However, the final equation is questionable because they made the assumption that $t = 0$. So for all time outside of this value the equation is invalid, therefore the equation should be,

$$\mathbf{A}(\mathbf{r}, t = 0) = \sqrt{\frac{4\pi}{3}} \int dk k^3 e^{-k} [\mathbf{A}_{1,1}^{TM}(k, \mathbf{r}) - i \mathbf{A}_{1,1}^{TE}(k, \mathbf{r})] + c.c. \quad (4.32)$$

This detracts from its use within their paper - as this exponential time dependency appears essential to forming the circularly polarised light beams. It can, therefore, be suggested that this approach is not suitable as a *complete* method for a multipole expansion on the Hopf-fields and, by extension, nor the experimental realisation. This chapter will move on to demonstrate a more general method that is correct for all knot types.³⁰

4.1.2 The Derivation of Jackson's Multipole Expansion Coefficients

To demonstrate that the method employed by, and the assumptions made by, Irvine and Bouwmeester [18] are not suitable, a derivation of the multipole coefficient equations, given by Jackson [2], must be shown. Jackson starts with the free-field Maxwell's equations,

$$\nabla \times \mathbf{E} = -\frac{\partial \mathbf{B}}{\partial t}, \quad \nabla \cdot \mathbf{E} = 0, \quad (4.33)$$

$$\nabla \times \mathbf{B} = \frac{1}{c^2} \frac{\partial \mathbf{E}}{\partial t}, \quad \nabla \cdot \mathbf{B} = 0.$$

At this point, Jackson assumes a time dependence of $e^{-i\omega t}$ for the electric and magnetic fields. One can assume this is because of the commonality of its inclusion in everyday problems. These equations become,

$$\nabla \times \mathbf{E} = i\omega \mathbf{B}, \quad \nabla \cdot \mathbf{E} = 0, \quad (4.34)$$

$$\nabla \times \mathbf{B} = \frac{-i\omega}{c^2} \mathbf{E}, \quad \nabla \cdot \mathbf{B} = 0.$$

As previously mentioned, this is the point within Jackson's derivation where this method becomes incompatible with the Hopf-knotted and torus-knotted fields. Neither of these sets of fields contain an exponential time dependence and, therefore, could not be reproduced using this set of Maxwell's equations. Also, without the exponential time dependency one cannot obtain Maxwell's equations in the form above. But the derivation will be continued, to display that there are no deviations that can rectify this. If one takes the curl of two of these equations, one obtains,

$$\nabla \times \nabla \times \mathbf{E} = i\omega \nabla \times \mathbf{B} = i\omega \frac{-i\omega}{c^2} \mathbf{E} = k^2 \mathbf{E}, \quad (4.35)$$

as $k = \omega/c$ - the wave number. The standard vector relations [36] give,

$$\nabla \times \nabla \times \mathbf{E} = \nabla(\nabla \cdot \mathbf{E}) - \nabla^2 \mathbf{E} = -\nabla^2 \mathbf{E}. \quad (4.36)$$

³⁰See section 4.2.

4.1. MULTIPOLAR EXPANSION OF THE VECTOR SPHERICAL
HARMONICS FOR THE HOPF-KNOTTED FIELDS

Thus,

$$\begin{aligned} -\nabla^2 \mathbf{E} &= k^2 \mathbf{E} \\ (\nabla^2 + k^2) \mathbf{E} &= 0. \end{aligned} \quad (4.37)$$

Following the same method for the other Maxwell equation,

$$(\nabla^2 + k^2) \mathbf{B} = 0. \quad (4.38)$$

These last two equations are the Helmholtz equation for each field [2]. The next step is to find the general solution to these equations for a scalar function ψ . In spherical polar coordinates,

$$\nabla^2 = \frac{1}{r^2} \frac{\partial}{\partial r} \left(r^2 \frac{\partial}{\partial r} \right) + \frac{1}{r^2 \sin(\theta)} \frac{\partial}{\partial \theta} \left(\sin(\theta) \frac{\partial}{\partial \theta} \right) + \frac{1}{r^2 \sin^2(\theta)} \frac{\partial^2}{\partial \phi^2}. \quad (4.39)$$

Inserting this into equations 4.37 and 4.38 and multiplying through by r^2 gives,

$$\frac{\partial}{\partial r} \left(r^2 \frac{\partial \psi}{\partial r} \right) + \frac{1}{\sin(\theta)} \frac{\partial}{\partial \theta} \left(\sin(\theta) \frac{\partial \psi}{\partial \theta} \right) + \frac{1}{\sin^2(\theta)} \frac{\partial^2 \psi}{\partial \phi^2} + r^2 k^2 \psi = 0. \quad (4.40)$$

Next, using separation of variables one can write,

$$\psi(r, \theta, \phi) = R(r) Y_l^m(\theta, \phi), \quad (4.41)$$

$$\frac{\partial}{\partial r} \left(r^2 \frac{\partial R(r) Y_l^m(\theta, \phi)}{\partial r} \right) + \frac{1}{\sin(\theta)} \frac{\partial}{\partial \theta} \left(\sin(\theta) \frac{\partial R(r) Y_l^m(\theta, \phi)}{\partial \theta} \right) + \frac{1}{\sin^2(\theta)} \frac{\partial^2 R(r) Y_l^m(\theta, \phi)}{\partial \phi^2} + r^2 k^2 R(r) Y_l^m(\theta, \phi) = 0. \quad (4.42)$$

Dividing through by $R(r) Y_l^m(\theta, \phi)$ and rearranging gives,

$$\frac{1}{R(r)} \frac{\partial}{\partial r} \left(r^2 \frac{\partial R(r)}{\partial r} \right) + r^2 k^2 = -\frac{1}{Y_l^m(\theta, \phi)} \frac{1}{\sin(\theta)} \frac{\partial}{\partial \theta} \left(\sin(\theta) \frac{\partial Y_l^m(\theta, \phi)}{\partial \theta} \right) - \frac{1}{Y_l^m(\theta, \phi)} \frac{1}{\sin^2(\theta)} \frac{\partial^2 Y_l^m(\theta, \phi)}{\partial \phi^2} = \text{Constant}. \quad (4.43)$$

Considering the angular part first, and letting the constant equal $l(l+1)$.

$$-\left[\frac{1}{\sin(\theta)} \frac{\partial}{\partial \theta} \left(\sin(\theta) \frac{\partial}{\partial \theta} \right) + \frac{1}{\sin^2(\theta)} \frac{\partial^2}{\partial \phi^2} \right] Y_l^m(\theta, \phi) = l(l+1) Y_l^m(\theta, \phi). \quad (4.44)$$

This is the differential equation that defines the spherical harmonics. Now, looking at the radial part.

$$\frac{\partial}{\partial r} \left(r^2 \frac{\partial R(r)}{\partial r} \right) + r^2 k^2 R(r) = l(l+1) R(r). \quad (4.45)$$

Using the product rule,

$$r^2 \frac{\partial^2 R(r)}{\partial r^2} + 2r \frac{\partial R(r)}{\partial r} + (r^2 k^2 - l(l+1)) R(r) = 0. \quad (4.46)$$

4.1. MULTIPOLAR EXPANSION OF THE VECTOR SPHERICAL
HARMONICS FOR THE HOPF-KNOTTED FIELDS

Let $z = kr$ and, therefore, $r^2 = \frac{z^2}{k^2}$, $\frac{\partial R}{\partial r} = k \frac{\partial R}{\partial z}$, and $\frac{\partial^2 R}{\partial r^2} = k^2 \frac{\partial^2 R}{\partial z^2}$. Substituting these into equation 4.46 gives,

$$z^2 \frac{\partial^2 R(r)}{\partial z^2} + 2z \frac{\partial R(r)}{\partial z} + (z^2 - l(l+1)) R(r) = 0. \quad (4.47)$$

This is equation 10.1.1 from textbook, *Handbook of Mathematical Functions With Formulas, Graphs, and Mathematical Tables* [60]. The standard solutions to this equation are spherical Bessel functions, but here using the Hankel function form,

$$R_l(z) = R_l(kr) = A_{l,m}^{(1)}(kr) h_l^{(1)}(kr) + A_{l,m}^{(2)}(kr) h_l^{(2)}(kr). \quad (4.48)$$

The solution to the Helmholtz equation for a particular l, m , is,

$$\psi(r, \theta, \phi) = [A_{l,m}^{(1)}(kr) h_l^{(1)}(kr) + A_{l,m}^{(2)}(kr) h_l^{(2)}(kr)] Y_l^m(\theta, \phi) \quad (4.49)$$

and the general solution is,

$$\psi(r, \theta, \phi) = \sum_{l=0}^{\infty} \sum_{m=-l}^l [A_{l,m}^{(1)}(kr) h_l^{(1)}(kr) + A_{l,m}^{(2)}(kr) h_l^{(2)}(kr)] Y_l^m(\theta, \phi). \quad (4.50)$$

The coefficients $A_{l,m}^{(1)}$ and $A_{l,m}^{(2)}$ are defined by the boundary conditions. From equation 4.37, one can write,

$$\mathbf{r} \cdot \nabla^2 \mathbf{E} + k^2 \mathbf{r} \cdot \mathbf{E} = 0. \quad (4.51)$$

Using the vector identity,

$$\nabla^2(\mathbf{r} \cdot \mathbf{A}) = \mathbf{r}(\nabla^2 A) + 2 \nabla \cdot \mathbf{A}, \quad (4.52)$$

for any vector field \mathbf{A} , let $\mathbf{A} = \mathbf{E}$:

$$\nabla^2(\mathbf{r} \cdot \mathbf{E}) = \mathbf{r}(\nabla^2 E) + 2 \nabla \cdot \mathbf{E} = \mathbf{r} \nabla^2 E. \quad (4.53)$$

Putting equation 4.53 into 4.51

$$\nabla^2(\mathbf{r} \cdot \mathbf{E}) + k^2 \mathbf{r} \cdot \mathbf{E} = (\nabla^2 + k^2) \mathbf{r} \cdot \mathbf{E} = 0. \quad (4.54)$$

$\mathbf{r} \cdot \mathbf{E}$ and $\mathbf{r} \cdot \mathbf{B}$, therefore both satisfy Helmholtz wave equations [2],

$$(\nabla^2 + k^2) \mathbf{r} \cdot \mathbf{E} = 0, \quad (4.55)$$

$$(\nabla^2 + k^2) \mathbf{r} \cdot \mathbf{B} = 0.$$

4.1. MULTIPOLAR EXPANSION OF THE VECTOR SPHERICAL
HARMONICS FOR THE HOPF-KNOTTED FIELDS

Knowing the solutions to these equations are given by equation 4.49, one can, therefore, define a magnetic multipole field of order l, m , as,

$$\mathbf{r} \cdot \mathbf{B}_{l,m} = \frac{l(l+1)}{k} \left[A_{l,m}^{(1)}(kr) h_l^{(1)}(kr) + A_{l,m}^{(2)}(kr) h_l^{(2)}(kr) \right] Y_l^m(\theta, \phi), \quad (4.56)$$

$$\mathbf{r} \cdot \mathbf{E}_{l,m} = 0.$$

The factor $\frac{l(l+1)}{k}$ is currently arbitrary, but can be addressed by the coefficients $A_{l,m}^{(1)}$ and $A_{l,m}^{(2)}$. It is taken out for convenience when later simplifying. Using equation 4.34,

$$\mathbf{r} \cdot \mathbf{B}_{l,m} = \frac{1}{i\omega} \mathbf{r} \cdot \nabla \times \mathbf{E} = \frac{1}{i\omega} (\mathbf{r} \times \nabla) \cdot \mathbf{E} = \frac{1}{\omega} \mathbf{L} \cdot \mathbf{E}. \quad (4.57)$$

Putting this back into equation 4.56,

$$\mathbf{L} \cdot \mathbf{E}_{l,m} = \frac{l(l+1)\omega}{k} \left[A_{l,m}^{(1)}(kr) h_l^{(1)}(kr) + A_{l,m}^{(2)}(kr) h_l^{(2)}(kr) \right] Y_l^m(\theta, \phi), \quad (4.58)$$

$$\mathbf{r} \cdot \mathbf{E}_{l,m} = 0.$$

The L operator does not act on the radial parts of the field, giving,

$$\mathbf{E}_{l,m} = \frac{\omega}{k} \left[A_{l,m}^{(1)}(kr) h_l^{(1)}(kr) + A_{l,m}^{(2)}(kr) h_l^{(2)}(kr) \right] \mathbf{L} Y_l^m(\theta, \phi), \quad (4.59)$$

because,

$$\mathbf{L}^2 Y_l^m(\theta, \phi) = l(l+1) Y_l^m(\theta, \phi). \quad (4.60)$$

The expressions for the electromagnetic fields of the magnetic multipole are,

$$\mathbf{E}_{l,m}^{(TE)} = \frac{\omega}{k} \left[A_{l,m}^{(1)}(kr) h_l^{(1)}(kr) + A_{l,m}^{(2)}(kr) h_l^{(2)}(kr) \right] \mathbf{L} Y_l^m(\theta, \phi), \quad (4.61)$$

$$\mathbf{B}_{l,m}^{(TE)} = -\frac{i}{\omega} \nabla \times \mathbf{E}_{l,m}.$$

Because the electric field, E , is transverse to the radius vector, these are called TE, rather than magnetic. The electric multipole fields can be derived similarly and for the same transverse properties to the radius vector are TM, giving:

$$\mathbf{B}_{l,m}^{(TM)} = f_l(kr) \mathbf{L} Y_l^m(\theta, \phi), \quad (4.62)$$

$$\mathbf{E}_{l,m}^{(TM)} = \frac{i\omega}{k} \nabla \times \mathbf{B}_{l,m}^{(E)}.$$

4.1. MULTIPOLAR EXPANSION OF THE VECTOR SPHERICAL
HARMONICS FOR THE HOPF-KNOTTED FIELDS

From these definitions one arrives at the vector spherical harmonics,

$$X_{l,m}(\theta, \phi) = \frac{1}{\sqrt{l(l+1)}} \mathbf{L} Y_{l,m}(\theta, \phi), \quad (4.63)$$

which have the orthogonality properties,

$$\begin{aligned} \int X_{l',m'}^* \cdot X_{l,m} d\Omega &= \delta_{l,l'} \delta_{m,m'} \\ \int X_{l',m'}^* \cdot (\mathbf{r} \times X_{l,m}) d\Omega &= 0, \end{aligned} \quad (4.64)$$

and $f_l(kr)$ is similar to the term in brackets in equation 4.61,

$$g_l(kr) = A_{l,m}^{(1)}(kr) h_l^{(1)}(kr) + A_{l,m}^{(2)}(kr) h_l^{(2)}(kr), \quad (4.65)$$

$$f_l(kr) = B_{l,m}^{(1)}(kr) h_l^{(1)}(kr) + B_{l,m}^{(2)}(kr) h_l^{(2)}(kr).$$

If one combines \mathbf{B} in both equation 4.61 and 4.62, and the same for \mathbf{E} ,

$$\begin{aligned} \mathbf{B} &= \sum_{l,m} \left(\mathbf{B}_{l,m}^{(TM)} + \mathbf{B}_{l,m}^{(TE)} \right) \\ &= \sum_{l,m} \left(\alpha_{l,m}^{TM}(k) f_l(kr) X_{l,m} - \frac{i}{\omega} \alpha_{l,m}^{TE}(k) \nabla \times g_l(kr) X_{l,m} \right), \end{aligned} \quad (4.66)$$

$$\begin{aligned} \mathbf{E} &= \sum_{l,m} \left(\mathbf{E}_{l,m}^{(TM)} + \mathbf{E}_{l,m}^{(TE)} \right) \\ &= \sum_{l,m} \left(\frac{i}{k} \alpha_{l,m}^{TM}(k) \nabla \times f_l(kr) X_{l,m} + \alpha_{l,m}^{TE}(k) g_l(kr) X_{l,m} \right), \end{aligned} \quad (4.67)$$

where the coefficients $\alpha_{l,m}^{TM}(k)$ and $\alpha_{l,m}^{TE}(k)$, specify the amounts of electric multipole and magnetic multipole fields of order (l, m) . These coefficients are also determined by the sources and boundary conditions. Operating with \mathbf{r} on equation 4.67,

$$\mathbf{r} \cdot \mathbf{E} = \sum_{l,m} \left(\frac{i}{k} \alpha_{l,m}^{TM}(k) \mathbf{r} \cdot \nabla \times f_l(kr) X_{l,m} + \alpha_{l,m}^{TE}(k) g_l(kr) \mathbf{r} \cdot X_{l,m} \right). \quad (4.68)$$

$X_{l,m}$ is given by equation 4.63. Putting that in the second term and using a vector identity on the first term gives,

$$\mathbf{r} \cdot \mathbf{E} = \sum_{l,m} \left(\frac{i}{k} \alpha_{l,m}^{TM}(k) (\mathbf{r} \times \nabla) \cdot f_l(kr) X_{l,m} + \alpha_{l,m}^{TE}(k) g_l(kr) \frac{1}{\sqrt{l(l+1)}} \mathbf{r} \cdot \mathbf{L} Y_{l,m} \right). \quad (4.69)$$

$\mathbf{L} = \frac{1}{i} \mathbf{r} \times \nabla$, and it is a vector identity that $\mathbf{r} \cdot \mathbf{r} \times \nabla = 0$, so the second term in equation 4.69 is zero. Therefore,

$$\begin{aligned} \mathbf{r} \cdot \mathbf{E} &= - \sum_{l,m} \left(\frac{i}{k} \alpha_{l,m}^{TM}(k) \mathbf{L} f_l(kr) X_{l,m} \right), \\ &= - \sum_{l,m} \left(\frac{i}{k} \alpha_{l,m}^{TM}(k) \mathbf{L} f_l(kr) \frac{1}{\sqrt{l(l+1)}} \mathbf{L} Y_{l,m} \right). \end{aligned} \quad (4.70)$$

4.1. MULTIPOLAR EXPANSION OF THE VECTOR SPHERICAL
HARMONICS FOR THE HOPF-KNOTTED FIELDS

\mathbf{L} only acts on angular coordinates, so it commutes through $f_l(kr)$,

$$\mathbf{r} \cdot \mathbf{E} = - \sum_{l,m} \left(\alpha_{l,m}^{TM}(k) f_l(kr) \frac{i}{k\sqrt{l(l+1)}} \mathbf{L}^2 Y_{l,m} \right). \quad (4.71)$$

But, by definition, $\mathbf{L}^2 Y_{l,m} = l(l+1) Y_{l,m}$, so,

$$\mathbf{r} \cdot \mathbf{E} = - \sum_{l,m} \left(\frac{i}{k} \alpha_{l,m}^{TM}(k) f_l(kr) \sqrt{l(l+1)} Y_{l,m} \right). \quad (4.72)$$

Multiplying by $Y_{l,m}^*$ and integrating over all angles. Knowing,

$$\int Y_{l',m'}^* Y_{l,m} d\Omega = \delta_{l,l'} \delta_{m,m'}, \quad (4.73)$$

so,

$$\alpha_{l,m}^{TM}(k) f_l(kr) = - \frac{k}{\sqrt{l(l+1)}} \int Y_{l,m}^* \mathbf{r} \cdot \mathbf{E} d\Omega. \quad (4.74)$$

A completely analogous calculation gives,

$$\alpha_{l,m}^{TE}(k) g_l(kr) = \frac{k}{\sqrt{l(l+1)}} \int Y_{l,m}^* \mathbf{r} \cdot \mathbf{B} d\Omega. \quad (4.75)$$

One can put the values obtained here back into equation 4.66 and 4.67 to express the fields as a multipole expansion around an electric or magnetic multipole and, therefore, potential field.

For Hopf-knotted solutions to Maxwell's equations, this derivation does not appear valid. There are two reasons for this: Firstly, Jackson, and therefore Irvine and Bouwmeester, have assumed an exponential time dependence, $e^{i\omega t}$, which the knotted fields do *not* have. Irvine and Bouwmeester attempt to circumvent this by assuming validity at $t = 0$, which brings this term to unity; Secondly, as previously stated, two of the equations in 4.34 rely on $e^{i\omega t}$ dependence. Without this assumption, the Helmholtz equations (4.37 and 4.38), and therefore everything that follows (equations 4.61 and 4.62) cannot be obtained. This makes the multipole coefficient equations impossible to derive. Because of this, the method employed by Irvine and Bouwmeester cannot be reconciled with the Hopf-knotted solutions to Maxwell's equations.

4.1.3 Irvine and Bouwmeester's Results Extended to Higher Knot Types

It would be quite simple to explore higher knotted potential fields, assuming that this method was valid. In a later paper by Irvine [15], this extension was considered and the equation given for all knot types was,

$$\mathbf{A}(\mathbf{r}, t) = \int dk k^3 e^{-k} \left[\mathbf{A}_{1,1}^{TM}(k, \mathbf{r}) - i \frac{p}{q} \mathbf{A}_{1,1}^{TE}(k, \mathbf{r}) \right] e^{-i\omega t} + c.c. \quad (4.76)$$

This suggests that, for all $p - q$ knot types, the potential field will always be a dipole, as $l = 1$. This result poses some problems: the higher the knotting number, the higher the concentration of field lines through the origin and, therefore, the quicker drop-off of magnitude from the centre of the pulse. In order to further analyse this, a calculation of the higher knotting number combinations was undertaken. In accordance with Irvine's work, the method used to obtain these results was precisely that derived in the first section of this chapter. However, this thesis, instead, uses the electric and magnetic field components for the different $p - q$ knot types. The initial field components for each $p - q$ knot type, and their associated multipolar coefficients, have been calculated using the same method, but have produced different results to those published in the original literature.

Before looking at the results directly, one should note the lowest 25 combinations of $p - q$ winding numbers that give different knot-types. These are shown, below, in the winding number tree ($p - q$ tree):

$$\begin{array}{c}
 p, q \\
 1, 1 \\
 1, 2 \quad 2, 2 \quad 2, 1 \\
 1, 3 \quad 2, 3 \quad 3, 3 \quad 3, 2 \quad 3, 1 \\
 1, 4 \quad 2, 4 \quad 3, 4 \quad 4, 4 \quad 4, 3 \quad 4, 2 \quad 4, 1 \\
 1, 5 \quad 2, 5 \quad 3, 5 \quad 4, 5 \quad 5, 5 \quad 5, 4 \quad 5, 3 \quad 5, 2 \quad 5, 1
 \end{array}$$

4.1. MULTIPOLAR EXPANSION OF THE VECTOR SPHERICAL
HARMONICS FOR THE HOPF-KNOTTED FIELDS

The $p - q$ number combinations in red show what knot-types have been calculated (using the method previously demonstrated by Irvine and Bouwmeester). Below are the individual multipole coefficient results for these different knot-types. For continuity, the coefficients have been brought inside the square roots for the magnetic vector potential equations, and the terms grouped so differences are easily comparable to published literature.³¹

$p = 1, q = 1$

Multipole coefficients and the potential field:

$$\begin{aligned}\alpha_{1,1}^{TM} &= \sqrt{\frac{4\pi}{3}} k^3 e^{-k} \\ \alpha_{1,1}^{TE} &= -i\alpha_{1,1}^{TM}\end{aligned}\tag{4.77}$$

$$\mathbf{A}(\mathbf{r}, t = 0) = \sqrt{\frac{4\pi}{3}} \int dk k^3 e^{-k} [\mathbf{A}_{1,1}^{TM}(k, \mathbf{r}) - i\mathbf{A}_{1,1}^{TE}(k, \mathbf{r})]\tag{4.78}$$

$p = 1, q = 2$

Multipole coefficients and the potential field:

$$\begin{aligned}\alpha_{2,2}^{TM} &= -\frac{4}{15} k^4 \sqrt{5} \sqrt{\pi} e^{-k} \\ \alpha_{2,2}^{TE} &= -i\alpha_{2,2}^{TM}\end{aligned}\tag{4.79}$$

$$\mathbf{A}(\mathbf{r}, t = 0) = -\sqrt{\frac{16\pi}{45}} \int dk k^4 e^{-k} [\mathbf{A}_{2,2}^{TM}(k, \mathbf{r}) - i\mathbf{A}_{2,2}^{TE}(k, \mathbf{r})]\tag{4.80}$$

$p = 1, q = 3$

Multipole coefficients and the potential field:

$$\begin{aligned}\alpha_{3,3}^{TM} &= \frac{2}{105} k^5 \sqrt{105} \sqrt{\pi} e^{-k} \\ \alpha_{3,3}^{TE} &= -i\alpha_{3,3}^{TM}\end{aligned}\tag{4.81}$$

$$\mathbf{A}(\mathbf{r}, t = 0) = \sqrt{\frac{4\pi}{105}} \int dk k^5 e^{-k} [\mathbf{A}_{3,3}^{TM}(k, \mathbf{r}) - i\mathbf{A}_{3,3}^{TE}(k, \mathbf{r})]\tag{4.82}$$

³¹To see the initial components of each electric ($\mathbf{E}(x, y, z, t)$) and magnetic ($\mathbf{B}(x, y, z, t)$) fields, please refer to the appendix A where they are stated at time $t = 0$.

4.1. MULTIPOLAR EXPANSION OF THE VECTOR SPHERICAL
HARMONICS FOR THE HOPF-KNOTTED FIELDS

$p = 2, q = 1$

Multipole coefficients and the potential field:

$$\alpha_{1,1}^{TM} = -\frac{2}{3} k^3 \sqrt{3} \sqrt{\pi} e^{-k} (k-2); \text{ and } \alpha_{2,1}^{TM} = -i \frac{2}{15} k^4 \sqrt{5} \sqrt{\pi} e^{-k} \quad (4.83)$$

$$\sum_{l=1}^2 \alpha_{l,1}^{TE} = -i \sum_{l=1}^2 \alpha_{l,1}^{TM}$$

$$\begin{aligned} \mathbf{A}(\mathbf{r}, t=0) = & \sqrt{\frac{4\pi}{9}} \int dk k^3 e^{-k} \left[(-\sqrt{3}(k-2) \mathbf{A}_{1,1}^{TM}(k, \mathbf{r}) - \frac{ik}{\sqrt{5}} \mathbf{A}_{2,1}^{TM}(k, \mathbf{r})) \right. \\ & \left. -i(-\sqrt{3}(k-2) \mathbf{A}_{1,1}^{TE}(k, \mathbf{r}) - \frac{ik}{\sqrt{5}} \mathbf{A}_{2,1}^{TE}(k, \mathbf{r})) \right] \end{aligned} \quad (4.84)$$

$p = 2, q = 2$

Multipole coefficients and the potential field:

$$\alpha_{2,2}^{TM} = \frac{8}{45} k^4 \sqrt{5} \sqrt{\pi} e^{-k} (k-3); \text{ and } \alpha_{3,2}^{TM} = \frac{4i}{315} k^5 \sqrt{70} \sqrt{\pi} e^{-k} \quad (4.85)$$

$$\sum_{l=2}^3 \alpha_{l,2}^{TE} = -i \sum_{l=2}^3 \alpha_{l,2}^{TM}$$

$$\begin{aligned} \mathbf{A}(\mathbf{r}, t=0) = & \sqrt{\frac{16\pi}{405}} \int dk k^4 e^{-k} \left[(\sqrt{4}(k-3) \mathbf{A}_{2,2}^{TM}(k, \mathbf{r}) + i \sqrt{\frac{2}{7}} k \mathbf{A}_{3,2}^{TM}(k, \mathbf{r})) \right. \\ & \left. -i(\sqrt{4}(k-3) \mathbf{A}_{2,2}^{TE}(k, \mathbf{r}) + i \sqrt{\frac{2}{7}} k \mathbf{A}_{3,2}^{TE}(k, \mathbf{r})) \right] \end{aligned} \quad (4.86)$$

4.1. MULTIPOLAR EXPANSION OF THE VECTOR SPHERICAL
HARMONICS FOR THE HOPF-KNOTTED FIELDS

$p = 3, q = 1$

Multipole coefficients and the potential field:

$$\alpha_{1,1}^{TM} = \frac{2}{5} k^3 \sqrt{3} \sqrt{\pi} e^{-k} (k^2 - 5k + 5); \quad \alpha_{2,1}^{TM} = \frac{2i}{15} k^4 \sqrt{5} \sqrt{\pi} e^{-k} (k - 3);$$

$$\text{and } \alpha_{3,1}^{TM} = -\frac{2}{105} k^5 \sqrt{7} \sqrt{\pi} e^{-k} \quad (4.87)$$

$$\sum_{l=1}^3 \alpha_{l,1}^{TE} = -i \sum_{l=1}^3 \alpha_{l,1}^{TM}$$

$$\mathbf{A}(\mathbf{r}, t = 0) = \sqrt{\frac{4\pi}{25}} \int dk k^3 e^{-k} \left[(\sqrt{3} (k^2 - 5k + 5) \mathbf{A}_{1,1}^{TM}(k, \mathbf{r}) \right.$$

$$+ i \sqrt{\frac{5}{9}} k (k - 3) \mathbf{A}_{2,1}^{TM}(k, \mathbf{r}) - \sqrt{\frac{1}{63}} k^2 \mathbf{A}_{3,1}^{TM}(k, \mathbf{r}))$$

$$\left. - i(\sqrt{3} (k^2 - 5k + 5) \mathbf{A}_{1,1}^{TE}(k, \mathbf{r}) + i \sqrt{\frac{5}{9}} k (k - 3) \mathbf{A}_{2,1}^{TE}(k, \mathbf{r}) - \sqrt{\frac{1}{63}} k^2 \mathbf{A}_{3,1}^{TE}(k, \mathbf{r})) \right] \quad (4.88)$$

Below, the $p - q$ tree is shown with the multipole coefficient terms, demonstrating the contributions for each different knot type.

				p, q $(\alpha_{1,1}^{TM})$					
		$(\alpha_{3,3}^{TM})$	$(\alpha_{2,2}^{TM})$	$(\alpha_{2,2}^{TM} \text{ and } \alpha_{3,2}^{TM})$	$(\alpha_{1,1}^{TM} \text{ and } \alpha_{2,1}^{TM})$		$(\alpha_{1,1}^{TM} \text{ and } \alpha_{2,1}^{TM} \text{ and } \alpha_{3,1}^{TM})$		
	1, 4	2, 4	3, 4	4, 4	5, 4		4, 2		4, 1
1, 5	2, 5	3, 5	4, 5	5, 5	5, 4		5, 3		5, 2 5, 1

This thesis' extension to the results of Irvine and Bouwmeester constructs a differing picture to that given by Irvine in his later paper [15], via equation (4.76). The prescription clearly shows that as one changes the winding number for q from 1 – 3, and hold $p = 1$ (red and green), the form of the field changes from a dipole ($l = 1$) to a quadrupole ($l = 2$) and then to an octupole ($l = 3$) for every next level of knot - with each change of q giving a pure form of each multipole. This changes when one holds $q = 1$ and increases the p winding number. When p changes from 1 – 3 and $q = 1$ (blue and green), the field gains contributions from the number of multipole fields dictated by p , and its starting point is defined by q . For example, if $p = 3$ and $q = 2$, the fields would have contributions from three multipole fields (as dictated by p) and the multipole field types - would start with a quadrupole (defined by $q = 2$) - where the other, higher contributions are from the higher levels of multipole field ($q = 3$ and $q = 4$). If you consider the topology of the field lines, this reinforces the assertions made in this thesis. As the field lines become more knotted, there will be a higher

density of field lines passing through the centre of the knot. This higher density will lead to a higher magnitude acting in the centre and a quicker fall-off of magnitude, with increasing radius. This would give rise to magnitudes falling off, with higher powered, inverse relationships with respect to their radii. This is in stark contrast to Irvine and his suggestion that all knot types have pure dipole multipole coefficients.

At this stage, one should assess the patterns which start to emerge, as the number of contributing coefficients increase. As the number of contributing multipole terms increases - for example, when p changes from 1 – 3 and $q = 1$ (blue and green), one starts to see extra coefficients emerge in powers of k from $k^0 - k^2$. For $p = 3$ and $q = 1$, there are three contributing terms for both the TM and TE parts. The first term has an extra quadratic factor in k ; the second term has an extra factor starting in k^1 ; and the third has no extra factor - which could be considered as a k^0 factor. One can also notice, whilst varying q , that the power of the original k term increases. For example, as one changes q from 1 – 3 and holds $p = 1$ (red and green), the power in k varies from 3 – 5. One could quite easily start assigning patterns for the derivation of the multipole coefficients in a similar vein to that employed with the zilches in terms of the $p - q$ winding numbers, k , and possibly the angular momentum numbers, l and m . For this limited set of results, this is conjecture and is considered retrospectively, with respect to exploring patterns that emerge in the generalised multipole coefficients.³²

4.2 Generalised Multipolar Expansion of the VSH of the Knotted Solutions to Maxwell's Equations Method

As this chapter has, hitherto, demonstrated, there are some issues with the published literature. This warrants the exploration of a new method. The aim of this section is to improve upon the results of Irvine and Bouwmeester and Irvine individually, by conducting a generalised multipole expansion for as many knot types as possible. A selection of equations produced in a book called *Theoretical Nuclear Physics*, by Blatt and Weisskopf, have been employed [61]. The equations state that an arbitrary

³²See section 4.2.2.

4.2. GENERALISED MULTIPOLAR EXPANSION OF THE VSH OF THE
KNOTTED SOLUTIONS TO MAXWELL'S EQUATIONS METHOD

vector field can be expanded in the following series,

$$\mathbf{A}(\mathbf{r}) = \sum_{l=0}^{\infty} \sum_{m=-l}^l \mathbf{A}_{l,m}(\mathbf{r}), \quad (4.89)$$

$$\mathbf{A}_{l,m}(\mathbf{r}) = r^{-1}[f_{l,m}(\mathbf{r})\mathbf{V}_{l,m} + g_{l,m}(\mathbf{r})\mathbf{W}_{l,m} + h_{l,m}(\mathbf{r})\mathbf{X}_{l,m}], \quad (4.90)$$

where, $\mathbf{V}_{l,m}$, $\mathbf{W}_{l,m}$, and $\mathbf{X}_{l,m}$ are the VSH, and the functions f , g , and h are the multipole coefficients. These were found from the following:

$$\begin{aligned} r^{-1}f_{l,m}(\mathbf{r}) &= \int [\mathbf{V}_{l,m}(\theta, \phi)]^* \cdot \mathbf{A}_{l,m}(\mathbf{r}) d\Omega, \\ r^{-1}g_{l,m}(\mathbf{r}) &= \int [\mathbf{W}_{l,m}(\theta, \phi)]^* \cdot \mathbf{A}_{l,m}(\mathbf{r}) d\Omega, \\ r^{-1}h_{l,m}(\mathbf{r}) &= \int [\mathbf{X}_{l,m}(\theta, \phi)]^* \cdot \mathbf{A}_{l,m}(\mathbf{r}) d\Omega. \end{aligned} \quad (4.91)$$

To find the multipole coefficients and determine the shape of the fields, the above equations must be solved. The VSH are derived in a paper by E. L. Hill [62]:

$$\begin{aligned} \mathbf{V}_{lm} &= \mathbf{r}_1 \left\{ -\left(\frac{l+1}{2l+1}\right)^{\frac{1}{2}} Y_l^m \right\} + \boldsymbol{\theta}_1 \left\{ \frac{1}{[(l+1)(2l+1)]^{\frac{1}{2}}} \frac{\partial Y_l^m}{\partial \theta} \right\} + \boldsymbol{\phi}_1 \left\{ \frac{i m Y_l^m}{[(l+1)(2l+1)]^{\frac{1}{2}} \sin(\theta)} \right\}, \\ \mathbf{X}_{lm} &= \boldsymbol{\theta}_1 \left\{ -\frac{m Y_l^m}{[l(l+1)]^{\frac{1}{2}} \sin(\theta)} \right\} + \boldsymbol{\phi}_1 \left\{ -\frac{i}{[l(l+1)]^{\frac{1}{2}}} \frac{\partial Y_l^m}{\partial \theta} \right\}, \\ \mathbf{W}_{lm} &= \mathbf{r}_1 \left\{ \left(\frac{l}{2l+1}\right)^{\frac{1}{2}} Y_l^m \right\} + \boldsymbol{\theta}_1 \left\{ \frac{1}{[l(2l+1)]^{\frac{1}{2}}} \frac{\partial Y_l^m}{\partial \theta} \right\} + \boldsymbol{\phi}_1 \left\{ \frac{i m Y_l^m}{[l(2l+1)]^{\frac{1}{2}} \sin(\theta)} \right\}, \end{aligned} \quad (4.92)$$

where,

$$\begin{aligned} \mathbf{r}_1 &= \mathbf{i} \sin(\theta) \cos(\phi) + \mathbf{j} \sin(\theta) \sin(\phi) + \mathbf{k} \cos(\theta), \\ \boldsymbol{\theta}_1 &= \mathbf{i} \cos(\theta) \cos(\phi) + \mathbf{j} \cos(\theta) \sin(\phi) - \mathbf{k} \sin(\theta), \\ \boldsymbol{\phi}_1 &= -\mathbf{i} \sin(\phi) + \mathbf{j} \cos(\phi). \end{aligned} \quad (4.93)$$

As $\mathbf{A}(\mathbf{r})$ is arbitrary, one can enter any vector field here. This means one can insert the magnetic vector potential directly into these equations. From these, one should be able to determine to which multipole type each knotted field belongs. This thesis will be considering the electric and magnetic fields and potentials - \mathbf{E} , \mathbf{B} , \mathbf{A} , and \mathbf{C} . In order to compare the results obtained during the course of this research to those of Irvine and Bouwmeester, it is necessary to outline the magnetic vector potential for the Hopf-knotted solutions to Maxwell's equations. One does not know at which angular momentum numbers the multipole coefficients will occur. This drastically

4.2. GENERALISED MULTIPOLAR EXPANSION OF THE VSH OF THE KNOTTED SOLUTIONS TO MAXWELL'S EQUATIONS METHOD

affects the VSH from above. The VSH will need to be derived for each set of angular momentum numbers tested, converted into Cartesian components, multiplied by the components of the magnetic vector potential via a dot product, then converted back to spherical polar coordinates. Finally, integrating the result over all angles - as stated in equation 4.91.

The program, *Maple*, was used extensively for this process: for efficiency when calculating multiple equations; but it was also used for its ability to create a script that can generate all the results by changing only the two input parameters - p and q . The script calculates the initial complex functions, α and β , along with their powers (the winding numbers p and q), which are then inserted into the equation for each component of the overall complex field, \mathbf{R} , and also the overall complex potential field, \mathbf{H} . When taking the real and imaginary parts, one can extract the electric and magnetic fields from \mathbf{R} , and the electric and magnetic vector potentials from \mathbf{H} (again all calculated at time $t = 0$). A separate script is required for each combination of winding numbers and for each different multipole coefficient functions f , g , and h - attached to their VSH, $\mathbf{V}_{l,m}$, $\mathbf{W}_{l,m}$ and $\mathbf{X}_{l,m}$ respectively. Within each script, the multipole coefficients were calculated for every combination of angular momentum numbers, from $l = 0, 1, \dots, 12, 13$ and $m = -l, -l + 1, \dots, l - 1, l$. This allowed the identification of exactly which multipole coefficients were finite and which were zero.

In total, three base scripts were needed for each of the multipole coefficient functions attached to their VSH. For simplicity and accuracy, the only input needed was the change of integer of the winding numbers, p and q . This thesis considers many combinations of the winding numbers from $p = 1 - 8$ and $q = 1 - 10$. This eventually gave 49 different knot types. Therefore, 147 scripts needed to be produced - considering each multipole coefficient.³³ As with the extension to the results of Irvine and Bouwmeester, a change in the winding number, p , produced multiple coefficients from the different contributions, and followed a prescription.³⁴ The multipole coefficients that were produced for each different knot type were tabulated.³⁵ This amounted to a collection of 3,680 multipole coefficient equations. As the scripts are all based off the same three initial scripts, there is a very high level of consistency in their production.

³³See figure 4.1 for the exact knot types and their $p - q$ combinations that were calculated.

³⁴See section 4.2.1.

³⁵A sample can be found in the appendix G.

p, q	
1,1	
1,2 2,2 2,1	
1,3 2,3 3,3 3,2 3,1	
1,4 2,4 3,4 4,4 4,3 4,2 4,1	
1,5 2,5 3,5 4,5 5,5 5,4 5,3 5,2 5,1	
1,6 2,6 3,6 4,6 5,6 6,6 6,5 6,4 6,3 6,2 6,1	
1,7 2,7 3,7 4,7 5,7 6,7 7,7 7,6 7,5 7,4 7,3 7,2 7,1	
1,8 2,8 3,8 4,8 5,8 6,8 7,8 8,8 8,7 8,6 8,5 8,4 8,3 8,2 8,1	
1,9 2,9 3,9 4,9 5,9 6,9 7,9 8,9 9,9 9,8 9,7 9,6 9,5 9,4 9,3 9,2 9,1	
1,10 2,10 3,10 4,10 5,10 6,10 7,10 8,10 9,10 10,10 10,9 10,8 10,7 10,6 10,5 10,4 10,3 10,2 10,1	

Figure 4.1: The exact knot types and their $p-q$ combinations that were calculated are shown in red, with the $p-q$ winding number tree showing the various combinations possible for $p = 1 - 10$ and $q = 1 - 10$.

4.2.1 Results from the Generalised Multipolar Method

A sample of the results for the magnetic vector potential is shown here at time $t = 0$. For continuity, the same knot types that were given in the extension to the work of Irvine and Bouwmeester [18][15] will be demonstrated for the potential field.³⁶ The form that the results take below are slightly different to those displayed in the appendices because their coefficients have been brought into the square-roots. The reason for this is that they are comparable with the extended results of Irvine and Bouwmeester. For each knot-type the multipole coefficients will be displayed, followed by the form of the potential field.

$p = 1, q = 1$

Multipole coefficients and the potential field at $t = 0$:

$$\begin{aligned}
 r^{-1} f_{l=1,m=\pm 1}(\mathbf{r}) &= -\sqrt{\frac{16\pi}{9}} \frac{ik^3 r^2}{(k^2 r^2 + 1)^2}, \\
 r^{-1} g_{l=1,m=\pm 1}(\mathbf{r}) &= -\sqrt{\frac{2\pi}{9}} \frac{ik(k^2 r^2 - 3)}{(k^2 r^2 + 1)^2}, \\
 r^{-1} h_{l=1,m=\pm 1}(\mathbf{r}) &= \sqrt{\frac{16\pi}{3}} \frac{k^2 r}{(k^2 r^2 + 1)^2}. \\
 A(\mathbf{r}, t = 0) &= r^{-1} \sqrt{\frac{2\pi}{3}} \frac{k}{(k^2 r^2 + 1)^2} \sum_{m=-1}^1 \left(-\sqrt{\frac{8}{3}} ik^2 r^2 \mathbf{V}_{1,m} - \frac{1}{\sqrt{3}} i(k^2 r^2 - 3) \mathbf{W}_{1,m} + \sqrt{\frac{8}{3}} kr \mathbf{X}_{1,m} \right).
 \end{aligned} \tag{4.94}$$

³⁶To see more multipole coefficients, please refer to the appendix G.

4.2. GENERALISED MULTIPOLAR EXPANSION OF THE VSH OF THE
KNOTTED SOLUTIONS TO MAXWELL'S EQUATIONS METHOD

$p = 1, q = 2$

Multipole coefficients and the potential field at $t = 0$:

$$\begin{aligned}
 r^{-1} f_{l=2,m=\pm 2}(\mathbf{r}) &= \left[\frac{m}{|m|} \right] \sqrt{\frac{512 \pi}{25}} \frac{i k^6 r^5}{(k^2 r^2 + 1)^4}, \\
 r^{-1} f_{l=3,m=\pm 2}(\mathbf{r}) &= \sqrt{\frac{2,048 \pi}{735}} \frac{k^5 r^4}{(k^2 r^2 + 1)^4}, \\
 r^{-1} g_{l=2,m=\pm 2}(\mathbf{r}) &= \left[\frac{m}{|m|} \right] \sqrt{\frac{64 \pi}{75}} \frac{i k^2 r (k^4 r^4 - 5)}{(k^2 r^2 + 1)^4}, \\
 r^{-1} g_{l=3,m=\pm 2}(\mathbf{r}) &= \sqrt{\frac{128 \pi}{2,205}} \frac{k^3 r^2 (k^2 r^2 + 7)}{(k^2 r^2 + 1)^4}, \\
 r^{-1} h_{l=2,m=\pm 2}(\mathbf{r}) &= - \left[\frac{m}{|m|} \right] \sqrt{\frac{1,024 \pi}{45}} \frac{k^3 r^2}{(k^2 r^2 + 1)^3}. \\
 A(\mathbf{r}, t = 0) &= r^{-1} \sqrt{\frac{64 \pi}{25}} \frac{k^2 r}{(k^2 r^2 + 1)^3} \sum_{m=-2}^2 \left[\frac{m}{|m|} \right] \left(\sqrt{8} \frac{i k^4 r^4}{(k^2 r^2 + 1)} \mathbf{V}_{2,m} + \sqrt{\frac{1}{3}} i \frac{(k^4 r^4 - 5)}{(k^2 r^2 + 1)} \mathbf{W}_{2,m} - \sqrt{\frac{80}{9}} k r \mathbf{X}_{2,m} \right) + \\
 &\left(\sqrt{\frac{160}{147}} \frac{k^3 r^3}{(k^2 r^2 + 1)} \mathbf{V}_{3,m} + \sqrt{\frac{10}{441}} \frac{k r (k^2 r^2 + 7)}{(k^2 r^2 + 1)} \mathbf{W}_{3,m} \right).
 \end{aligned} \tag{4.95}$$

$p = 1, q = 3$

Multipole coefficients and the potential field at $t = 0$:

$$\begin{aligned}
 r^{-1} f_{l=3,m=\pm 3}(\mathbf{r}) &= - \sqrt{\frac{36,864 \pi}{245}} \frac{i k^5 r^4 (k^2 r^2 - 1/3)}{(k^2 r^2 + 1)^5}, \\
 r^{-1} f_{l=4,m=\pm 3}(\mathbf{r}) &= - \left[\frac{m}{|m|} \right] \sqrt{\frac{16,384 \pi}{567}} \frac{k^6 r^5}{(k^2 r^2 + 1)^5}, \\
 r^{-1} g_{l=3,m=\pm 3}(\mathbf{r}) &= - \sqrt{\frac{768 \pi}{245}} \frac{i k^3 r^2 (k^4 r^4 + 2 k^2 r^2 - 7)}{(k^2 r^2 + 1)^5}, \\
 r^{-1} g_{l=4,m=\pm 3}(\mathbf{r}) &= - \left[\frac{m}{|m|} \right] \sqrt{\frac{1,024 \pi}{2,835}} \frac{k^4 r^3 (k^2 r^2 + 9)}{(k^2 r^2 + 1)^5}, \\
 r^{-1} h_{l=3,m=\pm 3}(\mathbf{r}) &= \sqrt{\frac{3,072 \pi}{35}} \frac{k^4 r^3}{(k^2 r^2 + 1)^4}. \\
 A(\mathbf{r}, t = 0) &= r^{-1} \sqrt{\pi} \frac{k^3 r^2}{(k^2 r^2 + 1)^4} \times \\
 &\sum_{m=-3}^3 \left(- \sqrt{\frac{36,864 \pi}{245}} \frac{i k^2 r^2 (k^2 r^2 - 1/3)}{(k^2 r^2 + 1)} \mathbf{V}_{3,m} - \sqrt{\frac{768 \pi}{245}} i \frac{(k^4 r^4 + 2 k^2 r^2 - 7)}{(k^2 r^2 + 1)} \mathbf{W}_{3,m} + \sqrt{\frac{3,072 \pi}{35}} k r \mathbf{X}_{3,m} \right) + \\
 &\left[\frac{m}{|m|} \right] \left(- \sqrt{\frac{16,384 \pi}{567}} \frac{k^3 r^3}{(k^2 r^2 + 1)} \mathbf{V}_{4,m} - \sqrt{\frac{1,024 \pi}{2,835}} \frac{k r (k^2 r^2 + 9)}{(k^2 r^2 + 1)} \mathbf{W}_{4,m} \right).
 \end{aligned} \tag{4.96}$$

4.2. GENERALISED MULTIPOLAR EXPANSION OF THE VSH OF THE
KNOTTED SOLUTIONS TO MAXWELL'S EQUATIONS METHOD

$\mathbf{p} = \mathbf{2}, \mathbf{q} = \mathbf{1}$

Multipole coefficients and the potential field at $t = 0$:

$$\begin{aligned}
 r^{-1} f_{l=1,m=\pm 1}(\mathbf{r}) &= -\sqrt{\frac{16\pi}{225}} \frac{i k^3 r^2 (5 k^4 r^4 + 6 k^2 r^2 - 23)}{(k^2 r^2 + 1)^4}, \\
 r^{-1} f_{l=2,m=\pm 1}(\mathbf{r}) &= -\left[\frac{m}{|m|} \right] \sqrt{\frac{512\pi}{25}} \frac{k^4 r^3}{(k^2 r^2 + 1)^4}, \\
 r^{-1} f_{l=3,m=\pm 1}(\mathbf{r}) &= -\sqrt{\frac{4,096\pi}{3,675}} \frac{i k^5 r^4}{(k^2 r^2 + 1)^4}, \\
 r^{-1} g_{l=1,m=\pm 1}(\mathbf{r}) &= -\sqrt{\frac{2\pi}{9}} \frac{i k (k^6 r^6 - \frac{63}{5} k^4 r^4 - k^2 r^2 + 3)}{(k^2 r^2 + 1)^4}, \\
 r^{-1} g_{l=2,m=\pm 1}(\mathbf{r}) &= \left[\frac{m}{|m|} \right] \sqrt{\frac{1,024\pi}{75}} \frac{k^4 r^3}{(k^2 r^2 + 1)^4}, \\
 r^{-1} g_{l=3,m=\pm 1}(\mathbf{r}) &= -\sqrt{\frac{256\pi}{11,025}} \frac{i k^3 r^2 (k^2 r^2 + 7)}{(k^2 r^2 + 1)^4}, \\
 r^{-1} h_{l=1,m=\pm 1}(\mathbf{r}) &= \sqrt{\frac{64\pi}{3}} \frac{k^2 r (k^2 r^2 - 1)}{(k^2 r^2 + 1)^3}, \\
 r^{-1} h_{l=2,m=\pm 1}(\mathbf{r}) &= -\left[\frac{m}{|m|} \right] \sqrt{\frac{256\pi}{45}} \frac{i k^3 r^2}{(k^2 r^2 + 1)^3}.
 \end{aligned}$$

$$\begin{aligned}
 A(\mathbf{r}, t = 0) &= r^{-1} \sqrt{\pi} \frac{k}{(k^2 r^2 + 1)^3} \times \\
 &\sum_{m=-1}^1 \left[\left(-\sqrt{\frac{16}{225}} \frac{i k^2 r^2 (5 k^4 r^4 + 6 k^2 r^2 - 23)}{(k^2 r^2 + 1)} \mathbf{V}_{1,m} - \sqrt{\frac{2}{9}} \frac{i (k^6 r^6 - \frac{63}{5} k^4 r^4 - k^2 r^2 + 3)}{(k^2 r^2 + 1)} \mathbf{W}_{1,m} + \sqrt{\frac{64}{3}} k r (k^2 r^2 - 1) \mathbf{X}_{1,m} \right) + \right. \\
 &\left. \left[\frac{m}{|m|} \right] \left(-\sqrt{\frac{512}{25}} \frac{k^3 r^3}{(k^2 r^2 + 1)} \mathbf{V}_{2,m} + \sqrt{\frac{1,024}{75}} \frac{k^3 r^3}{(k^2 r^2 + 1)} \mathbf{W}_{2,m} - \sqrt{\frac{256}{45}} i k^2 r^2 \mathbf{X}_{2,m} \right) + \right. \\
 &\left. \left(-\sqrt{\frac{4,096}{3,675}} \frac{i k^4 r^4}{(k^2 r^2 + 1)} \mathbf{V}_{3,m} - \sqrt{\frac{256}{11,025}} \frac{i k^2 r^2 (k^2 r^2 + 7)}{(k^2 r^2 + 1)} \mathbf{W}_{3,m} \right) \right].
 \end{aligned} \tag{4.97}$$

4.2. GENERALISED MULTIPOLAR EXPANSION OF THE VSH OF THE
KNOTTED SOLUTIONS TO MAXWELL'S EQUATIONS METHOD

$\mathbf{p} = 2, \mathbf{q} = 2$

Multipole coefficients and the potential field at $t = 0$:

$$r^{-1} f_{l=2,m=\pm 2}(\mathbf{r}) = - \left[\frac{m}{|m|} \right] \sqrt{\frac{512 \pi}{25}} \frac{i k^4 r^3 \left(k^2 r^2 - \frac{5}{3} \right)}{(k^2 r^2 + 1)^4},$$

$$r^{-1} f_{l=3,m=\pm 2}(\mathbf{r}) = - \left[\frac{m}{|m|} \right] \sqrt{\frac{8,192 \pi}{735}} \frac{k^5 r^4}{(k^2 r^2 + 1)^4},$$

$$r^{-1} g_{l=2,m=\pm 2}(\mathbf{r}) = - \left[\frac{m}{|m|} \right] \sqrt{\frac{64 \pi}{75}} \frac{i k^2 r \left(k^4 r^4 - 10 k^2 r^2 + 5 \right)}{(k^2 r^2 + 1)^4},$$

$$r^{-1} g_{l=3,m=\pm 2}(\mathbf{r}) = - \left[\frac{m}{|m|} \right] \sqrt{\frac{512 \pi}{2,205}} \frac{k^3 r^2 \left(k^2 r^2 - 7 \right)}{(k^2 r^2 + 1)^4},$$

$$r^{-1} h_{l=2,m=\pm 2}(\mathbf{r}) = - \left[\frac{m}{|m|} \right] - \sqrt{\frac{4,096 \pi}{45}} \frac{k^3 r^2 \left(k^2 r^2 - 1 \right)}{(k^2 r^2 + 1)^4},$$

$$r^{-1} h_{l=3,m=\pm 2}(\mathbf{r}) = - \left[\frac{m}{|m|} \right] \sqrt{\frac{8,192 \pi}{315}} \frac{i k^4 r^3}{(k^2 r^2 + 1)^4}.$$

$$A(\mathbf{r}, t = 0) = r^{-1} \sqrt{\pi} \frac{k^2 r}{(k^2 r^2 + 1)^4} \times$$

$$\left[\sum_{m=-2}^2 \left[\frac{m}{|m|} \right] \left(\sqrt{\frac{512}{25}} i k^2 r^2 \left(k^2 r^2 - \frac{5}{3} \right) \mathbf{v}_{2,m} + \sqrt{\frac{64}{75}} i \left(k^4 r^4 - 10 k^2 r^2 + 5 \right) \mathbf{w}_{2,m} - \sqrt{\frac{4,096}{45}} k r \left(k^2 r^2 - 1 \right) \mathbf{x}_{2,m} \right) + \right. \\ \left. \left(\sqrt{\frac{8,192}{735}} k^3 r^3 \mathbf{v}_{3,m} + \sqrt{\frac{512}{2,205}} k r \left(k^2 r^2 - 7 \right) \mathbf{w}_{3,m} + \sqrt{\frac{8,192}{315}} i k^2 r^2 \mathbf{x}_{3,m} \right) \right].$$

(4.98)

4.2. GENERALISED MULTIPOLAR EXPANSION OF THE VSH OF THE
KNOTTED SOLUTIONS TO MAXWELL'S EQUATIONS METHOD

$\mathbf{p} = \mathbf{3}, \mathbf{q} = \mathbf{1}$

Multipole coefficients and the potential field at $t = 0$:

$$\begin{aligned}
 r^{-1} f_{l=1,m=\pm 1}(\mathbf{r}) &= - \left[\frac{m}{|m|} \right] - \sqrt{\frac{16 \pi}{225} \frac{i k^3 r^2 (5 k^6 r^6 + 3 k^4 r^4 - 81 k^2 r^2 + 49)}{(k^2 r^2 + 1)^5}}, \\
 r^{-1} f_{l=2,m=\pm 1}(\mathbf{r}) &= - \left[\frac{m}{|m|} \right] - \sqrt{\frac{247,808 \pi}{1,225} \frac{k^4 r^3 (k^2 r^2 - \frac{13}{11})}{(k^2 r^2 + 1)^5}}, \\
 r^{-1} f_{l=3,m=\pm 1}(\mathbf{r}) &= - \left[\frac{m}{|m|} \right] - \sqrt{\frac{12,288 \pi}{1,225} \frac{k^5 r^4 (k^2 r^2 - 3)}{(k^2 r^2 + 1)^5}}, \\
 r^{-1} f_{l=4,m=\pm 1}(\mathbf{r}) &= - \left[\frac{m}{|m|} \right] - \sqrt{\frac{16,384 \pi}{3,969} \frac{k^6 r^5}{(k^2 r^2 + 1)^5}}, \\
 r^{-1} g_{l=1,m=\pm 1}(\mathbf{r}) &= - \left[\frac{m}{|m|} \right] - \sqrt{\frac{2 \pi}{9} \frac{i k (k^8 r^8 - \frac{144}{5} k^6 r^6 + \frac{162}{5} k^4 r^4 + 8 k^2 r^2 - 3)}{(k^2 r^2 + 1)^5}}, \\
 r^{-1} g_{l=2,m=\pm 1}(\mathbf{r}) &= - \left[\frac{m}{|m|} \right] \sqrt{\frac{248,832 \pi}{1,225} \frac{k^4 r^3 (k^2 r^2 - \frac{7}{9})}{(k^2 r^2 + 1)^5}}, \\
 r^{-1} g_{l=3,m=\pm 1}(\mathbf{r}) &= - \left[\frac{m}{|m|} \right] - \sqrt{\frac{256 \pi}{1,225} \frac{i k^3 r^2 (k^4 r^4 + 18 k^2 r^2 - 7)}{(k^2 r^2 + 1)^5}}, \\
 r^{-1} g_{l=4,m=\pm 1}(\mathbf{r}) &= - \left[\frac{m}{|m|} \right] - \sqrt{\frac{1,024 \pi}{19,845} \frac{k^4 r^3 (k^2 r^2 + 9)}{(k^2 r^2 + 1)^5}}, \\
 r^{-1} h_{l=1,m=\pm 1}(\mathbf{r}) &= - \left[\frac{m}{|m|} \right] \sqrt{48 \pi} \frac{k^2 r (k^4 r^4 - \frac{14}{5} k^2 r^2 + 1)}{(k^2 r^2 + 1)^4}, \\
 r^{-1} h_{l=2,m=\pm 1}(\mathbf{r}) &= - \left[\frac{m}{|m|} \right] - \sqrt{\frac{256 \pi}{5} \frac{i k^3 r^2 (k^2 r^2 - 1)}{(k^2 r^2 + 1)^4}}, \\
 r^{-1} h_{l=3,m=\pm 1}(\mathbf{r}) &= - \left[\frac{m}{|m|} \right] - \sqrt{\frac{1,024 \pi}{175} \frac{k^4 r^3}{(k^2 r^2 + 1)^4}}.
 \end{aligned}$$

$$\begin{aligned}
 A(\mathbf{r}, t = 0) &= r^{-1} \sqrt{\pi} \frac{k}{(k^2 r^2 + 1)^4} \times \\
 &\left[\sum_{m=-1}^1 \left[\frac{m}{|m|} \right] \left(-\sqrt{\frac{16}{225} \frac{i k^2 r^2 (5 k^6 r^6 + 3 k^4 r^4 - 81 k^2 r^2 + 49)}{(k^2 r^2 + 1)}} \mathbf{V}_{1,m} - \sqrt{\frac{2}{9} \frac{i (k^8 r^8 - \frac{144}{5} k^6 r^6 + \frac{162}{5} k^4 r^4 + 8 k^2 r^2 - 3)}{(k^2 r^2 + 1)}} \mathbf{W}_{1,m} + \right. \right. \\
 &\left. \left. \sqrt{48} k r \left(k^4 r^4 - \frac{14}{5} k^2 r^2 + 1 \right) \mathbf{X}_{1,m} \right) + \right. \\
 &\left(-\sqrt{\frac{247,808}{1,225} \frac{k^3 r^3 (k^2 r^2 - \frac{13}{11})}{(k^2 r^2 + 1)}} \mathbf{V}_{2,m} + \sqrt{\frac{248,832}{1,225} \frac{k^3 r^3 (k^2 r^2 - \frac{7}{9})}{(k^2 r^2 + 1)}} \mathbf{W}_{2,m} - \sqrt{\frac{256}{5}} i k^2 r^2 (k^2 r^2 - 1) \mathbf{X}_{2,m} \right) + \\
 &\left(-\sqrt{\frac{12,288}{1,225} \frac{k^4 r^4 (k^2 r^2 - 3)}{(k^2 r^2 + 1)}} \mathbf{V}_{3,m} - \sqrt{\frac{256}{1,225} \frac{i k^2 r^2 (k^4 r^4 + 18 k^2 r^2 - 7)}{(k^2 r^2 + 1)}} \mathbf{W}_{3,m} - \sqrt{\frac{1,024}{175}} k^3 r^3 \mathbf{X}_{3,m} \right) + \\
 &\left. \left(-\sqrt{\frac{16,384}{3,969} \frac{k^5 r^5}{(k^2 r^2 + 1)}} \mathbf{V}_{4,m} - \sqrt{\frac{1,024}{19,845} \frac{k^3 r^3 (k^2 r^2 + 9)}{(k^2 r^2 + 1)}} \mathbf{W}_{4,m} \right) \right].
 \end{aligned}$$

(4.99)

In their entirety, the results show that there is a prescription to their generation, relating the number of multipolar coefficients, the starting angular momentum number, l , and the winding numbers, p and q . This prescription is similar to this thesis' extension to the work of Irvine and Bouwmeester, where the potential fields, \mathbf{A} and \mathbf{C} , have a number of multipole coefficients determined by: $p + 1$ if $p \neq q$; and by p if $p = q$ - for the f and g multipole coefficient functions. They always start with $l = q$ and increase for the next coefficient in integers, and $m = \pm q$ for all coefficients. For example, for the $p = 3$ and $q = 2$ knot, considering the $\mathbf{V}_{l,m}$ VSH, you would have $r^{-1} f_{l=2,m=\pm 2}(\mathbf{r})$, $r^{-1} f_{l=3,m=\pm 2}(\mathbf{r})$, $r^{-1} f_{l=4,m=\pm 2}(\mathbf{r})$, $r^{-1} f_{l=5,m=\pm 2}(\mathbf{r})$. For h , the number of multipole coefficients is determined by p , and they always start with $l = q$. Using the same example, for the $\mathbf{X}_{l,m}$ VSH, you would have $r^{-1} h_{l=2,m=\pm 2}(\mathbf{r})$, $r^{-1} h_{l=3,m=\pm 2}(\mathbf{r})$, $r^{-1} h_{l=4,m=\pm 2}(\mathbf{r})$. The electric and magnetic fields, \mathbf{E} and \mathbf{B} , are slightly different, having the number of multipolar coefficients determined by p , but still start with $l = q$. These results serve as a more accurate set in comparison to that given and suggested by Irvine and Bouwmeester.

4.2.2 Investigating the Patterns Occurring in the Multipole Coefficients

Whilst generating the 3,680 multipole coefficients, it was noted that there was some sort of pattern emerging between each term. Initially, simple relationships were recorded, like the powers of k increasing by one for each change of p or q , or by two for a change in both. As Chapter Three states, zilches can be written in terms of the winding numbers for the different knot types and the properties of the fields - it is the contention here that a similar occurrence might be possible.

It became fairly obvious that there was an expansion of the terms occurring. The higher ordered knot types resulted in terms appearing with a descending power series of kr . The assumption was made, initially, that each term would be a multiplication of a pre-factor, \mathcal{H} , and a factor of the form, $(k^2 r^2 + 1)^\zeta$, where ζ was related to the order in which the multipole coefficient appeared. Within the pre-factor was found a combination of two binomial expansion terms - which can be written in terms of gamma functions.

After a process of trial and error, *Maple* scripts were completed that allowed the user to input: which knot type was required; what multipole term was needed, according

4.2. GENERALISED MULTIPOLAR EXPANSION OF THE VSH OF THE
KNOTTED SOLUTIONS TO MAXWELL'S EQUATIONS METHOD

to the angular momentum number, l ; and what type of field the user was looking at. The script would then give the correct form for the multipole coefficient. The final results have been triple checked for all 3,680 terms. Whether this remains true for all values to infinity is not known, as these have not been solved analytically. The final forms of each script narrow down the set of total equations from 3,680 to just 18. The equations shown below relate to the potential fields for each corresponding multipole coefficient type for each VSH. There are labels: 'The last term'; 'The second last term' etc. - these refer to the contributing coefficients for the different knot types. For example, as previously stated, if one uses the $p = 3$ and $q = 2$ knot, this would have four contributing coefficients for f and the $\mathbf{V}_{l,m}$ VSH. The last term out of these is the fourth coefficient. If one considers the $p = 1$ and $q = 1$ knot, there are only two contributing coefficients, therefore the last term is the second coefficient. The reason they have been labelled this way is because the last term always has the smallest expansion in kr for every knot type, and the higher expansions appear in the second and third last terms - in that order.

For: $r^{-1} f_{l,m}(\mathbf{r})$ attached to $\mathbf{V}_{l,m}$ for the \mathbf{A} and \mathbf{C} fields:

The pre-factor:

$$\mathcal{H} = \left[\frac{m}{|m|} \right]^{2(p+q)-l+\delta_f} \frac{2^{p+q+l+1} (p+q) p! q! l! (-1)^{l+p-\delta_{pq}+\delta_f} (-i)^{3l+5q+2p-2\delta_{pq}+\delta_f} k^{l+2} r^{l+1}}{(p+q+l+1)! (k^2 r^2 + 1)^{p+q+1-\delta_{pq}}} \left(\frac{\Gamma(l)\Gamma(l+q+1)l\pi}{\Gamma(q)^2\Gamma(l-q+1)\Gamma(l+2)} \right)^{\frac{1}{2}} \quad (4.100)$$

The last term:

$$r^{-1} f_{l,m}(\mathbf{r}) = \mathcal{H} \frac{(-p^2 + q^2 - p + q + 2\delta_{pq}q(p+q))}{2q(p+q)}. \quad (4.101)$$

The second last term:

$$r^{-1} f_{l,m}(\mathbf{r}) = \mathcal{H} \frac{(Z^{1-\delta_{fg}}(p+q-\delta_{pq}))(q-p+1+\delta_{pq}(8p^2-6p)+2\delta_{fg})}{2q(4p)^{\delta_{pq}}}. \quad (4.102)$$

The third last term:

$$\begin{aligned} r^{-1} f_{l,m}(\mathbf{r}) = & \mathcal{H} \frac{p+q-1}{8q(p+q)} \left((-2p^3 + (-2q+7)p^2 + (2q^2+8q-7)p + 2q^3 + q^2 \right. \\ & \left. - 5q + 2 + \delta_{pq}(16q^3 - 60q^2 + 52q - 14)) Z^2 \right. \\ & \left. - \frac{4(-p^3+(q-2)p^2+(q^2-8q+5)p-q^3-6q^2+7q-2-\delta_{pq}(-64q^3+56q^2-16q))}{p-q+\delta_{pq}(2q-1)} Z \right. \\ & \left. + \frac{4(p^4+(-2q+1)p^3+(q-1)p^2+(2q^3+3q^2+4q-3)p-q^4-5q^3+13q^2-9q+2+\delta_{pq}(-64q^4+112q^3-108q^2+40q-4))}{p-q+\delta_{pq}(2q-1)^2} \right) \end{aligned} \quad (4.103)$$

4.2. GENERALISED MULTIPOLAR EXPANSION OF THE VSH OF THE
KNOTTED SOLUTIONS TO MAXWELL'S EQUATIONS METHOD

Where,

$$Z = k^2 r^2 - \frac{p(2-\delta_{pq})-q\delta_{pq}-l-3\delta_{pq}}{p(2-\delta_{pq})-q\delta_{pq}-l+\delta_{pq}-2-\delta_{fg}},$$

$$\delta_{pq} = \begin{cases} 1, & \text{If } p = q. \\ 0, & \text{Otherwise.} \end{cases} \quad (4.104)$$

$$\delta_f = \begin{cases} 1, & \text{Potential field.} \\ 0, & \text{Dual potential field.} \end{cases}$$

For: $r^{-1} g_{l,m}(\mathbf{r})$ attached to $\mathbf{W}_{l,m}$ for the \mathbf{A} and \mathbf{C} fields:

The pre-factor:

$$\mathcal{H} = \left[\frac{m}{|m|} \right]^{l+\delta_f} \frac{2^{p+q+l-2} p! q! l! (-1)^{q-\delta_{pq}+\delta_f} (-i)^{2p+q-l+\delta_f} k^l r^{l-1}}{(p+q+l)! (k^2 r^2 + 1)^{p+q+1-\delta_{pq}}} \left(\frac{\Gamma(l) \Gamma(l+q+1) (l+1) \pi}{\Gamma(q)^2 \Gamma(l-q+1) \Gamma(l+2)} \right)^{\frac{1}{2}} \quad (4.105)$$

The last term:

$$r^{-1} g_{l,m}(\mathbf{r}) = \mathcal{H} \frac{2(q-p+\frac{1}{2}\delta_{pq})(4p-3)^{\delta_{pq}}}{q(2(p+q-1)+3-4\delta_{pq})} Z. \quad (4.106)$$

The second last term:

$$r^{-1} g_{l,m}(\mathbf{r}) = \frac{\mathcal{H}}{q} ((p-q-1-\delta_{pq})(2p-2)) Z^2 + (6p^2-6q^2-4p-2+\delta_{pq}(24p^2-12p+4)) Z + (8p^3+(8q-6)p^2+(-8q^2-1)p-8q^3+6q^2-3q-1+\delta_{pq}(-64p^3+56p^2-2p-2)). \quad (4.107)$$

The third last term:

$$r^{-1} g_{l,m}(\mathbf{r}) = \mathcal{H} \frac{(p+q-1)}{q} \left(\frac{(p-q-2+\delta_{pq}(4q^2-7q+5))}{2(\delta_{pq}(p+q)-1)} \right) Z^3 + \frac{4(p^3+(q-4)p^2+(-q^2-8q+\frac{17}{4})p-q^3-4q^2+\frac{7}{4}q-\frac{1}{2})+\delta_{pq}(16q^3+8q^2+31q-13)}{(-\delta_{pq}(p+q)+2q+2p-1)} Z^2 + (2(-p^3+(-q+8)p^2+(q^2+20q-11)p+q^3+12q^2-q-2)+\delta_{pq}(16q^3-180q^2+162q-50)) Z + (-12p^3+(-44q+24)p^2+(-52q^2+32q+4)p-20q^3+8q^2+12q-8)+\delta_{pq}(32q^3+184q^2-228q+68) \quad (4.108)$$

Where,

$$Z = k^2 r^2 + (-1)^{p+q-l} (p+q-\delta_{pq}+l+1).$$

$$\delta_{pq} = \begin{cases} 1, & \text{If } p = q. \\ 0, & \text{Otherwise.} \end{cases} \quad (4.109)$$

$$\delta_f = \begin{cases} 1, & \text{Potential field.} \\ 0, & \text{Dual potential field.} \end{cases}$$

4.2. GENERALISED MULTIPOLAR EXPANSION OF THE VSH OF THE
KNOTTED SOLUTIONS TO MAXWELL'S EQUATIONS METHOD

For: $r^{-1} h_{l,m}(\mathbf{r})$ attached to $\mathbf{X}_{l,m}$ for the **A**, **C**, **E** and **B** fields:

The pre-factor:

$$\mathcal{H} = \left[\frac{m}{|m|} \right]^{l+\delta_f} \frac{2^{p+q+l+1-\delta_{pf}} (p+q)^{1-\delta_{pf}} p! q! l! (-1)^{l-p+\delta_{pf}} (-i)^{2p+q-l-\delta_f-1+2\delta_{pf}} k^{l+2-\delta_{pf}} r^l}{(p+q+l)! (k^2 r^2 + 1)^{p+q+1-\delta_{pf}}} \left(\frac{\Gamma(l) \Gamma(l+q+1) (2l+1) \pi}{\Gamma(q)^2 \Gamma(l-q+1) \Gamma(l+2)} \right)^{\frac{1}{2}} \quad (4.110)$$

The last term:

$$r^{-1} h_{l,m}(\mathbf{r}) = \mathcal{H}. \quad (4.111)$$

The second last term:

$$r^{-1} h_{l,m}(\mathbf{r}) = \mathcal{H} (p+q-1) Z. \quad (4.112)$$

The third last term:

$$r^{-1} h_{l,m}(\mathbf{r}) = \mathcal{H} (p+q-2) \left(\frac{(2p+2q-3)}{4} Z^2 - Z - 1 \right) \quad (4.113)$$

The fourth last term:

$$r^{-1} h_{l,m}(\mathbf{r}) = \mathcal{H} (p+q-2) (p+q-3) Z \left(\frac{(2p+2q-5)}{12} Z^2 - Z - 1 \right) \quad (4.114)$$

Where,

$$\begin{aligned} Z &= k^2 r^2 - 1. \\ \delta_{pf} &= \begin{cases} 1, & \text{Potential field.} \\ 0, & \text{Field.} \end{cases} \\ \delta_f &= \begin{cases} 1, & \text{Magnetic, or magnetic vector potential.} \\ 0, & \text{Electric, or dual potential.} \end{cases} \end{aligned} \quad (4.115)$$

4.3 Summary

The aim of this chapter was to understand the methods used by Irvine and Bouwmeester, and later, Irvine, to conduct a multipole expansion on the Hopf-knotted and torus-knotted fields. It has shown that, although their results were remarkable at the time, they are no longer suitable for application in their proposed experimental verification. This is primarily due to the limitations forced upon them by their own assumptions. It has been demonstrated that the equations, initially derived by Jackson, cannot be obtained without the variable t , always being valid. Therefore, the multipole coefficient equations cannot be derived, if fixing $t = 0$ - as is the case in the work of Irvine and Bouwmeester. In addition, the Hopf-knotted fields do not contain an exponential time-dependency.

An extension to the results of Irvine and Bouwmeester was undertaken and showed drastically different results to those published in Irvine's later paper. The results displayed a prescription that: as the winding number q got higher, whilst $p = 1$, a pure multipole would appear - giving a higher pure multipole term for each increasing value of q ; or if p and q varied, then coefficients would have contributions from the number of multipole terms dictated by p , starting with angular momentum number, $l = q$.

As the published literature proved insufficient, this chapter aimed to provide an alternative approach. Utilising a method given by Blatt and Weisskopf, a completely general multipole expansion was applied to the Hopf-knotted and torus-knotted fields and potentials. This method successfully produced all the multipole coefficients for the first 49 different combinations of knots. Patterns between the multipolar coefficients were recorded and relationships between the fields and potentials emerged. Triangular numbers also appeared integral, as binomial expansion coefficients were found in *all* the multipole coefficients. As these patterns were further investigated, a complete set of scripts, and therefore equations, were produced to describe each field and potential in terms of the winding numbers, p and q , the radius, r , and the angular momentum numbers, l and m . This apparent relation is one that requires further investigation - ideally to find an analytic solution.³⁷

³⁷See Chapter Five for suggestions of further work.

CONCLUSIONS

This thesis has described a project that has advanced the knowledge of knotted electromagnetic fields and electromagnetism. It has focused on two distinct areas: Lipkin's zilches in unusual electromagnetic fields; and the conduct of a multipole expansion on the vector spherical harmonics of the knotted electromagnetic fields. As such, this concluding chapter is devoted to the research chapters discussing these areas. The remaining chapter, Chapter Two of this thesis, consisted of a detailed analysis of the literature and background to the science on which this thesis is based. It allowed for deeper understanding of the current academic landscape and afforded a suitable position from which to start the research chapters.

For the last 55 years, physical understanding of Lipkin's zilch has remained elusive. Chapter Three presented the components of the zilch in three examples that provide a new way of viewing them, which sheds considerable light on their interpretation. The examples involved three sets of families of vacuum electromagnetic solutions - all of which were developed in the same manner - through Bateman's construction. It was found that all solutions deliberated resulted in converging values - when their densities were integrated over all space. When taking into account their scalar field plots (for constant magnitude, $\phi_{1,2}$), they all produced closed surfaces. Chapter Three identified two, core findings into which the results can be divided: the zilches can be written entirely in terms of the known conserved quantities of the field (energy, momentum, angular momentum and helicity); and it ascertained that the zilches contain information about the topology of the fields. Further to this, second strand, more detailed and specific properties were established for the knotted fields the crossing and unknotting numbers were found, in terms of the $Z_{p,q}^{110}$. Finally, the chapter observed

an unquantified correlation between the zilches and the degree of chirality in the field.

Future work on the zilches might involve exploring further examples to attempt to determine a general theory confirming or denying the conjecture given here - suggesting that these results are only possible in convergent solutions. Further exploration of the topological nature of the zilches, and the exact mechanism that causes it, would be of worth because it could allow them to be used experimentally to determine how the topology of fields changes with time. Strong links between the zilches and the topology of these fields has been established. Rather than continuing to pursue a physical interpretation, a more fruitful way of viewing them is one of a topological invariant.

An interpretation of the components of zilch have been demonstrated in a number of examples of this class of fields, in terms of both the physically conserved properties associated with the electromagnetic fields, and in terms of their topology. It is speculated that this may only be possible for fields of which properties are convergent. Exploration to find any through diverging solutions were unsuccessful. This chapter has taken the opportunity to investigate the zilches in a previously unconsidered arena - knotted electromagnetic fields - and gave a fresh insight into their properties. These properties are expected to give the zilches a more central role in future electromagnetic theory.

The second aspect of this thesis concentrated on the multipole expansion of the knotted fields and potentials. Chapter Four ascertained that the work of Irvine, and the collaborative work of Irvine and Bouwmeester, in conducting a multipole expansion of the vector spherical harmonics, is no longer applicable for application in their proffered experimental validation. It was established, here, that the multipole coefficient equations cannot be obtained without the variable, t , being valid. Therefore, this thesis claims that the multipole coefficient equations cannot be derived if fixing $t = 0$. Additionally, it was maintained that the Hopf-knotted fields do not contain an exponential time-dependency in their equations.

This thesis went on to provide an extension to the results of Irvine and Bouwmeester. Subsequent results were distinct from those previously published by Irvine. It was found that: when holding the winding number $p = 1$ and increasing the value of q , a pure multipole would appear - giving a higher pure multipole term for each higher

value of q ; or if p and q were both varied, then coefficients would have contributions from the number of multipole terms dictated by p , starting with angular momentum number, $l = q$.

Finally, Chapter Four gave an alternative approach to that of Irvine and Bouwmeester. A general, multipole expansion was applied to Hopf-knotted and torus-knotted fields and potentials. This resulted in the successful production of all multipole coefficients for the first 49 combinations of knots. As patterns were observed, a complete script, and therefore equations, were formed to portray each field and potential in terms of the winding numbers, p and q , the radius, r , and the angular momentum numbers, l and m .

This work has stated that, to an extent, the original work of Irvine and Bouwmeester is unfitting. This dictates that their final experimental verification is affected and requires attention. Further work in this area might possibly take two routes: an attempt to improve upon the original results of Irvine and Bouwmeester, to achieve experimental verification of the knotted solutions to Maxwell's equations; or an effort to find an analytic solution that describes the multipole coefficients indefinitely. The former of these routes would need to consider the method of Irvine and Bouwmeester in generating the knotted solutions through circularly polarised plane waves. The possibility of this producing tangible results may be affected by the fact there is no exponential time dependency in the new multipolar expansion solutions.

As the knotted electric and magnetic field lines fill all of space, the likelihood that they can be experimentally verified globally through superpositions of plane waves is unlikely. There could be a possibility of creating a local approximation to them experimentally for an instant in time, but as the fields expand out radially with the speed of light and propagate linearly in the z -direction at the same time, it is unlikely that this could be fulfilled at later times.

The aim of this thesis was to contribute to the body of knowledge of electromagnetic theory through exploration of two, distinct projects, related through a topological formalism of Maxwell's equations and the Hopf fibration. This thesis' exploration of Lipkin's zilches in unusual, electromagnetic fields has enhanced our understanding by providing unique insight which identifies the zilches' deep connection with topology. The subsequent work on the multipolar expansion of the vector spherical harmonics of

the knotted electromagnetic fields has provided a thorough study into the assumptions made in the current literature and presented a viable alternative. The hope is that this work can inspire further progression within the area of electromagnetism and advance our overall understanding.

BIBLIOGRAPHY

- [1] Maxwell JC. A Dynamical Theory of the Electromagnetic Field. Philosophical transactions of the Royal Society of London. 1865;155:459–512.
- [2] Jackson JD. Classical Electrodynamics. AAPT; 1999.
- [3] Rañada AF. A Topological Theory of the Electromagnetic Field. Letters in Mathematical Physics. 1989;18(2):97–106.
- [4] Robinson I. Null Electromagnetic Fields. Journal of Mathematical Physics. 1961;2(3):290–291.
- [5] Trautman A. Solutions of the Maxwell and Yang-Mills equations associated with Hopf fibrings. International Journal of Theoretical Physics. 1977;16(8):561–565.
- [6] Bateman H. The Mathematical Analysis of Electrical and Optical Wave-motion on the Basis of Maxwell's Equations: By H. Bateman... University press; 1915.
- [7] Lyons DW. An Elementary Introduction to the Hopf Fibration. Mathematics magazine. 2003;76(2):87–98.
- [8] Ranada AF. Knotted Solutions of the Maxwell Equations in Vacuum. Journal of Physics A: Mathematical and General. 1990;23(16):L815.
- [9] Ranada AF. On Topology and Electromagnetism. Annalen der Physik. 2012;524(2).
- [10] Ranada AF, Trueba JL. A Topological Mechanism of Discretization for the Electric Charge. Physics Letters B. 1998;422(1):196–200.
- [11] Rañada AF, Trueba JL. Electromagnetic Knots. Physics Letters A. 1995;202(5-6):337–342.

- [12] Rañada AF, Trueba JL. Two Properties of Electromagnetic Knots. *Physics Letters A*. 1997;232(1-2):25–33.
- [13] Bialynicki-Birula I. Electromagnetic Vortex Lines Riding atop Null Solutions of the Maxwell Equations. *Journal of Optics A: Pure and Applied Optics*. 2004;6(5):S181.
- [14] Robinson I, Trautman A. *New Theories in Physics: Proc. Warsaw Symp. on Elementary Particle Physics* ed Z Ajduk et al. Singapore: World Scientific; 1989.
- [15] Irvine WTM. Linked and Knotted Beams of Light, Conservation of Helicity and the Flow of Null Electromagnetic Fields. *Journal of Physics A: Mathematical and Theoretical*. 2010;43(38):385203.
- [16] Kedia H, Bialynicki-Birula I, Peralta-Salas D, Irvine WTM. Tying Knots in Light Fields. *Physical review letters*. 2013;111(15):150404.
- [17] Milnor J. *Singular Points of Complex Hypersurfaces.(AM-61)*. vol. 61. Princeton University Press; 2016.
- [18] Irvine WTM, Bouwmeester D. Linked and Knotted Beams of Light. *Nature Physics*. 2008;4(9):716–720.
- [19] Thomson W. VI.on Vortex Motion. *Earth and Environmental Science Transactions of the Royal Society of Edinburgh*. 1868;25(1):217–260.
- [20] Knots PTO. I, II, III. *Scientific Papers I*. Cambridge University Press, Cambridge; 1898.
- [21] Michelson AA, Morley EW. On the Relative Motion of the Earth and of the Luminiferous Ether. *Sidereal Messenger*, vol 6, pp 306-310. 1887;6:306–310.
- [22] Adams CC. *The Knot Book: An Elementary Introduction to the Mathematical Theory of Knots*. American Mathematical Soc.; 2004.
- [23] Brasher R, Scharein RG, Vazquez M. *New Biologically Motivated Knot Table*. Portland Press Limited; 2013.
- [24] Thurston WP. *The Geometry and Topology of Three-Manifolds*. Princeton University Princeton, NJ; 1979.

- [25] Chris T. Nested Tori; 2012. 2019-01-10.
<http://www.nestedtori.com/2012/10/welcome-to-nested-tori.html>.
- [26] Scharlemann MG. Unknotting Number One Knots are Prime. *Inventiones mathematicae*. 1985;82(1):37–55.
- [27] Alexander JW. Topological Invariants of Knots and Links. *Transactions of the American Mathematical Society*. 1928;30(2):275–306.
- [28] Jones VFR. A Polynomial Invariant for Knots via Von Neumann Algebras. In: *Fields Medallists' Lectures*. World Scientific; 1997. p. 448–458.
- [29] Hopf H. Über die Abbildungen der Dreidimensionalen Sphäre auf die Kugelfläche. *Mathematische Annalen*. 1931;104(1):637–665.
- [30] May JP. *A Concise Course in Algebraic Topology*. University of Chicago press; 1999.
- [31] Urbantke HK. The Hopf Fibration Seven Times in Physics. *Journal of Geometry and Physics*. 2003;46(2):125–150.
- [32] Ryder LH. Dirac Monopoles and the Hopf Map S^3 to S^2 . *Journal of Physics A: Mathematical and General*. 1980;13(2):437.
- [33] Hogan PA. Bateman Electromagnetic waves. *Proceedings of the Royal Society of London Series A, Mathematical and Physical Sciences*. 1984;p. 199–204.
- [34] Silberstein L. Elektromagnetische Grundgleichungen in Bivektorieller Behandlung. *Annalen der Physik*. 1907;327(3):579–586.
- [35] Penrose R. Twistor Algebra. *Journal of Mathematical physics*. 1967;8(2):345–366.
- [36] Griffiths DJ. *Introduction to Electrodynamics*. Prentice Hall; 1962.
- [37] Dennis MR, King RP, Jack B, OHolleran K, Padgett MJ. Isolated Optical Vortex Knots. *Nature Physics*. 2010;6(2):118–121.
- [38] Smith G, Strange P. Lipkin's Conservation Law in Vacuum Electromagnetic Fields. *Journal of Physics A: Mathematical and Theoretical*. 2018;.

- [39] Smith G, Strange P. Properties of null knotted solutions to Maxwell's equations. ProcSPIE. 2017;10120:10120 – 10120 – 6. Available from: <https://doi.org/10.1117/12.2260484>.
- [40] Hoyos C, Sircar N, Sonnenschein J. New Knotted Solutions of Maxwell's Equations. Journal of Physics A: Mathematical and Theoretical. 2015;48(25):255204. Available from: <http://stacks.iop.org/1751-8121/48/i=25/a=255204>.
- [41] Surot. Inside-Out Torus; 2008. 2019-01-10. [https://en.wikipedia.org/wiki/File:Inside-out_torus_\(animated,_s_mall\).gif](https://en.wikipedia.org/wiki/File:Inside-out_torus_(animated,_s_mall).gif).
- [42] Banchoff T. The Flat Torus in the Three-Sphere;. 2019-01-11. <http://www.geom.uiuc.edu/~banchoff/script/b3d/hypertorus.html>.
- [43] University of Oxford MI. Dupin Cyclides; 2015. 2019-01-11. <https://www.maths.ox.ac.uk/about-us/departmental-art/dupin-cyclides>.
- [44] Lipkin DM. Existence of a New Conservation Law in Electromagnetic Theory. Journal of Mathematical Physics. 1964;5(5):696–700.
- [45] Candlin DJ. Analysis of the New Conservation Law in Electromagnetic Theory. Il Nuovo Cimento (1955-1965). 1965;37(4):1390–1395.
- [46] Morgan TA. Two Classes of New Conservation Laws for the Electromagnetic Field and for other Massless Fields. Journal of Mathematical Physics. 1964;5(11):1659–1660.
- [47] O'Connell RF, Tompkins DR. Generalized Solutions for Massless Free Fields and Consequent Generalized Conservation Laws. Journal of Mathematical Physics. 1965;6(12):1952–1954.
- [48] Kibble TWB. Conservation Laws for Free Fields. Journal of Mathematical Physics. 1965;6(7):1022–1026.
- [49] Noether E. Invariante Variationsprobleme, Nachr. d. König. Gesellsch. d. Wiss. zu Göttingen, Math-phys. Klasse (1918), 235-257. English Reprint: [physics/0503066](https://arxiv.org/abs/physics/0503066). 1918;p. 57.
- [50] Cameron RP, Barnett SM, Yao AM. Optical Helicity, Optical Spin and Related Quantities in Electromagnetic Theory. New Journal of Physics. 2012;14(5):053050. Available from: <http://stacks.iop.org/1367-2630/14/i=5/a=053050>.

- [51] Philbin TG. Lipkin's Conservation Law, Noether's Theorem, and the Relation to Optical Helicity. *Physical Review A*. 2013;87(4):043843.
- [52] Calkin MG. An Invariance Property of the Free Electromagnetic Field. *American Journal of Physics*. 1965;33(11):958–960.
- [53] Przanowski M, Rajca B, Tosiek J. On Some Conservation Laws in the Maxwell Electrodynamics in Vacuum. *Acta Physica Polonica Series B*. 1994;25(7):1065–1077.
- [54] Tang Y, Cohen AE. Optical Chirality and its Interaction with Matter. *Physical Review Letters*. 2010;104(16):163901.
- [55] Yang N, Cohen AE. Local Geometry of Electromagnetic Fields and its Role in Molecular Multipole Transitions. *The Journal of Physical Chemistry B*. 2011;115(18):5304–5311.
- [56] Bliokh KY, Nori F. Characterizing Optical Chirality. *Physical Review A*. 2011;83(2):021803.
- [57] Coles MM, Andrews DL. Chirality and Angular Momentum in Optical Radiation. *Physical Review A*. 2012;85(6):063810.
- [58] Andrews DL, Coles MM. Measures of Chirality and Angular Momentum in the Electromagnetic Field. *Optics letters*. 2012;37(15):3009–3011.
- [59] Chandrasekhar S, Kendall PC. On Force-Free Magnetic Fields. *The Astrophysical Journal*. 1957;126:457.
- [60] Abramowitz M, Stegun IA. *Handbook of Mathematical Functions: with Formulas, Graphs, and Mathematical Tables*. vol. 55. Courier Corporation; 1964.
- [61] Blatt JM, Weisskopf VF. *Theoretical Nuclear Physics*. Springer Science & Business Media; 2012.
- [62] Hill EL. The Theory of Vector Spherical Harmonics. *American Journal of Physics*. 1954;22(4):211–214.

FIELD COMPONENTS FOR THE DIFFERENT $P - Q$
KNOT-TYPES

$p = 1, q = 2$

Initial Field Components:

$$\mathbf{E}(\mathbf{r}, t = 0) = -\frac{16}{(1+r^2)^4} \begin{pmatrix} x^3 - 3xy^2 - xz^2 - 2yz + x, \\ 3x^2y - y^3 + yz^2 - 2zx - y, \\ 2(x^2z - y^2z + 2xy) \end{pmatrix} \quad (\text{A.1})$$

$$\mathbf{B}(\mathbf{r}, t = 0) = -\frac{16}{(1+r^2)^4} \begin{pmatrix} -3x^2y + y^3 + yz^2 - 2zx - y, \\ x^3 - 3xy^2 + xz^2 + 2yz - x, \\ 2(-2xyz + x^2 - y^2) \end{pmatrix}$$

$p = 1, q = 3$

Initial Field Components:

$$\mathbf{E}(\mathbf{r}, t = 0) = -\frac{48}{(1+r^2)^5} \begin{pmatrix} x^4 - 6x^2y^2 - x^2z^2 + y^4 + y^2z^2 - 4xyz + x^2 - y^2, \\ 2(2x^3y - 2xy^3 + xyz^2 - x^2z + y^2z - xy), \\ 2(x^3z - 3xy^2z + 3x^2y - y^3) \end{pmatrix}$$
$$\mathbf{B}(\mathbf{r}, t = 0) = -\frac{48}{(1+r^2)^5} \begin{pmatrix} 2(-2x^3y + 2xy^3 + xyz^2 - x^2z + y^2z - xy), \\ x^4 - 6x^2y^2 + x^2z^2 + y^4 - y^2z^2 + 4xyz - x^2 + y^2, \\ 2(-3x^2yz + y^3z + x^3 - 3xy^2) \end{pmatrix} \quad (\text{A.2})$$

$p = 2, q = 1$

Initial Field Components:

$$\begin{aligned}
\mathbf{E}(\mathbf{r}, t = 0) &= -\frac{8}{(1+r^2)^4} \begin{pmatrix} x^4 - y^4 - 2y^2z^2 - z^4 + 4xyz + 2y^2 + 6z^2 - 1, \\ 2(x^3y + xy^3 + xyz^2 - 2x^2z - 2z^3 - xy + 2z), \\ 2(x^3z + xy^2z + xz^3 + x^2y + y^3 + 3yz^2 - 3xz - y) \end{pmatrix} \\
\mathbf{B}(\mathbf{r}, t = 0) &= -\frac{8}{(1+r^2)^4} \begin{pmatrix} 2(-x^3y - xy^3 - xyz^2 - 2y^2z - 2z^3 + xy + 2z), \\ x^4 + 2x^2z^2 - y^4 + z^4 + 4xyz - 2x^2 - 6z^2 + 1, \\ 2(-x^2yz - y^3z - yz^3 + x^3 + xy^2 + 3xz^2 + 3yz - x) \end{pmatrix}
\end{aligned} \tag{A.3}$$

$p = 2, q = 2$

Initial Field Components:

$$\begin{aligned}
\mathbf{E}(\mathbf{r}, t = 0) &= -\frac{32}{(1+r^2)^5} \begin{pmatrix} x^5 - 2x^3y^2 - 3xy^4 - 4xy^2z^2 - xz^4 + 4x^2yz - 4y^3z - 4yz^3 + 4xy^2 + 6xz^2 + 4yz - x, \\ 3x^4y + 2x^2y^3 + 4x^2yz^2 - y^5 + yz^4 - 4x^3z + 4xy^2z - 4xz^3 - 4x^2y - 6yz^2 + 4xz + y, \\ 2(x^4z + x^2z^3 - y^4z - y^2z^3 + 2x^3y + 2xy^3 + 6xyz^2 - 3x^2z + 3y^2z - 2xy) \end{pmatrix} \\
\mathbf{B}(\mathbf{r}, t = 0) &= -\frac{32}{(1+r^2)^5} \begin{pmatrix} -3x^4y - 2x^2y^3 - 2x^2yz^2 + y^5 + 2y^3z^2 + yz^4 - 8xy^2z - 4xz^3 + 2x^2y - 2y^3 - 6yz^2 + 4xz + y, \\ x^5 - 2x^3y^2 + 2x^3z^2 - 3xy^4 - 2xy^2z^2 + xz^4 + 8x^2yz + 4yz^3 - 2x^3 + 2xy^2 - 6xz^2 - 4yz + x, \\ 2(-2x^3yz - 2xy^3z - 2xyz^3 + x^4 + 3x^2z^2 - y^4 - 3y^2z^2 + 6xyz - x^2 + y^2) \end{pmatrix}
\end{aligned} \tag{A.4}$$

$p = 3, q = 1$

Initial Field Components:

$$\begin{aligned}
\mathbf{E}(\mathbf{r}, t = 0) &= -\frac{12}{(1+r^2)^7} \begin{pmatrix} x^6 + x^4y^2 + x^2z^2 - x^2y^4 - 2x^2y^2z^2 - x^2z^4 - y^6 - 3y^4z^2 - 3y^2z^4 - z^6 + 8x^3yz + 8xy^3z + 8xyz^3 - x^4 + 2x^2y^2 + 6x^2z^2 + 3y^4 + 18y^2z^2 + 15z^4 - 8xyz - x^2 - 3y^2 - 15z^2 + 1, \\ 2(x^5y + 2x^3y^3 + 2x^3yz^2 + xy^5 + 2xy^3z^2 + xyz^4 - 3x^4z - 2x^2y^2z - 6x^2z^3 + y^4z - 2y^2z^3 - 3z^5 - 2x^3y - 2xy^3 - 6xyz^2 + 6x^2z + 2y^2z + 10z^3 + xy - 3z), \\ 2(x^5z + 2x^3y^2z + 2x^3z^3 + xy^4z + 2xy^2z^3 + xz^5 + x^4y + 2x^2y^3 + 6x^2yz^2 + y^5 + 6y^3z^2 + 5yz^4 - 6x^3z - 6xy^2z - 10xz^3 - 2x^2y - 2y^3 - 10yz^2 + 5xz + y), \\ 2(-x^5y - 2x^3y^3 - 2x^3yz^2 - xy^5 - 2xy^3z^2 - xyz^4 + x^4z - 2x^2y^2z - 2x^2z^3 - 3y^4z - 6y^2z^3 - 3z^5 + 2x^3y + 2xy^3 + 6xyz^2 + 2x^2z + 6y^2z + 10z^3 - xy - 3z), \end{pmatrix} \\
\mathbf{B}(\mathbf{r}, t = 0) &= -\frac{12}{(1+r^2)^7} \begin{pmatrix} x^6 + x^4y^2 + 3x^4z^2 - x^2y^4 + 2x^2y^2z^2 + 3x^2z^4 - y^6 - y^4z^2 + y^2z^4 + z^6 + 8x^3yz + 8xy^3z + 8xyz^3 - 3x^4 - 2x^2y^2 - 18x^2z^2 + y^4 - 6y^2z^2 - 15z^4 - 8xyz + 3x^2 + y^2 + 15z^2 - 1, \\ 2(-x^4yz - 2x^2y^3z - 2x^2yz^3 - y^5z - 2y^3z^3 - yz^5 + x^5 + 2x^3y^2 + 6x^3z^2 + xy^4 + 6xy^2z^2 + 5xz^4 + 6x^2yz + 6y^3z + 10yz^3 - 2x^3 - 2xy^2 - 10xz^2 - 5yz + x) \end{pmatrix}
\end{aligned} \tag{A.5}$$

MULTIPOLE COEFFICIENT GENERATION, $R^{-1}F_{L,M}$,
FOR THE V-VSH, FOR THE ELECTRIC (C) AND
MAGNETIC (A) VECTOR POTENTIALS

Below is the Maple script used to generate the multipole coefficients, $r^{-1}f_{l,m}$, for the Electric and Magnetic Vector Potentials in terms of only their windings numbers p and q , their angular momentum numbers l and m , and the radius, r .

> # *V – Vector Spherical Harmonic (VSPH) – Electric Potential field (C), & Magnetic Potential field (A)*

> # *Writing the Multipole Coefficients in terms of the Winding numbers of the Torus knots, and the radius*

This script has been written to determine the form of the multipolar coefficients for the V vector – spherical-harmonic (VSPH) term of the magnetic potential field (A) and electric potential field (C). To use this script, simply input your choice of variables into the 'Input Variables Required' section, then run the whole script using the buttons ctrl + shift + enter. Then look for the required multipole term below. The variables below have the following meanings : p, q, are the winding numbers; k, is a scaling constant with dimensions of inverse length; r, is the radius with dimensions of length; l, m are the angular momentum numbers.

> restart

> # *Input Variables Required*

> p := 5

$$p := 5 \quad (1)$$

> q := 5

$$q := 5 \quad (2)$$

> l := 7

$$l := 7 \quad (3)$$

> m := 5

$$m := -5 \quad (4)$$

> *Field := electric* # *Input either 'electric' or 'magnetic' here*
Field := electric

(5)

> *if Field = magnetic then F := 1 else F := 0 end if*
F := 0

(6)

> *if p = q then p_q := 1 else p_q := 0 end if*

$$p_q := 1 \quad (7)$$

> *if -2·p + l + 2 + p_q = 0 then Fg := 1 else Fg := 0 end if*
Fg := 1

(8)

$$Z := \left(k^2 r^2 - \frac{p \cdot (2 - p_q) - q \cdot (p_q) - l - 3 \cdot p_q}{p \cdot (2 - p_q) - q \cdot (p_q) - l + p_q - 2 - Fg} \right)$$

$$Z := k^2 r^2 - \frac{10}{9} \quad (9)$$

$$\text{Prefactor} := \text{simplify} \left(\left(\frac{m}{(m^2)^{\frac{1}{2}}} \right)^{2 \cdot p + 2 \cdot q - l + F} \cdot \frac{1}{(p + q + l + 1)! \cdot (k^2 \cdot r^2 + 1)^{p + q + 1 - p_q}} \left(2^{p + q + l + 1} \cdot (p + q) \cdot p! \cdot (q)! \cdot l! \cdot (-1)^l \right)^{+p - p_q + F} \cdot (-1)^{3 \cdot l + 5 \cdot q + 2 \cdot p - 2 \cdot p_q + F} \cdot k^{l + 2} \cdot r^{l + 1} \cdot (\text{binomial}(l - 1, q - 1)) \right)$$

$$\cdot \text{binomial}(q+l, q-1) \cdot l \cdot \pi \left. \right)^{\frac{1}{2}} \left. \right)$$

$$\text{Prefactor} := -\frac{204800}{459459} \frac{k^9 r^8 \sqrt{231} \sqrt{\pi}}{(k^2 r^2 + 1)^{10}} \quad (10)$$

$$> \text{Last_term} := \frac{\text{Prefactor} \cdot (-p^2 + q^2 - p + q + p_q \cdot (2 \cdot q \cdot (p + q)))}{2 \cdot q \cdot (p + q)}$$

$$\text{Last_term} := -\frac{204800}{459459} \frac{k^9 r^8 \sqrt{231} \sqrt{\pi}}{(k^2 r^2 + 1)^{10}} \quad (11)$$

$$> \text{Second_Last_Term} := \frac{\text{Prefactor} \cdot Z^{1-Fg} \cdot (p + q - p_q) \cdot (q - p + 1 + p_q \cdot (8 \cdot p^2 - 6 \cdot p) + 2 \cdot Fg)}{2 \cdot q \cdot (4 \cdot p)^{p-q}}$$

$$\text{Second_Last_Term} := -\frac{177152}{51051} \frac{k^9 r^8 \sqrt{231} \sqrt{\pi}}{(k^2 r^2 + 1)^{10}} \quad (12)$$

$$> \text{Third_Last_Term} := \text{simplify} \left(\text{expand} \left(\frac{(\text{Prefactor}) \cdot (q-1+p)}{8 \cdot q \cdot (p+q)} \cdot \left((-2p^3 + (-2q+7)p^2 \right. \right. \right.$$

$$\left. \left. \left. + (2q^2 + 8q - 7)p + 2q^3 + q^2 - 5q + 2 + p_q \cdot (16q^3 - 60q^2 + 52q - 14) \right) \cdot Z^2 \right. \right.$$

$$\left. \left. - \frac{1}{(p-q+p_q \cdot (2q-1))} \left(4 \cdot (-p^3 + (q-2) \cdot p^2 + (q^2 - 8q + 5) \cdot p - q^3 - 6 \cdot q^2 + 7 \cdot q \right. \right. \right.$$

$$\left. \left. \left. - 2 \right) - p_q \cdot (-64q^3 + 56q^2 - 16q) \right) \cdot Z + \frac{1}{(p-q+p_q \cdot (2q-1))^2} \left(4 \cdot (p^4 + (-2 \right.$$

$$\left. \left. \left. \cdot q + 1) \cdot p^3 + (q-1) \cdot p^2 + (2 \cdot q^3 + 3 \cdot q^2 + 4 \cdot q - 3) \cdot p - q^4 - 5 \cdot q^3 + 13 \cdot q^2 - 9 \cdot q + 2 \right) \right. \right.$$

$$\left. \left. \left. + p_q \cdot (-64q^4 + 112q^3 - 108q^2 + 40q - 4) \right) \right) \right), 'size')$$

$$\text{Third_Last_Term} := -\frac{32768}{51051} \frac{k^9 r^8 \sqrt{231} \sqrt{\pi} (17k^4 r^4 - 47k^2 r^2 + 26)}{(k^2 r^2 + 1)^{10}} \quad (13)$$

[>

MULTIPOLE COEFFICIENT GENERATION, $R^{-1}F_{L,M}$,
FOR THE V-VSH, FOR THE ELECTRIC (E) AND
MAGNETIC (B) FIELDS

Below is the Maple script used to generate the multipole coefficients, $r^{-1}f_{l,m}$, for the Electric and Magnetic fields in terms of only their windings numbers p and q , their angular momentum numbers l and m , and the radius, r .

> # **V – Vector Spherical Harmonic (VSPH) – Electric field (E), & Magnetic field (B)**

> # **Writing the Multipole Coefficients in terms of the Winding numbers of the Torus knots, angular momentum numbers and the radius**

This script has been written to determine the form of the multipolar coefficients for the **V vector – spherical-harmonic (VSPH)** term of the **electric field (E)** and **magnetic field (B)**. To use this script, simply input your choice of variables into the **'Input Variables Required'** section, then run the whole script using the buttons **ctrl + shift + enter**. Then look for the required multipole term below. The variables below have the following meanings : $p, q,$ are the winding numbers; $k,$ is a scaling constant with dimensions of inverse length; $r,$ is the radius with dimensions of length; l, m are the angular momentum numbers.

> restart

> # **Input Variables Required**

> $p := 2$

$$p := 2 \quad (1)$$

> $q := 3$

$$q := 3 \quad (2)$$

> $l := 5$

$$l := 5 \quad (3)$$

> $m := 1$

$$m := 1 \quad (4)$$

> **Field := magnetic** # **Input either 'electric' or 'magnetic' here**
Field := magnetic

(5)

> **if Field = magnetic then F := 1 else F := 0 end if**
F := 1

(6)

> $Z := \left(k^2 r^2 - \frac{l+3}{l+1} \right)$

$$Z := k^2 r^2 - \frac{4}{3} \quad (7)$$

> $Last_term := simplify \left(\left(\frac{m}{(m^2)^{\frac{1}{2}}} \right)^{l+F} \cdot \frac{2^{p+q+l+1} \cdot p! \cdot q! \cdot l! \cdot (-1)^{l+p} \cdot (-1)^{2 \cdot p+q-l-F} \cdot k^{l+3} \cdot r^{l+1} \cdot \left(\frac{\pi \cdot (l+1) \cdot (q+l)!}{(l-q)!} \right)^{\frac{1}{2}}}{(q-1)! \cdot (p+q+l)! \cdot (k^2 \cdot r^2 + 1)^{p+q+1}} \right)$

$$Last_term := \frac{1024}{105} I k^8 r^6 \sqrt{210} \sqrt{\pi} (k^2 r^2 + 1)^6 \quad (8)$$

> $Second_Last_Term := (Last_term) \cdot (p+q-1) \cdot Z$

$$\text{Second_Last_Term} := \frac{\frac{4096}{105} 1 k^8 r^6 \sqrt{210} \sqrt{\pi} \left(k^2 r^2 - \frac{4}{3} \right)}{(k^2 r^2 + 1)^6} \quad (9)$$

$$\text{Third_Last_Term} := \text{simplify} \left(\text{expand} \left((\text{Last_term}) \cdot \left(\frac{(p+q-2) \cdot (2 \cdot p + 2 \cdot q - 3)}{4} \cdot Z^2 - (p+q-1) \cdot Z - \frac{(p+q-1) \cdot (p+q+1)}{(p+q-2)} \right) \right), 'size' \right)$$

$$\text{Third_Last_Term} := \frac{\frac{256}{315} 1 k^8 r^6 \sqrt{210} \sqrt{\pi} (63 k^4 r^4 - 216 k^2 r^2 + 80)}{(k^2 r^2 + 1)^6} \quad (10)$$

$$\text{Fourth_Last_Term} := \text{simplify} \left(\text{expand} \left((\text{Last_term}) \cdot (p+q-2) \cdot \left(\frac{(p+q-3) \cdot (2 \cdot p + 2 \cdot q - 5)}{12} \cdot Z^3 - (p+q-2) \cdot Z^2 - \frac{((p+q-1)^2 + 1)}{(p+q-3)} \cdot Z - \frac{8 \cdot (p+q-1)}{3 \cdot (p+q-3)^2} \right) \right), 'size' \right)$$

$$\text{Fourth_Last_Term} := \frac{\frac{512}{2835} 1 k^8 r^6 \sqrt{210} \sqrt{\pi} (135 k^6 r^6 - 1026 k^4 r^4 + 639 k^2 r^2 + 220)}{(k^2 r^2 + 1)^6} \quad (11)$$

MULTIPOLE COEFFICIENT GENERATION, $R^{-1}G_{L,M}$,
FOR THE W-VSH, FOR THE ELECTRIC (A) AND
MAGNETIC (C) VECTOR POTENTIALS

Below is the Maple script used to generate the multipole coefficients, $r^{-1}g_{l,m}$, for the Electric and Magnetic Vector Potentials in terms of only their windings numbers p and q , their angular momentum numbers l and m , and the radius, r .

> #**W—Vector Spherical Harmonic (VSPH) – Electric Potential field (C),**
 & **Magnetic Potential field (A)**

> #**Writing the Multipole Coefficients in terms of the Winding numbers of the Torus knots, and the radius**

This script has been written to determine the form of the multipolar coefficients for the **W vector – spherical-harmonic (VSPH)** term of the **magnetic potential field (A)** and the **electric potential field (C)**. To use this script, simply input your choice of variables into the **'Input Variables Required'** section, then run the whole script using the buttons **ctrl + shift + enter**. Then look for the required multipole term below. The variables below have the following meanings : p, q , are the winding numbers; k , is a scaling constant with dimensions of inverse length; r , is the radius with dimensions of length; l, m are the angular momentum numbers.

> restart

> #**Input Variables Required**

> $p := 5$

$$p := 5 \quad (1)$$

> $q := 2$

$$q := 2 \quad (2)$$

> $l := 5$

$$l := 5 \quad (3)$$

> $m := 2$

$$m := 2 \quad (4)$$

> **Field := electric** # **Input either 'electric' or 'magnetic' here**
 Field := electric

(5)

> **if Field = magnetic then F := 1 else F := 0 end if**
 F := 0

(6)

> **if p = q then p_q := 1 else p_q := 0 end if**

$$p_q := 0 \quad (7)$$

> $Z := (k^2 r^2 + (-1)^{p+q-l} \cdot (p+q-p_q+l+1))$

$$Z := k^2 r^2 + 13 \quad (8)$$

> Prefactor := simplify $\left(\left(\frac{m}{(m^2)^{\frac{1}{2}}} \right)^{l+F} \cdot \frac{1}{(p+q+l)! \cdot (k^2 \cdot r^2 + 1)^{p+q+1-p_q}} \left(2^{p+q+l-2} \cdot p! \cdot q! \cdot l! \cdot (-1)^{q-p_q+F} \cdot (-1)^{2 \cdot p+q-l+F} \cdot k^l \cdot r^{l-1} \cdot \left((l+1) \cdot \pi \cdot (\text{binomial}(l-1, q-1)) \right) \cdot (\text{binomial}(q+l, q-1)) \right)^{\frac{1}{2}} \right)$

$$\text{Prefactor} := \frac{256}{2079} \frac{1 k^5 r^4 \sqrt{42} \sqrt{\pi}}{(k^2 r^2 + 1)^8} \quad (9)$$

$$\begin{aligned}
& \text{Last_term} := \text{simplify} \left(\text{expand} \left(\frac{2 \cdot \left(q - p + \frac{1}{2} \cdot p \cdot q \right) \cdot (4 \cdot p - 3)^{p-q} \cdot \text{Prefactor}}{q \cdot (2 \cdot (p + q - 1) + 3 - 4 \cdot p \cdot q)} \cdot (Z) \right), 'size' \right) \\
& \text{Last_term} := - \frac{\frac{256}{10395} \text{I} k^5 r^4 \sqrt{42} \sqrt{\pi} (k^2 r^2 + 13)}{(k^2 r^2 + 1)^8} \tag{10}
\end{aligned}$$

$$\begin{aligned}
& \text{Second_Last_Term} := \text{simplify} \left(\text{expand} \left(\frac{(\text{Prefactor})}{q} \cdot \left((p - q - 1 - p \cdot q \cdot (2 \cdot p - 2)) \cdot Z^2 \right. \right. \right. \\
& \quad \left. \left. + (6 \cdot p^2 - 6 \cdot q^2 - 4 \cdot p - 2 + p \cdot q \cdot (24 \cdot p^2 - 12 \cdot p + 4)) \cdot Z + (8 \cdot p^3 + (8 \cdot q - 6) \cdot p^2 + (-8 \right. \right. \\
& \quad \left. \left. \cdot q^2 - 1) \cdot p - 8 \cdot q^3 + 6 \cdot q^2 - 3 \cdot q - 1 + p \cdot q \cdot (-64 \cdot p^3 + 56 \cdot p^2 - 2 \cdot p - 2) \right) \right), 'size' \right) \\
& \text{Second_Last_Term} := - \frac{\frac{256}{2079} \text{I} k^5 r^4 \sqrt{42} \sqrt{\pi} (k^4 r^4 + 78 k^2 r^2 + 1364)}{(k^2 r^2 + 1)^8} \tag{11}
\end{aligned}$$

$$\begin{aligned}
& \text{Third_Last_Term} := \text{simplify} \left(\text{expand} \left(\frac{(p + q - 1) \cdot (\text{Prefactor})}{q} \right. \right. \\
& \quad \cdot \left(\left(\frac{(p - q - 2 + p \cdot q \cdot (4 q^2 - 7 q + 5))}{2 \cdot (p \cdot q \cdot (p + q) - 1)} \cdot Z^3 \right. \right. \\
& \quad \left. \left. + \frac{1}{(-p \cdot q \cdot (p + q) + 2 \cdot q + 2 \cdot p - 1)} \left(4 \cdot \left(p^3 + (q - 4) \cdot p^2 + \left(-q^2 - 8 \cdot q + \frac{17}{4} \right) \cdot p \right. \right. \right. \right. \\
& \quad \left. \left. - q^3 - 4 \cdot q^2 + \frac{7}{4} \cdot q - \frac{1}{2} \right) + p \cdot q \cdot (16 q^3 + 8 q^2 + 31 q - 13) \right) \cdot Z^2 + (2 \cdot (-p^3 + (-q \right. \\
& \quad \left. + 8) \cdot p^2 + (q^2 + 20 \cdot q - 11) \cdot p + q^3 + 12 \cdot q^2 - q - 2) + p \cdot q \cdot (16 q^3 - 180 q^2 + 162 q \right. \\
& \quad \left. - 50) \right) \cdot Z + (-12 p^3 + (-44 q + 24) p^2 + (-52 q^2 + 32 q + 4) p - 20 q^3 + 8 q^2 + 12 q \\
& \quad \left. - 8) + p \cdot q \cdot (32 q^3 + 184 q^2 - 228 q + 68) \right) \right), 'size' \right) \\
& \text{Third_Last_Term} := - \frac{\frac{128}{693} \text{I} k^5 \left(k^6 r^6 + \frac{705}{13} k^4 r^4 - 65 k^2 r^2 + 11 \right) \sqrt{42} r^4 \sqrt{\pi}}{(k^2 r^2 + 1)^8} \tag{12}
\end{aligned}$$

>
>

MULTIPOLE COEFFICIENT GENERATION, $R^{-1}G_{L,M}$,
FOR THE W-VSH, FOR THE ELECTRIC (E) AND
MAGNETIC (B) FIELDS

Below is the Maple script used to generate the multipole coefficients, $r^{-1}g_{l,m}$, for the Electric and Magnetic fields in terms of only their windings numbers p and q , their angular momentum numbers l and m , and the radius, r .

> **#W-Vector Spherical Harmonic (VSPH) - Electric field (E), & Magnetic field (B)**

> **#Writing the Multipole Coefficients in terms of the Winding numbers of the Torus knots, and the radius**

This script has been written to determine the form of the multipolar coefficients for the **W vector -spherical-harmonic (VSPH)** term of the **electric field (E)** and **magnetic field (B)**. To use this script, simply input your choice of variables into the **'Input Variables Required'** section, then run the whole script using the buttons **ctrl + shift + enter**. Then look for the required multipole term below. The variables below have the following meanings : p, q , are the winding numbers; k , is a scaling constant with dimensions of inverse length; r , is the radius with dimensions of length; l, m are the angular momentum numbers.

> restart

> **#Input Variables Required**

> $p := 6$

$$p := 6 \quad (1)$$

> $q := 6$

$$q := 6 \quad (2)$$

> $l := 8$

$$l := 8 \quad (3)$$

> $m := 6$

$$m := 6 \quad (4)$$

> **Field := electric # Input either 'electric' or 'magnetic' here**
Field := electric

(5)

> **if Field = magnetic then F := 1 else F := 0 end if**
F := 0

(6)

> $Z := (k^2 r^2 - (2 \cdot l + 1))$

$$Z := k^2 r^2 - 17 \quad (7)$$

> Prefactor := simplify $\left(\left(\frac{m}{(m^2)^{\frac{1}{2}}} \right)^{l+F} \cdot \frac{1}{(p+q+l)! \cdot (k^2 \cdot r^2 + 1)^{p+q+1}} \left(2^{p+q+l} \cdot p! \cdot q! \cdot l! \cdot (-1)^{l-p+1} \cdot (-1)^{2 \cdot p+q-l+2-F} \cdot k^{l+1} \cdot r^{l-1} \cdot \left(\text{binomial}(l-1, q-1) \cdot \text{binomial}(q+l, q-1) \cdot (l+1) \cdot \pi \right)^{\frac{1}{2}} \right) \right)$

$$\text{Prefactor} := - \frac{131072}{692835} \frac{k^9 r^7 \sqrt{858} \sqrt{\pi}}{(k^2 r^2 + 1)^{13}} \quad (8)$$

> Last_term := Prefactor \cdot Z

$$\text{Last_term} := - \frac{131072}{692835} \frac{k^9 r^7 \sqrt{858} \sqrt{\pi} (k^2 r^2 - 17)}{(k^2 r^2 + 1)^{13}} \quad (9)$$

> Second_Last_Term := simplify(expand((Prefactor) \cdot ((p+q-1) \cdot (Z^2 + 2 \cdot (p+q-4) \cdot Z - 4 \cdot (2 \cdot p + 2 \cdot q - 3)))), 'size'))

$$\text{Second_Last_Term} := -\frac{131072}{62985} \frac{k^9 r^7 \sqrt{858} \sqrt{\pi} (k^4 r^4 - 18 k^2 r^2 - 67)}{(k^2 r^2 + 1)^{13}} \quad (10)$$

> $\text{Third_Last_Term} := \text{simplify}\left(\text{expand}\left((\text{Prefactor}) \cdot (p + q - 2) \cdot \left(\frac{(2 \cdot p + 2 \cdot q - 3)}{4} \cdot Z^3 + (2 \cdot p^2 + (4 \cdot q - 13) \cdot p + 2 \cdot q^2 - 13 \cdot q + 12) \cdot Z^2 - (-2 p^3 + (-6 \cdot q + 31) \cdot p^2 + (-6 \cdot q^2 + 62 \cdot q - 94) \cdot p - 2 \cdot q^3 + 31 \cdot q^2 - 94 \cdot q + 66) \cdot Z - (16 p^3 + (48 q - 104) p^2 + (48 q^2 - 208 q + 208) p + 16 q^3 - 104 q^2 + 208 q - 120)\right)\right), 'size'\right)$

$$\text{Third_Last_Term} := -\frac{65536}{46189} \frac{k^9 r^7 \sqrt{858} \sqrt{\pi} (7 k^6 r^6 - 165 k^4 r^4 - 387 k^2 r^2 - 191)}{(k^2 r^2 + 1)^{13}} \quad (11)$$

> $\text{Fourth_Last_Term} := \text{simplify}\left(\text{expand}\left((\text{Prefactor}) \cdot (p + q - 2) \cdot (p + q - 3) \cdot \left(\frac{(2 \cdot p + 2 \cdot q - 5)}{12} \cdot Z^4 + \frac{(2 \cdot p^2 + (4 \cdot q - 17) \cdot p + 2 \cdot q^2 - 17 \cdot q + 24)}{2} \cdot Z^3 + (2 \cdot p^3 + (6 \cdot q - 33) \cdot p^2 + (6 \cdot q^2 - 66 \cdot q + 132) \cdot p + 2 \cdot q^3 - 33 \cdot q^2 + 132 \cdot q - 130) \cdot Z^2 + \frac{1}{3} \left((4 \cdot p^4 + (16 \cdot q - 130) \cdot p^3 + (24 \cdot q^2 - 390 \cdot q + 960) \cdot p^2 + (16 \cdot q^3 - 390 \cdot q^2 + 1920 \cdot q - 2482) \cdot p + 4 \cdot q^4 - 130 \cdot q^3 + 960 \cdot q^2 - 2482 \cdot q + 1888)\right) \cdot Z - (16 \cdot p^4 + (64 \cdot q - 208) \cdot p^3 + (96 \cdot q^2 - 624 \cdot q + 964) \cdot p^2 + (64 \cdot q^3 - 624 \cdot q^2 + 1928 \cdot q - 1840) \cdot p + 16 \cdot q^4 - 208 \cdot q^3 + 964 \cdot q^2 - 1840 \cdot q + 1148)\right)\right), 'size'\right)$

$\text{Fourth_Last_Term} :=$

$$-\frac{65536}{2431} \frac{k^9 \sqrt{\pi} r^7 \left(k^8 r^8 - \frac{644}{19} k^6 r^6 + \frac{1794}{19} k^4 r^4 - 76 k^2 r^2 + 17\right) \sqrt{858}}{(k^2 r^2 + 1)^{13}} \quad (12)$$



MULTIPOLE COEFFICIENT GENERATION, $R^{-1}H_{L,M}$,
FOR THE X-VSH, FOR THE ELECTRIC (E) AND
MAGNETIC (B) FIELDS, AND THE ELECTRIC (A) AND
MAGNETIC (C) VECTOR POTENTIALS

Below is the Maple script used to generate the multipole coefficients, $r^{-1}h_{l,m}$, for the Electric and Magnetic fields, and the Electric and Magnetic Vector Potentials in terms of only their windings numbers p and q , their angular momentum numbers l and m , and the radius, r .

> # **X – Vector Spherical Harmonic (VSPH) – Electric field (E),
Magnetic field (B), Electric Potential field (C),
& Magnetic Potential field (A)**

> # **Writing the Multipole Coefficients in terms of the Winding numbers of the Torus knots, and the radius**

This script has been written to determine the form of the multipolar coefficients for the **X vector – spherical-harmonic (VSPH)** term of the **electric field (E)**, **magnetic field (B)**, **magnetic potential field (A)** and the **electric potential field (C)**. To use this script, simply input your choice of variables into the **'Input Variables Required'** section, then run the whole script using the buttons **ctrl + shift + enter**. Then look for the required multipole term below.

The variables below have the following meanings : p, q , are the winding numbers; k , is a scaling constant with dimensions of inverse length; r , is the radius with dimensions of length; l, m are the angular momentum numbers.

> restart

> # **Input Variables Required**

> $p := 5$

$$p := 5 \quad (1)$$

> $q := 1$

$$q := 1 \quad (2)$$

> $l := 5$

$$l := 5 \quad (3)$$

> $m := 1$

$$m := 1 \quad (4)$$

> **Field := electric** # **Input either 'electric' or 'magnetic' here**
 $Field := electric$

(5)

> **PotentialField := No** # **Input either 'Yes' or 'No' here to say if it is a potential field or not**
 $PotentialField := No$

(6)

> **if PotentialField = Yes then PF := 1 else PF := 0 end if**
 $PF := 0$

(7)

> **if Field = magnetic then F := 1 else F := 0 end if**
 $F := 0$

(8)

> **if p = q then p_q := 1 else p_q := 0 end if**
 $p_q := 0$

(9)

> $Z := (k^2 r^2 - 1)$

$$Z := k^2 r^2 - 1 \quad (10)$$

> $Last_term := simplify \left(\left(\frac{m}{(m^2)^{\frac{1}{2}}} \right)^{l+F} \cdot \frac{1}{(p+q+l)! \cdot (k^2 \cdot r^2 + 1)^{p+q+1-PF}} \left(2^{p+q+l+1-PF} \cdot (p+q)^{1-PF} \cdot p! \cdot q! \cdot l! \cdot \right) \right)$

$$\begin{aligned}
& -1)^{l-p+PF} \cdot (-1)^{2 \cdot p+q-l-F-1+2 \cdot PF} \cdot k^{l+2-PF} \cdot r^l \cdot \left(\text{binomial}(l-1, q-1) \right. \\
& \left. \cdot \text{binomial}(q+l, q-1) \cdot (2 \cdot l+1) \cdot \pi^{\frac{1}{2}} \right) \Bigg) \\
& \text{Last_term} := - \frac{\frac{2048}{231} I k^7 r^5 \sqrt{11} \sqrt{\pi}}{(k^2 r^2 + 1)^7} \tag{11}
\end{aligned}$$

$$\begin{aligned}
& > \text{Second_Last_Term} := (\text{Last_term}) \cdot (p+q-1) \cdot Z \\
& \text{Second_Last_Term} := - \frac{\frac{10240}{231} I k^7 r^5 \sqrt{11} \sqrt{\pi} (k^2 r^2 - 1)}{(k^2 r^2 + 1)^7} \tag{12}
\end{aligned}$$

$$\begin{aligned}
& > \text{Third_Last_Term} := \text{simplify} \left(\text{expand} \left((\text{Last_term}) \cdot (p+q-2) \cdot \left(\frac{(2 \cdot p+2 \cdot q-3)}{4} \cdot Z^2 - Z \right. \right. \right. \\
& \left. \left. \left. - 1 \right) \right), 'size' \right) \\
& \text{Third_Last_Term} := - \frac{\frac{2048}{231} I k^7 r^5 \sqrt{11} \sqrt{\pi} (9 k^4 r^4 - 22 k^2 r^2 + 9)}{(k^2 r^2 + 1)^7} \tag{13}
\end{aligned}$$

$$\begin{aligned}
& > \text{Fourth_Last_Term} := \text{simplify} \left(\text{expand} \left((\text{Last_term}) \cdot (p+q-2) \cdot (p+q-3) \cdot Z \right. \right. \\
& \left. \left. \cdot \left(\frac{(2 \cdot p+2 \cdot q-5)}{12} \cdot Z^2 - Z - 1 \right) \right), 'size' \right) \\
& \text{Fourth_Last_Term} := - \frac{\frac{2048}{231} I k^7 r^5 \sqrt{11} \sqrt{\pi} (7 k^6 r^6 - 33 k^4 r^4 + 33 k^2 r^2 - 7)}{(k^2 r^2 + 1)^7} \tag{14}
\end{aligned}$$

>
>
>

TABULATED MULTIPOLE COEFFICIENTS

Below is a sample of the tabulated multipolar coefficients.

Table G.1: The Generalised Multipolar Coefficients For the Vector Spherical Harmonics, Knot type: p=1; q=1

p=1, q=1, Electric and Magnetic Fields			
l	m	E-field	B-field
$r^{-1}f_{l,m}$			
1	1	$-16/3 \frac{k^4 r^2 \sqrt{\pi}}{(k^2 r^2 + 1)^3}$	$-16/3 \frac{ik^4 r^2 \sqrt{\pi}}{(k^2 r^2 + 1)^3}$
1	-1	$16/3 \frac{k^4 r^2 \sqrt{\pi}}{(k^2 r^2 + 1)^3}$	$\frac{-16/3 ik^4 r^2 \sqrt{\pi}}{(k^2 r^2 + 1)^3}$
$r^{-1}g_{l,m}$			
1	1	$-4/3 \frac{\sqrt{2}k^2 \sqrt{\pi} (k^2 r^2 - 3)}{(k^2 r^2 + 1)^3}$	$\frac{-4/3 i\sqrt{2}k^2 \sqrt{\pi} (k^2 r^2 - 3)}{(k^2 r^2 + 1)^3}$
1	-1	$4/3 \frac{\sqrt{2}k^2 \sqrt{\pi} (k^2 r^2 - 3)}{(k^2 r^2 + 1)^3}$	$\frac{-4/3 i\sqrt{2}k^2 \sqrt{\pi} (k^2 r^2 - 3)}{(k^2 r^2 + 1)^3}$
$r^{-1}h_{l,m}$			
1	1	$\frac{-16/3 ik^3 r \sqrt{3} \sqrt{\pi}}{(k^2 r^2 + 1)^3}$	$16/3 \frac{k^3 r \sqrt{3} \sqrt{\pi}}{(k^2 r^2 + 1)^3}$
1	-1	$\frac{16/3 ik^3 r \sqrt{3} \sqrt{\pi}}{(k^2 r^2 + 1)^3}$	$16/3 \frac{k^3 r \sqrt{3} \sqrt{\pi}}{(k^2 r^2 + 1)^3}$

p=1, q=1, Electric and Magnetic Potential Fields			
l	m	A-field	C-field
$r^{-1}f_{l,m}$			
1	1	$\frac{-4/3 ik^3 r^2 \sqrt{\pi}}{(k^2 r^2 + 1)^2}$	$-4/3 \frac{k^3 r^2 \sqrt{\pi}}{(k^2 r^2 + 1)^2}$
1	-1	$\frac{-4/3 ik^3 r^2 \sqrt{\pi}}{(k^2 r^2 + 1)^2}$	$4/3 \frac{k^3 r^2 \sqrt{\pi}}{(k^2 r^2 + 1)^2}$
$r^{-1}g_{l,m}$			
1	1	$\frac{-i/3k \sqrt{2}\sqrt{\pi} (k^2 r^2 - 3)}{(k^2 r^2 + 1)^2}$	$-1/3 \frac{k \sqrt{2}\sqrt{\pi} (k^2 r^2 - 3)}{(k^2 r^2 + 1)^2}$
1	-1	$\frac{-i/3k \sqrt{2}\sqrt{\pi} (k^2 r^2 - 3)}{(k^2 r^2 + 1)^2}$	$1/3 \frac{k \sqrt{2}\sqrt{\pi} (k^2 r^2 - 3)}{(k^2 r^2 + 1)^2}$
$r^{-1}h_{l,m}$			
1	1	$4/3 \frac{k^2 r \sqrt{3}\sqrt{\pi}}{(k^2 r^2 + 1)^2}$	$\frac{-4/3 ik^2 r \sqrt{3}\sqrt{\pi}}{(k^2 r^2 + 1)^2}$
1	-1	$4/3 \frac{k^2 r \sqrt{3}\sqrt{\pi}}{(k^2 r^2 + 1)^2}$	$\frac{4/3 ik^2 r \sqrt{3}\sqrt{\pi}}{(k^2 r^2 + 1)^2}$

Table G.4: The Generalised Multipolar Coefficients For the Vector Spherical Harmonics, Knot type: p=1; q=2

p=1, q=2, Electric and Magnetic Fields			
l	m	E-field	B-field
$r^{-1}f_{l,m}$			
2	2	$\frac{64\sqrt{2}k^5r^3\sqrt{\pi}}{5(k^2r^2+1)^4}$	$\frac{\frac{64i}{5}\sqrt{2}k^5r^3\sqrt{\pi}}{(k^2r^2+1)^4}$
2	-2	$\frac{64\sqrt{2}k^5r^3\sqrt{\pi}}{5(k^2r^2+1)^4}$	$\frac{-\frac{64i}{5}\sqrt{2}k^5r^3\sqrt{\pi}}{(k^2r^2+1)^4}$
3	2	0	0
3	-2	0	0
$r^{-1}g_{l,m}$			
2	2	$\frac{32\sqrt{\pi}\sqrt{3}k^3r(k^2r^2-5)}{15(k^2r^2+1)^4}$	$\frac{\frac{32i}{15}\sqrt{\pi}\sqrt{3}k^3r(k^2r^2-5)}{(k^2r^2+1)^4}$
2	-2	$\frac{32\sqrt{\pi}\sqrt{3}k^3r(k^2r^2-5)}{15(k^2r^2+1)^4}$	$\frac{-\frac{32i}{15}\sqrt{\pi}\sqrt{3}k^3r(k^2r^2-5)}{(k^2r^2+1)^4}$
3	2	0	0
3	-2	0	0
$r^{-1}h_{l,m}$			
2	2	$\frac{\frac{64i}{5}\sqrt{5}k^4r^2\sqrt{\pi}}{(k^2r^2+1)^4}$	$-\frac{64\sqrt{5}k^4r^2\sqrt{\pi}}{5(k^2r^2+1)^4}$
2	-2	$\frac{\frac{64i}{5}\sqrt{5}k^4r^2\sqrt{\pi}}{(k^2r^2+1)^4}$	$\frac{64\sqrt{5}k^4r^2\sqrt{\pi}}{5(k^2r^2+1)^4}$
3	2	0	0
3	-2	0	0

Table G.6: The Generalised Multipolar Coefficients For the Vector Spherical Harmonics, Knot type: p=1; q=2

p=1, q=2, Electric and Magnetic Potential Fields			
l	m	A-field	C-field
$r^{-1}f_{l,m}$			
2	2	$\frac{16^i r^5 \sqrt{2} k^6 \sqrt{\pi}}{(k^2 r^2 + 1)^4}$	$\frac{16 r^5 \sqrt{2} k^6 \sqrt{\pi}}{5 (k^2 r^2 + 1)^4}$
2	-2	$\frac{-16^i r^5 \sqrt{2} k^6 \sqrt{\pi}}{(k^2 r^2 + 1)^4}$	$\frac{16 r^5 \sqrt{2} k^6 \sqrt{\pi}}{5 (k^2 r^2 + 1)^4}$
3	2	$\frac{32 \sqrt{30} k^5 r^4 \sqrt{\pi}}{105 (k^2 r^2 + 1)^4}$	$\frac{-32^i \sqrt{30} k^5 r^4 \sqrt{\pi}}{(k^2 r^2 + 1)^4}$
3	-2	$\frac{32 \sqrt{30} k^5 r^4 \sqrt{\pi}}{105 (k^2 r^2 + 1)^4}$	$\frac{32^i \sqrt{30} k^5 r^4 \sqrt{\pi}}{(k^2 r^2 + 1)^4}$
$r^{-1}g_{l,m}$			
2	2	$\frac{\frac{8^i}{15} \sqrt{\pi} r \sqrt{3} k^2 (k^4 r^4 - 5)}{(k^2 r^2 + 1)^4}$	$\frac{8 \sqrt{\pi} r \sqrt{3} k^2 (k^4 r^4 - 5)}{15 (k^2 r^2 + 1)^4}$
2	-2	$\frac{-\frac{8^i}{15} \sqrt{\pi} r \sqrt{3} k^2 (k^4 r^4 - 5)}{(k^2 r^2 + 1)^4}$	$\frac{8 \sqrt{\pi} r \sqrt{3} k^2 (k^4 r^4 - 5)}{15 (k^2 r^2 + 1)^4}$
3	2	$\frac{8 \sqrt{\pi} \sqrt{10} k^3 r^2 (k^2 r^2 + 7)}{105 (k^2 r^2 + 1)^4}$	$\frac{-\frac{8^i}{105} \sqrt{\pi} \sqrt{10} k^3 r^2 (k^2 r^2 + 7)}{(k^2 r^2 + 1)^4}$
3	-2	$\frac{8 \sqrt{\pi} \sqrt{10} k^3 r^2 (k^2 r^2 + 7)}{105 (k^2 r^2 + 1)^4}$	$\frac{\frac{8^i}{105} \sqrt{\pi} \sqrt{10} k^3 r^2 (k^2 r^2 + 7)}{(k^2 r^2 + 1)^4}$
$r^{-1}h_{l,m}$			
2	2	$-\frac{32 k^3 \sqrt{5} r^2 \sqrt{\pi}}{15 (k^2 r^2 + 1)^3}$	$\frac{\frac{32^i}{15} k^3 \sqrt{5} r^2 \sqrt{\pi}}{(k^2 r^2 + 1)^3}$
2	-2	$\frac{32 k^3 \sqrt{5} r^2 \sqrt{\pi}}{15 (k^2 r^2 + 1)^3}$	$\frac{\frac{32^i}{15} k^3 \sqrt{5} r^2 \sqrt{\pi}}{(k^2 r^2 + 1)^3}$
3	2	0	0
3	-2	0	0

Table G.8: The Generalised Multipolar Coefficients For the Vector Spherical Harmonics, Knot type: p=1; q=3

p=1, q=3, Electric and Magnetic Fields			
l	m	E-field	B-field
$r^{-1}f_{l,m}$			
3	3	$-\frac{768 k^6 r^4 \sqrt{5} \sqrt{\pi}}{35 (k^2 r^2 + 1)^5}$	$-\frac{768 i r^4 k^6 \sqrt{5} \sqrt{\pi}}{35 (k^2 r^2 + 1)^5}$
3	-3	$\frac{768 k^6 r^4 \sqrt{5} \sqrt{\pi}}{35 (k^2 r^2 + 1)^5}$	$-\frac{768 i r^4 k^6 \sqrt{5} \sqrt{\pi}}{35 (k^2 r^2 + 1)^5}$
4	3	0	0
4	-3	0	0
$r^{-1}g_{l,m}$			
3	3	$-\frac{64 \sqrt{5} \sqrt{3} k^4 r^2 \sqrt{\pi} (k^2 r^2 - 7)}{35 (k^2 r^2 + 1)^5}$	$-\frac{64 i \sqrt{5} \sqrt{3} k^4 r^2 \sqrt{\pi} (k^2 r^2 - 7)}{35 (k^2 r^2 + 1)^5}$
3	-3	$\frac{64 \sqrt{5} \sqrt{3} k^4 r^2 \sqrt{\pi} (k^2 r^2 - 7)}{35 (k^2 r^2 + 1)^5}$	$-\frac{64 i \sqrt{5} \sqrt{3} k^4 r^2 \sqrt{\pi} (k^2 r^2 - 7)}{35 (k^2 r^2 + 1)^5}$
4	3	0	0
4	-3	0	0
$r^{-1}h_{l,m}$			
3	3	$-\frac{256 i k^5 r^3 \sqrt{3} \sqrt{35} \sqrt{\pi}}{35 (k^2 r^2 + 1)^5}$	$\frac{256 k^5 r^3 \sqrt{3} \sqrt{35} \sqrt{\pi}}{35 (k^2 r^2 + 1)^5}$
3	-3	$\frac{256 i k^5 r^3 \sqrt{3} \sqrt{35} \sqrt{\pi}}{35 (k^2 r^2 + 1)^5}$	$\frac{256 k^5 r^3 \sqrt{3} \sqrt{35} \sqrt{\pi}}{35 (k^2 r^2 + 1)^5}$
4	3	0	0
4	-3	0	0

Table G.10: The Generalised Multipolar Coefficients For the Vector Spherical Harmonics, Knot type: p=1; q=3

p=1, q=3, Electric and Magnetic Potential Fields			
l	m	A-field	C-field
$r^{-1}f_{l,m}$			
3	3	$-\frac{192i}{35}\sqrt{5}r^4\sqrt{\pi}k^5(k^2r^2-1/3)$ $(k^2r^2+1)^5$	$-\frac{192\sqrt{5}r^4\sqrt{\pi}k^5(k^2r^2-1/3)}{35(k^2r^2+1)^5}$
3	-3	$-\frac{192i}{35}\sqrt{5}r^4\sqrt{\pi}k^5(k^2r^2-1/3)$ $(k^2r^2+1)^5$	$\frac{192\sqrt{5}r^4\sqrt{\pi}k^5(k^2r^2-1/3)}{35(k^2r^2+1)^5}$
4	3	$-\frac{128k^6r^5\sqrt{7}\sqrt{\pi}}{63(k^2r^2+1)^5}$	$\frac{\frac{128i}{63}k^6r^5\sqrt{7}\sqrt{\pi}}{(k^2r^2+1)^5}$
4	-3	$\frac{128k^6r^5\sqrt{7}\sqrt{\pi}}{63(k^2r^2+1)^5}$	$\frac{\frac{128i}{63}k^6r^5\sqrt{7}\sqrt{\pi}}{(k^2r^2+1)^5}$
$r^{-1}g_{l,m}$			
3	3	$-\frac{16i}{35}k^3\sqrt{3}\sqrt{5}r^2\sqrt{\pi}(k^4r^4+2k^2r^2-7)$ $(k^2r^2+1)^5$	$-\frac{16k^3\sqrt{3}\sqrt{5}r^2\sqrt{\pi}(k^4r^4+2k^2r^2-7)}{35(k^2r^2+1)^5}$
3	-3	$-\frac{16i}{35}k^3\sqrt{3}\sqrt{5}r^2\sqrt{\pi}(k^4r^4+2k^2r^2-7)$ $(k^2r^2+1)^5$	$\frac{16k^3\sqrt{3}\sqrt{5}r^2\sqrt{\pi}(k^4r^4+2k^2r^2-7)}{35(k^2r^2+1)^5}$
4	3	$-\frac{32k^4\sqrt{35}r^3\sqrt{\pi}(k^2r^2+9)}{315(k^2r^2+1)^5}$	$\frac{\frac{32i}{315}k^4\sqrt{35}r^3\sqrt{\pi}(k^2r^2+9)}{(k^2r^2+1)^5}$
4	-3	$\frac{32k^4\sqrt{35}r^3\sqrt{\pi}(k^2r^2+9)}{315(k^2r^2+1)^5}$	$\frac{\frac{32i}{315}k^4\sqrt{35}r^3\sqrt{\pi}(k^2r^2+9)}{(k^2r^2+1)^5}$
$r^{-1}h_{l,m}$			
3	3	$\frac{32k^4r^3\sqrt{3}\sqrt{35}\sqrt{\pi}}{35(k^2r^2+1)^4}$	$-\frac{\frac{32i}{35}k^4r^3\sqrt{3}\sqrt{35}\sqrt{\pi}}{(k^2r^2+1)^4}$
3	-3	$\frac{32k^4r^3\sqrt{3}\sqrt{35}\sqrt{\pi}}{35(k^2r^2+1)^4}$	$\frac{\frac{32i}{35}k^4r^3\sqrt{3}\sqrt{35}\sqrt{\pi}}{(k^2r^2+1)^4}$
4	3	0	0
4	-3	0	0

Table G.12: The Generalised Multipolar Coefficients For the Vector Spherical Harmonics, Knot type: p=1; q=4

p=1, q=4, Electric and Magnetic Fields			
l	m	E-field	B-field
$r^{-1}f_{l,m}$			
4	4	$\frac{2048 \sqrt{14}k^7r^5 \sqrt{\pi}}{63 (k^2r^2 + 1)^6}$	$\frac{\frac{2048i}{63} \sqrt{14}k^7r^5 \sqrt{\pi}}{(k^2r^2 + 1)^6}$
4	-4	$\frac{2048 \sqrt{14}k^7r^5 \sqrt{\pi}}{63 (k^2r^2 + 1)^6}$	$\frac{-\frac{2048i}{63} \sqrt{14}k^7r^5 \sqrt{\pi}}{(k^2r^2 + 1)^6}$
5	4	0	0
5	-4	0	0
$r^{-1}g_{l,m}$			
4	4	$\frac{512 \sqrt{\pi} \sqrt{70}k^5r^3 (k^2r^2 - 9)}{315 (k^2r^2 + 1)^6}$	$\frac{\frac{512i}{315} \sqrt{\pi} \sqrt{70}k^5r^3 (k^2r^2 - 9)}{(k^2r^2 + 1)^6}$
4	-4	$\frac{512 \sqrt{\pi} \sqrt{70}k^5r^3 (k^2r^2 - 9)}{315 (k^2r^2 + 1)^6}$	$\frac{-\frac{512i}{315} \sqrt{\pi} \sqrt{70}k^5r^3 (k^2r^2 - 9)}{(k^2r^2 + 1)^6}$
5	4	0	0
5	-4	0	0
$r^{-1}h_{l,m}$			
4	4	$\frac{\frac{1024i}{21} \sqrt{14}k^6r^4 \sqrt{\pi}}{(k^2r^2 + 1)^6}$	$-\frac{1024 \sqrt{14}k^6r^4 \sqrt{\pi}}{21 (k^2r^2 + 1)^6}$
4	-4	$\frac{\frac{1024i}{21} \sqrt{14}k^6r^4 \sqrt{\pi}}{(k^2r^2 + 1)^6}$	$\frac{1024 \sqrt{14}k^6r^4 \sqrt{\pi}}{21 (k^2r^2 + 1)^6}$
5	4	0	0
5	-4	0	0

Table G.14: The Generalised Multipolar Coefficients For the Vector Spherical Harmonics, Knot type: p=1; q=4

p=1, q=4, Electric and Magnetic Potential Fields			
l	m	A-field	C-field
$r^{-1}f_{l,m}$			
4	4	$\frac{512i k^6 r^5 \sqrt{\pi} (k^2 r^2 - 1/2) \sqrt{14}}{(k^2 r^2 + 1)^6}$	$\frac{512 k^6 r^5 \sqrt{\pi} (k^2 r^2 - 1/2) \sqrt{14}}{63 (k^2 r^2 + 1)^6}$
4	-4	$-\frac{512i k^6 r^5 \sqrt{\pi} (k^2 r^2 - 1/2) \sqrt{14}}{(k^2 r^2 + 1)^6}$	$\frac{512 k^6 r^5 \sqrt{\pi} (k^2 r^2 - 1/2) \sqrt{14}}{63 (k^2 r^2 + 1)^6}$
5	4	$\frac{512 k^7 \sqrt{3} \sqrt{35} r^6 \sqrt{\pi}}{385 (k^2 r^2 + 1)^6}$	$-\frac{512i k^7 \sqrt{3} \sqrt{35} r^6 \sqrt{\pi}}{(k^2 r^2 + 1)^6}$
5	-4	$\frac{512 k^7 \sqrt{3} \sqrt{35} r^6 \sqrt{\pi}}{385 (k^2 r^2 + 1)^6}$	$\frac{512i k^7 \sqrt{3} \sqrt{35} r^6 \sqrt{\pi}}{(k^2 r^2 + 1)^6}$
$r^{-1}g_{l,m}$			
4	4	$\frac{\frac{128i}{315} \sqrt{\pi} k^4 \sqrt{70} r^3 (k^4 r^4 + 4 k^2 r^2 - 9)}{(k^2 r^2 + 1)^6}$	$\frac{128 \sqrt{\pi} k^4 \sqrt{70} r^3 (k^4 r^4 + 4 k^2 r^2 - 9)}{315 (k^2 r^2 + 1)^6}$
4	-4	$-\frac{128i \sqrt{\pi} k^4 \sqrt{70} r^3 (k^4 r^4 + 4 k^2 r^2 - 9)}{(k^2 r^2 + 1)^6}$	$\frac{128 \sqrt{\pi} k^4 \sqrt{70} r^3 (k^4 r^4 + 4 k^2 r^2 - 9)}{315 (k^2 r^2 + 1)^6}$
5	4	$\frac{128 \sqrt{\pi} k^5 \sqrt{14} r^4 (k^2 r^2 + 11)}{385 (k^2 r^2 + 1)^6}$	$-\frac{128i \sqrt{\pi} k^5 \sqrt{14} r^4 (k^2 r^2 + 11)}{(k^2 r^2 + 1)^6}$
5	-4	$\frac{128 \sqrt{\pi} k^5 \sqrt{14} r^4 (k^2 r^2 + 11)}{385 (k^2 r^2 + 1)^6}$	$\frac{128i \sqrt{\pi} k^5 \sqrt{14} r^4 (k^2 r^2 + 11)}{(k^2 r^2 + 1)^6}$
$r^{-1}h_{l,m}$			
4	4	$-\frac{512 \sqrt{14} k^5 r^4 \sqrt{\pi}}{105 (k^2 r^2 + 1)^5}$	$\frac{\frac{512i}{105} \sqrt{14} k^5 r^4 \sqrt{\pi}}{(k^2 r^2 + 1)^5}$
4	-4	$\frac{512 \sqrt{14} k^5 r^4 \sqrt{\pi}}{105 (k^2 r^2 + 1)^5}$	$\frac{\frac{512i}{105} \sqrt{14} k^5 r^4 \sqrt{\pi}}{(k^2 r^2 + 1)^5}$
5	4	0	0
5	-4	0	0

Table G.16: The Generalised Multipolar Coefficients For the Vector Spherical Harmonics, Knot type: p=1; q=5

p=1, q=5, Electric and Magnetic Fields			
l	m	E-field	B-field
$r^{-1}f_{l,m}$			
5	5	$-\frac{10240 k^8 r^6 \sqrt{6} \sqrt{7} \sqrt{\pi}}{231 (k^2 r^2 + 1)^7}$	$-\frac{10240 i r^6 k^8 \sqrt{6} \sqrt{7} \sqrt{\pi}}{231 (k^2 r^2 + 1)^7}$
5	-5	$\frac{10240 k^8 r^6 \sqrt{6} \sqrt{7} \sqrt{\pi}}{231 (k^2 r^2 + 1)^7}$	$\frac{-10240 i r^6 k^8 \sqrt{6} \sqrt{7} \sqrt{\pi}}{231 (k^2 r^2 + 1)^7}$
6	5	0	0
6	-5	0	0
$r^{-1}g_{l,m}$			
5	5	$-\frac{1024 \sqrt{5} \sqrt{7} k^6 r^4 \sqrt{\pi} (k^2 r^2 - 11)}{231 (k^2 r^2 + 1)^7}$	$-\frac{1024 i \sqrt{5} \sqrt{7} k^6 r^4 \sqrt{\pi} (k^2 r^2 - 11)}{231 (k^2 r^2 + 1)^7}$
5	-5	$\frac{1024 \sqrt{5} \sqrt{7} k^6 r^4 \sqrt{\pi} (k^2 r^2 - 11)}{231 (k^2 r^2 + 1)^7}$	$\frac{-1024 i \sqrt{5} \sqrt{7} k^6 r^4 \sqrt{\pi} (k^2 r^2 - 11)}{231 (k^2 r^2 + 1)^7}$
6	5	0	0
6	-5	0	0
$r^{-1}h_{l,m}$			
5	5	$\frac{-\frac{2048 i}{231} k^7 \sqrt{77} \sqrt{30} r^5 \sqrt{\pi}}{(k^2 r^2 + 1)^7}$	$\frac{2048 k^7 \sqrt{77} \sqrt{30} r^5 \sqrt{\pi}}{231 (k^2 r^2 + 1)^7}$
5	-5	$\frac{\frac{2048 i}{231} k^7 \sqrt{77} \sqrt{30} r^5 \sqrt{\pi}}{(k^2 r^2 + 1)^7}$	$\frac{2048 k^7 \sqrt{77} \sqrt{30} r^5 \sqrt{\pi}}{231 (k^2 r^2 + 1)^7}$
6	5	0	0
6	-5	0	0

Table G.18: The Generalised Multipolar Coefficients For the Vector Spherical Harmonics, Knot type: p=1; q=5

p=1, q=5, Electric and Magnetic Potential Fields			
l	m	A-field	C-field
$r^{-1}f_{l,m}$			
5	5	$\frac{-\frac{2560i}{231}k^7\sqrt{7}\sqrt{\pi}(k^2r^2-3/5)r^6\sqrt{6}}{(k^2r^2+1)^7}$	$-\frac{2560k^7\sqrt{7}\sqrt{\pi}(k^2r^2-3/5)r^6\sqrt{6}}{231(k^2r^2+1)^7}$
5	-5	$\frac{-\frac{2560i}{231}k^7\sqrt{7}\sqrt{\pi}(k^2r^2-3/5)r^6\sqrt{6}}{(k^2r^2+1)^7}$	$\frac{2560k^7\sqrt{7}\sqrt{\pi}(k^2r^2-3/5)r^6\sqrt{6}}{231(k^2r^2+1)^7}$
6	5	$-\frac{4096k^8r^7\sqrt{11}\sqrt{\pi}}{429(k^2r^2+1)^7}$	$\frac{\frac{4096i}{429}k^8r^7\sqrt{11}\sqrt{\pi}}{(k^2r^2+1)^7}$
6	-5	$\frac{4096k^8r^7\sqrt{11}\sqrt{\pi}}{429(k^2r^2+1)^7}$	$\frac{\frac{4096i}{429}k^8r^7\sqrt{11}\sqrt{\pi}}{(k^2r^2+1)^7}$
$r^{-1}g_{l,m}$			
5	5	$\frac{-\frac{256i}{231}k^5\sqrt{5}\sqrt{7}r^4\sqrt{\pi}(k^4r^4+6k^2r^2-11)}{(k^2r^2+1)^7}$	$-\frac{256k^5\sqrt{5}\sqrt{7}r^4\sqrt{\pi}(k^4r^4+6k^2r^2-11)}{231(k^2r^2+1)^7}$
5	-5	$\frac{-\frac{256i}{231}k^5\sqrt{5}\sqrt{7}r^4\sqrt{\pi}(k^4r^4+6k^2r^2-11)}{(k^2r^2+1)^7}$	$\frac{256k^5\sqrt{5}\sqrt{7}r^4\sqrt{\pi}(k^4r^4+6k^2r^2-11)}{231(k^2r^2+1)^7}$
6	5	$-\frac{1024k^6\sqrt{6}\sqrt{77}r^5\sqrt{\pi}(k^2r^2+13)}{9009(k^2r^2+1)^7}$	$\frac{\frac{1024i}{9009}k^6\sqrt{6}\sqrt{77}r^5\sqrt{\pi}(k^2r^2+13)}{(k^2r^2+1)^7}$
6	-5	$\frac{1024k^6\sqrt{6}\sqrt{77}r^5\sqrt{\pi}(k^2r^2+13)}{9009(k^2r^2+1)^7}$	$\frac{\frac{1024i}{9009}k^6\sqrt{6}\sqrt{77}r^5\sqrt{\pi}(k^2r^2+13)}{(k^2r^2+1)^7}$
$r^{-1}h_{l,m}$			
5	5	$\frac{512r^5\sqrt{30}\sqrt{77}k^6\sqrt{\pi}}{693(k^2r^2+1)^6}$	$\frac{-\frac{512i}{693}r^5\sqrt{30}\sqrt{77}k^6\sqrt{\pi}}{(k^2r^2+1)^6}$
5	-5	$\frac{512r^5\sqrt{30}\sqrt{77}k^6\sqrt{\pi}}{693(k^2r^2+1)^6}$	$\frac{\frac{512i}{693}r^5\sqrt{30}\sqrt{77}k^6\sqrt{\pi}}{(k^2r^2+1)^6}$
6	5	0	0
6	-5	0	0

Table G.20: The Generalised Multipolar Coefficients For the Vector Spherical Harmonics, Knot type: p=1; q=6

p=1, q=6, Electric and Magnetic Fields			
l	m	E-field	B-field
$r^{-1}f_{l,m}$			
6	6	$\frac{16384 k^9 r^7 \sqrt{33} \sqrt{\pi}}{143 (k^2 r^2 + 1)^8}$	$\frac{\frac{16384 i}{143} k^9 r^7 \sqrt{33} \sqrt{\pi}}{(k^2 r^2 + 1)^8}$
6	-6	$\frac{16384 k^9 r^7 \sqrt{33} \sqrt{\pi}}{143 (k^2 r^2 + 1)^8}$	$\frac{-\frac{16384 i}{143} k^9 r^7 \sqrt{33} \sqrt{\pi}}{(k^2 r^2 + 1)^8}$
7	6	0	0
7	-6	0	0
$r^{-1}g_{l,m}$			
6	6	$\frac{4096 \sqrt{\pi} k^7 \sqrt{2} \sqrt{77} r^5 (k^2 r^2 - 13)}{1001 (k^2 r^2 + 1)^8}$	$\frac{\frac{4096 i}{1001} \sqrt{\pi} k^7 \sqrt{2} \sqrt{77} r^5 (k^2 r^2 - 13)}{(k^2 r^2 + 1)^8}$
6	-6	$\frac{4096 \sqrt{\pi} k^7 \sqrt{2} \sqrt{77} r^5 (k^2 r^2 - 13)}{1001 (k^2 r^2 + 1)^8}$	$\frac{-\frac{4096 i}{1001} \sqrt{\pi} k^7 \sqrt{2} \sqrt{77} r^5 (k^2 r^2 - 13)}{(k^2 r^2 + 1)^8}$
7	6	0	0
7	-6	0	0
$r^{-1}h_{l,m}$			
6	6	$\frac{\frac{8192 i}{143} k^8 \sqrt{143} \sqrt{2} r^6 \sqrt{\pi}}{(k^2 r^2 + 1)^8}$	$-\frac{8192 k^8 \sqrt{143} \sqrt{2} r^6 \sqrt{\pi}}{143 (k^2 r^2 + 1)^8}$
6	-6	$\frac{4096 k^7 \sqrt{143} \sqrt{2} r^6 \sqrt{\pi}}{1001 (k^2 r^2 + 1)^7}$	$\frac{\frac{4096 i}{1001} k^7 \sqrt{143} \sqrt{2} r^6 \sqrt{\pi}}{(k^2 r^2 + 1)^7}$
7	6	0	0
7	-6	0	0

p=1, q=6, Electric and Magnetic Potential Fields		
l	m	C-field
A-field		C-field
		$r^{-1}f_{l,m}$
6	6	$\frac{4096^i \sqrt{33} \sqrt{\pi} r^7 k^8 (k^2 r^2 - 2/3)}{(k^2 r^2 + 1)^8}$
6	-6	$\frac{4096 \sqrt{33} \sqrt{\pi} r^7 k^8 (k^2 r^2 - 2/3)}{143 (k^2 r^2 + 1)^8}$
7	6	$\frac{8192 \sqrt{2} \sqrt{1001} \sqrt{3} r^8 k^9 \sqrt{\pi}}{9009 (k^2 r^2 + 1)^8}$
7	-6	$\frac{8192 \sqrt{2} \sqrt{1001} \sqrt{3} r^8 k^9 \sqrt{\pi}}{9009 (k^2 r^2 + 1)^8}$
		$r^{-1}g_{l,m}$
6	6	$\frac{1024^i k^6 \sqrt{2} \sqrt{77} r^5 \sqrt{\pi} (k^4 r^4 + 8 k^2 r^2 - 13)}{(k^2 r^2 + 1)^8}$
6	-6	$\frac{1024 k^6 \sqrt{2} \sqrt{77} r^5 \sqrt{\pi} (k^4 r^4 + 8 k^2 r^2 - 13)}{1001 (k^2 r^2 + 1)^8}$
7	6	$\frac{2048 \sqrt{\pi} k^7 \sqrt{3} \sqrt{143} r^6 (k^2 r^2 + 15)}{9009 (k^2 r^2 + 1)^8}$
7	-6	$\frac{2048 \sqrt{\pi} k^7 \sqrt{3} \sqrt{143} r^6 (k^2 r^2 + 15)}{9009 (k^2 r^2 + 1)^8}$
		$r^{-1}h_{l,m}$
6	6	$\frac{4096 k^7 \sqrt{143} \sqrt{2} r^6 \sqrt{\pi}}{1001 (k^2 r^2 + 1)^7}$
6	-6	$\frac{4096^i k^7 \sqrt{143} \sqrt{2} r^6 \sqrt{\pi}}{1001 (k^2 r^2 + 1)^7}$

p=1,q=6 Magnetic Potential Field continued	
6	$\frac{4096 k^7 \sqrt{143} \sqrt{2r^6} \sqrt{\pi}}{1001 (k^2 r^2 + 1)^7}$
7	$\frac{4096 i k^7 \sqrt{143} \sqrt{2r^6} \sqrt{\pi}}{1001 (k^2 r^2 + 1)^7}$
7	0
7	0
End of Table	

Table G.23: The Generalised Multipolar Coefficients For the Vector Spherical Harmonics, Knot type: p=2; q=1

p=2, q=1, Electric and Magnetic Fields			
l	m	E-field	B-field
$r^{-1}f_{l,m}$			
1	1	$-\frac{32k^4\sqrt{\pi}r^2(k^2r^2-2)}{3(k^2r^2+1)^4}$	$-\frac{\frac{32i}{3}k^4\sqrt{\pi}r^2(k^2r^2-2)}{(k^2r^2+1)^4}$
1	-1	$\frac{32k^4\sqrt{\pi}r^2(k^2r^2-2)}{3(k^2r^2+1)^4}$	$-\frac{\frac{32i}{3}k^4\sqrt{\pi}r^2(k^2r^2-2)}{(k^2r^2+1)^4}$
2	1	$\frac{\frac{32i}{5}k^5r^3\sqrt{2}\sqrt{\pi}}{(k^2r^2+1)^4}$	$-\frac{32k^5r^3\sqrt{2}\sqrt{\pi}}{5(k^2r^2+1)^4}$
2	-1	$\frac{\frac{32i}{5}k^5r^3\sqrt{2}\sqrt{\pi}}{(k^2r^2+1)^4}$	$\frac{32k^5r^3\sqrt{2}\sqrt{\pi}}{5(k^2r^2+1)^4}$
3	1	0	0
3	-1	0	0
$r^{-1}g_{l,m}$			
1	1	$-8/3\frac{\sqrt{2}k^2\sqrt{\pi}(k^4r^4-8k^2r^2+3)}{(k^2r^2+1)^4}$	$-\frac{8/3i\sqrt{2}k^2\sqrt{\pi}(k^4r^4-8k^2r^2+3)}{(k^2r^2+1)^4}$
1	-1	$8/3\frac{\sqrt{2}k^2\sqrt{\pi}(k^4r^4-8k^2r^2+3)}{(k^2r^2+1)^4}$	$-\frac{8/3i\sqrt{2}k^2\sqrt{\pi}(k^4r^4-8k^2r^2+3)}{(k^2r^2+1)^4}$
2	1	$\frac{\frac{16i}{15}k^3\sqrt{3}\sqrt{\pi}r(k^2r^2-5)}{(k^2r^2+1)^4}$	$-\frac{16k^3\sqrt{3}\sqrt{\pi}r(k^2r^2-5)}{15(k^2r^2+1)^4}$
2	-1	$\frac{\frac{16i}{15}k^3\sqrt{3}\sqrt{\pi}r(k^2r^2-5)}{(k^2r^2+1)^4}$	$\frac{16k^3\sqrt{3}\sqrt{\pi}r(k^2r^2-5)}{15(k^2r^2+1)^4}$
3	1	0	0
3	-1	0	0
$r^{-1}h_{l,m}$			
1	1	$-\frac{16ik^3\sqrt{3}\sqrt{\pi}r(k^2r^2-1)}{(k^2r^2+1)^4}$	$\frac{(16k^5r^3-16k^3r)\sqrt{3}\sqrt{\pi}}{(k^2r^2+1)^4}$
1	-1	$\frac{16ik^3\sqrt{3}\sqrt{\pi}r(k^2r^2-1)}{(k^2r^2+1)^4}$	$\frac{(16k^5r^3-16k^3r)\sqrt{3}\sqrt{\pi}}{(k^2r^2+1)^4}$
2	1	$-\frac{32k^4r^2\sqrt{5}\sqrt{\pi}}{5(k^2r^2+1)^4}$	$-\frac{\frac{32i}{5}k^4r^2\sqrt{5}\sqrt{\pi}}{(k^2r^2+1)^4}$
2	-1	$-\frac{32k^4r^2\sqrt{5}\sqrt{\pi}}{5(k^2r^2+1)^4}$	$\frac{\frac{32i}{5}k^4r^2\sqrt{5}\sqrt{\pi}}{(k^2r^2+1)^4}$
3	1	0	0
3	-1	0	0

Table G.25: The Generalised Multipolar Coefficients For the Vector Spherical Harmonics, Knot type: p=2; q=1

p=2, q=1, Electric and Magnetic Potential Fields			
l	m	A-field	C-field
		$r^{-1}f_{l,m}$	
1	1	$\frac{-\frac{4i}{15}k^3\sqrt{\pi}r^2(5k^4r^4+6k^2r^2-23)}{(k^2r^2+1)^4}$	$\frac{4k^3\sqrt{\pi}r^2(5k^4r^4+6k^2r^2-23)}{15(k^2r^2+1)^4}$
1	-1	$\frac{-\frac{4i}{15}k^3\sqrt{\pi}r^2(5k^4r^4+6k^2r^2-23)}{(k^2r^2+1)^4}$	$\frac{4k^3\sqrt{\pi}r^2(5k^4r^4+6k^2r^2-23)}{15(k^2r^2+1)^4}$
2	1	$-\frac{16k^4r^3\sqrt{2}\sqrt{\pi}}{5(k^2r^2+1)^4}$	$\frac{\frac{16i}{5}k^4r^3\sqrt{2}\sqrt{\pi}}{(k^2r^2+1)^4}$
2	-1	$\frac{16k^4r^3\sqrt{2}\sqrt{\pi}}{5(k^2r^2+1)^4}$	$\frac{\frac{16i}{5}k^4r^3\sqrt{2}\sqrt{\pi}}{(k^2r^2+1)^4}$
3	1	$-\frac{\frac{64i}{105}k^5r^4\sqrt{3}\sqrt{\pi}}{(k^2r^2+1)^4}$	$-\frac{64k^5r^4\sqrt{3}\sqrt{\pi}}{105(k^2r^2+1)^4}$
3	-1	$-\frac{\frac{64i}{105}k^5r^4\sqrt{3}\sqrt{\pi}}{(k^2r^2+1)^4}$	$\frac{64k^5r^4\sqrt{3}\sqrt{\pi}}{105(k^2r^2+1)^4}$
		$r^{-1}g_{l,m}$	
1	1	$\frac{-i/3\sqrt{2}k\sqrt{\pi}}{(k^2r^2+1)^4}\left(k^6r^6-\frac{63k^4r^4}{5}-k^2r^2+3\right)$	$-1/3\frac{\sqrt{2}k\sqrt{\pi}}{(k^2r^2+1)^4}\left(k^6r^6-\frac{63k^4r^4}{5}-k^2r^2+3\right)$
1	-1	$\frac{-i/3\sqrt{2}k\sqrt{\pi}}{(k^2r^2+1)^4}\left(k^6r^6-\frac{63k^4r^4}{5}-k^2r^2+3\right)$	$1/3\frac{\sqrt{2}k\sqrt{\pi}}{(k^2r^2+1)^4}\left(k^6r^6-\frac{63k^4r^4}{5}-k^2r^2+3\right)$
2	1	$\frac{32k^4r^3\sqrt{3}\sqrt{\pi}}{15(k^2r^2+1)^4}$	$\frac{-\frac{32i}{15}k^4r^3\sqrt{3}\sqrt{\pi}}{(k^2r^2+1)^4}$

p=2,q=1 Magnetic Potential Field continued			
2	-1	$-\frac{32 k^4 r^3 \sqrt{3} \sqrt{\pi}}{15 (k^2 r^2 + 1)^4}$	$-\frac{32^i k^4 r^3 \sqrt{3} \sqrt{\pi}}{(k^2 r^2 + 1)^4}$
3	1	$-\frac{16^i k^3 \sqrt{\pi r^2 (k^2 r^2 + 7)}}{(k^2 r^2 + 1)^4}$	$-\frac{16 k^3 \sqrt{\pi r^2 (k^2 r^2 + 7)}}{105 (k^2 r^2 + 1)^4}$
3	-1	$-\frac{16^i k^3 \sqrt{\pi r^2 (k^2 r^2 + 7)}}{(k^2 r^2 + 1)^4}$	$\frac{16 k^3 \sqrt{\pi r^2 (k^2 r^2 + 7)}}{105 (k^2 r^2 + 1)^4}$
$r^{-1} h_{l,m}$			
1	1	$1/3 \frac{(8 k^4 r^3 - 8 k^2 r) \sqrt{3} \sqrt{\pi}}{(k^2 r^2 + 1)^3}$	$\frac{-8/3 i k^2 \sqrt{3} \sqrt{\pi r (k^2 r^2 - 1)}}{(k^2 r^2 + 1)^3}$
1	-1	$1/3 \frac{(8 k^4 r^3 - 8 k^2 r) \sqrt{3} \sqrt{\pi}}{(k^2 r^2 + 1)^3}$	$\frac{8/3 i k^2 \sqrt{3} \sqrt{\pi r (k^2 r^2 - 1)}}{(k^2 r^2 + 1)^3}$
2	1	$-\frac{16^i k^3 r^2 \sqrt{5} \sqrt{\pi}}{(k^2 r^2 + 1)^3}$	$-\frac{16 k^3 r^2 \sqrt{5} \sqrt{\pi}}{15 (k^2 r^2 + 1)^3}$
2	-1	$\frac{16^i k^3 r^2 \sqrt{5} \sqrt{\pi}}{(k^2 r^2 + 1)^3}$	$-\frac{16 k^3 r^2 \sqrt{5} \sqrt{\pi}}{15 (k^2 r^2 + 1)^3}$
3	1	0	0
3	-1	0	0
End of Table			

Table G.26: The Generalised Multipolar Coefficients For the Vector Spherical Harmonics, Knot type: p=2; q=2

p=2, q=2, Electric and Magnetic Fields			
l	m	E-field	B-field
$r^{-1}f_{l,m}$			
2	2	$\frac{128\sqrt{2}(k^2r^2 - 5/3)r^3k^5\sqrt{\pi}}{5(k^2r^2 + 1)^5}$	$\frac{\frac{128i}{5}\sqrt{2}(k^2r^2 - 5/3)r^3k^5\sqrt{\pi}}{(k^2r^2 + 1)^5}$
2	-2	$\frac{128\sqrt{2}(k^2r^2 - 5/3)r^3k^5\sqrt{\pi}}{5(k^2r^2 + 1)^5}$	$\frac{-\frac{128i}{5}\sqrt{2}(k^2r^2 - 5/3)r^3k^5\sqrt{\pi}}{(k^2r^2 + 1)^5}$
3	2	$\frac{-\frac{512i}{105}k^6r^4\sqrt{30}\sqrt{\pi}}{(k^2r^2 + 1)^5}$	$\frac{512k^6r^4\sqrt{30}\sqrt{\pi}}{105(k^2r^2 + 1)^5}$
3	-2	$\frac{\frac{512i}{105}k^6r^4\sqrt{30}\sqrt{\pi}}{(k^2r^2 + 1)^5}$	$\frac{512k^6r^4\sqrt{30}\sqrt{\pi}}{105(k^2r^2 + 1)^5}$
$r^{-1}g_{l,m}$			
2	2	$\frac{64\sqrt{\pi}r\sqrt{3}k^3(k^4r^4 - 10k^2r^2 + 5)}{15(k^2r^2 + 1)^5}$	$\frac{\frac{64i}{15}\sqrt{\pi}r\sqrt{3}k^3(k^4r^4 - 10k^2r^2 + 5)}{(k^2r^2 + 1)^5}$
2	-2	$\frac{64\sqrt{\pi}r\sqrt{3}k^3(k^4r^4 - 10k^2r^2 + 5)}{15(k^2r^2 + 1)^5}$	$\frac{-\frac{64i}{15}\sqrt{\pi}r\sqrt{3}k^3(k^4r^4 - 10k^2r^2 + 5)}{(k^2r^2 + 1)^5}$
3	2	$\frac{-\frac{128i}{105}\sqrt{\pi}k^4\sqrt{10}r^2(k^2r^2 - 7)}{(k^2r^2 + 1)^5}$	$\frac{128\sqrt{\pi}k^4\sqrt{10}r^2(k^2r^2 - 7)}{105(k^2r^2 + 1)^5}$
3	-2	$\frac{\frac{128i}{105}\sqrt{\pi}k^4\sqrt{10}r^2(k^2r^2 - 7)}{(k^2r^2 + 1)^5}$	$\frac{128\sqrt{\pi}k^4\sqrt{10}r^2(k^2r^2 - 7)}{105(k^2r^2 + 1)^5}$
$r^{-1}h_{l,m}$			
2	2	$\frac{\frac{512i}{15}\sqrt{\pi}\sqrt{5}k^4r^2(k^2r^2 - 1)}{(k^2r^2 + 1)^5}$	$-\frac{512\sqrt{\pi}\sqrt{5}k^4r^2(k^2r^2 - 1)}{15(k^2r^2 + 1)^5}$
2	-2	$\frac{\frac{512i}{15}\sqrt{\pi}\sqrt{5}k^4r^2(k^2r^2 - 1)}{(k^2r^2 + 1)^5}$	$\frac{512\sqrt{\pi}\sqrt{5}k^4r^2(k^2r^2 - 1)}{15(k^2r^2 + 1)^5}$
3	2	$\frac{512k^5\sqrt{70}r^3\sqrt{\pi}}{105(k^2r^2 + 1)^5}$	$\frac{\frac{512i}{105}k^5\sqrt{70}r^3\sqrt{\pi}}{(k^2r^2 + 1)^5}$
3	-2	$-\frac{512k^5\sqrt{70}r^3\sqrt{\pi}}{105(k^2r^2 + 1)^5}$	$\frac{\frac{512i}{105}k^5\sqrt{70}r^3\sqrt{\pi}}{(k^2r^2 + 1)^5}$

Table G.28: The Generalised Multipolar Coefficients For the Vector Spherical Harmonics, Knot type: p=2; q=2

p=2, q=2, Electric and Magnetic Potential Fields			
l	m	A-field	C-field
$r^{-1}f_{l,m}$			
2	2	$\frac{16i}{5}\sqrt{2}(k^2r^2 - 5/3)r^3k^4\sqrt{\pi}$ $(k^2r^2 + 1)^4$	$\frac{16\sqrt{2}(k^2r^2 - 5/3)r^3k^4\sqrt{\pi}}{5(k^2r^2 + 1)^4}$
2	-2	$-\frac{16i}{5}\sqrt{2}(k^2r^2 - 5/3)r^3k^4\sqrt{\pi}$ $(k^2r^2 + 1)^4$	$\frac{16\sqrt{2}(k^2r^2 - 5/3)r^3k^4\sqrt{\pi}}{5(k^2r^2 + 1)^4}$
3	2	$\frac{64\sqrt{30}r^4k^5\sqrt{\pi}}{105(k^2r^2 + 1)^4}$	$-\frac{64i}{105}k^5r^4\sqrt{30}\sqrt{\pi}$ $(k^2r^2 + 1)^4$
3	-2	$\frac{64\sqrt{30}r^4k^5\sqrt{\pi}}{105(k^2r^2 + 1)^4}$	$\frac{64i}{105}k^5r^4\sqrt{30}\sqrt{\pi}$ $(k^2r^2 + 1)^4$
$r^{-1}g_{l,m}$			
2	2	$\frac{8i}{15}\sqrt{\pi}\sqrt{3}k^2r(k^4r^4 - 10k^2r^2 + 5)$ $(k^2r^2 + 1)^4$	$\frac{8\sqrt{\pi}\sqrt{3}k^2r(k^4r^4 - 10k^2r^2 + 5)}{15(k^2r^2 + 1)^4}$
2	-2	$-\frac{8i}{15}\sqrt{\pi}\sqrt{3}k^2r(k^4r^4 - 10k^2r^2 + 5)$ $(k^2r^2 + 1)^4$	$\frac{8\sqrt{\pi}\sqrt{3}k^2r(k^4r^4 - 10k^2r^2 + 5)}{15(k^2r^2 + 1)^4}$
3	2	$\frac{16\sqrt{\pi}k^3\sqrt{10}r^2(k^2r^2 - 7)}{105(k^2r^2 + 1)^4}$	$-\frac{16i}{105}\sqrt{\pi}k^3\sqrt{10}r^2(k^2r^2 - 7)$ $(k^2r^2 + 1)^4$
3	-2	$\frac{16\sqrt{\pi}k^3\sqrt{10}r^2(k^2r^2 - 7)}{105(k^2r^2 + 1)^4}$	$\frac{16i}{105}\sqrt{\pi}k^3\sqrt{10}r^2(k^2r^2 - 7)$ $(k^2r^2 + 1)^4$
$r^{-1}h_{l,m}$			
2	2	$-\frac{64\sqrt{\pi}r^2\sqrt{5}k^3(k^2r^2 - 1)}{15(k^2r^2 + 1)^4}$	$\frac{64i}{15}\sqrt{\pi}r^2\sqrt{5}k^3(k^2r^2 - 1)$ $(k^2r^2 + 1)^4$
2	-2	$\frac{64\sqrt{\pi}r^2\sqrt{5}k^3(k^2r^2 - 1)}{15(k^2r^2 + 1)^4}$	$\frac{64i}{15}\sqrt{\pi}r^2\sqrt{5}k^3(k^2r^2 - 1)$ $(k^2r^2 + 1)^4$
3	2	$\frac{64i}{105}k^4\sqrt{70}r^3\sqrt{\pi}$ $(k^2r^2 + 1)^4$	$\frac{64k^4\sqrt{70}r^3\sqrt{\pi}}{105(k^2r^2 + 1)^4}$
3	-2	$\frac{64i}{105}k^4\sqrt{70}r^3\sqrt{\pi}$ $(k^2r^2 + 1)^4$	$-\frac{64k^4\sqrt{70}r^3\sqrt{\pi}}{105(k^2r^2 + 1)^4}$

Table G.30: The Generalised Multipolar Coefficients For the Vector Spherical Harmonics, Knot type: p=2; q=3

p=2, q=3, Electric and Magnetic Fields			
l	m	E-field	B-field
$r^{-1}f_{l,m}$			
3	3	$-\frac{(1536 k^2 r^2 - 2304) \sqrt{5} \sqrt{\pi} k^6 r^4}{35 (k^2 r^2 + 1)^6}$	$-\frac{1536 i}{35} (k^2 r^2 - 3/2) \sqrt{5} \sqrt{\pi} k^6 r^4 / (k^2 r^2 + 1)^6$
3	-3	$\frac{(1536 k^2 r^2 - 2304) \sqrt{5} \sqrt{\pi} k^6 r^4}{35 (k^2 r^2 + 1)^6}$	$-\frac{1536 i}{35} (k^2 r^2 - 3/2) \sqrt{5} \sqrt{\pi} k^6 r^4 / (k^2 r^2 + 1)^6$
4	3	$\frac{512 i k^7 r^5 \sqrt{7} \sqrt{\pi}}{21 (k^2 r^2 + 1)^6}$	$-\frac{512 k^7 r^5 \sqrt{7} \sqrt{\pi}}{21 (k^2 r^2 + 1)^6}$
4	-3	$\frac{512 i k^7 r^5 \sqrt{7} \sqrt{\pi}}{21 (k^2 r^2 + 1)^6}$	$\frac{512 k^7 r^5 \sqrt{7} \sqrt{\pi}}{21 (k^2 r^2 + 1)^6}$
5	3	0	0
5	-3	0	0
$r^{-1}g_{l,m}$			
3	3	$\frac{128 \sqrt{2} (k^2 r^2 - 5/3) r^3 k^5 \sqrt{\pi}}{5 (k^2 r^2 + 1)^5}$	$\frac{128 i}{5} \sqrt{2} (k^2 r^2 - 5/3) r^3 k^5 \sqrt{\pi} / (k^2 r^2 + 1)^5$
3	-3	$\frac{128 \sqrt{2} (k^2 r^2 - 5/3) r^3 k^5 \sqrt{\pi}}{5 (k^2 r^2 + 1)^5}$	$-\frac{128 i}{5} \sqrt{2} (k^2 r^2 - 5/3) r^3 k^5 \sqrt{\pi} / (k^2 r^2 + 1)^5$
4	3	$-\frac{512 i k^6 r^4 \sqrt{30} \sqrt{\pi}}{105 (k^2 r^2 + 1)^5}$	$\frac{512 k^6 r^4 \sqrt{30} \sqrt{\pi}}{105 (k^2 r^2 + 1)^5}$
4	-3	$\frac{512 i k^6 r^4 \sqrt{30} \sqrt{\pi}}{105 (k^2 r^2 + 1)^5}$	$\frac{512 k^6 r^4 \sqrt{30} \sqrt{\pi}}{105 (k^2 r^2 + 1)^5}$
5	3	0	0
5	-3	0	0
$r^{-1}h_{l,m}$			
3	3	$\frac{128 \sqrt{2} (k^2 r^2 - 5/3) r^3 k^5 \sqrt{\pi}}{5 (k^2 r^2 + 1)^5}$	$\frac{128 i}{5} \sqrt{2} (k^2 r^2 - 5/3) r^3 k^5 \sqrt{\pi} / (k^2 r^2 + 1)^5$
3	-3	$\frac{128 \sqrt{2} (k^2 r^2 - 5/3) r^3 k^5 \sqrt{\pi}}{5 (k^2 r^2 + 1)^5}$	$-\frac{128 i}{5} \sqrt{2} (k^2 r^2 - 5/3) r^3 k^5 \sqrt{\pi} / (k^2 r^2 + 1)^5$
4	3	$-\frac{512 i k^6 r^4 \sqrt{30} \sqrt{\pi}}{105 (k^2 r^2 + 1)^5}$	$\frac{512 k^6 r^4 \sqrt{30} \sqrt{\pi}}{105 (k^2 r^2 + 1)^5}$
4	-3	$\frac{512 i k^6 r^4 \sqrt{30} \sqrt{\pi}}{105 (k^2 r^2 + 1)^5}$	$\frac{512 k^6 r^4 \sqrt{30} \sqrt{\pi}}{105 (k^2 r^2 + 1)^5}$
5	3	0	0
5	-3	0	0

Table G.32: The Generalised Multipolar Coefficients For the Vector Spherical Harmonics, Knot type: p=2; q=3

p=2, q=3, Electric and Magnetic Potential Fields			
l	m	A-field	C-field
$r^{-1}f_{l,m}$			
3	3	$\frac{-\frac{64i}{315}k^5r^4(27k^4r^4 - 32k^2r^2 - 19)\sqrt{5}\sqrt{\pi}}{(k^2r^2 + 1)^6}$	$-\frac{64k^5r^4(27k^4r^4 - 32k^2r^2 - 19)\sqrt{5}\sqrt{\pi}}{315(k^2r^2 + 1)^6}$
3	-3	$\frac{-\frac{64i}{315}k^5r^4(27k^4r^4 - 32k^2r^2 - 19)\sqrt{5}\sqrt{\pi}}{(k^2r^2 + 1)^6}$	$\frac{64k^5r^4(27k^4r^4 - 32k^2r^2 - 19)\sqrt{5}\sqrt{\pi}}{315(k^2r^2 + 1)^6}$
4	3	$-\frac{256k^8r^7\sqrt{7}\sqrt{\pi}}{63(k^2r^2 + 1)^6}$	$\frac{\frac{256i}{63}k^8r^7\sqrt{7}\sqrt{\pi}}{(k^2r^2 + 1)^6}$
4	-3	$\frac{256k^8r^7\sqrt{7}\sqrt{\pi}}{63(k^2r^2 + 1)^6}$	$\frac{\frac{256i}{63}k^8r^7\sqrt{7}\sqrt{\pi}}{(k^2r^2 + 1)^6}$
5	3	$\frac{\frac{512i}{3465}k^7r^6\sqrt{6}\sqrt{35}\sqrt{\pi}}{(k^2r^2 + 1)^6}$	$\frac{512k^7r^6\sqrt{35}\sqrt{6}\sqrt{\pi}}{3465(k^2r^2 + 1)^6}$
5	-3	$\frac{\frac{512i}{3465}k^7r^6\sqrt{6}\sqrt{35}\sqrt{\pi}}{(k^2r^2 + 1)^6}$	$-\frac{512k^7r^6\sqrt{35}\sqrt{6}\sqrt{\pi}}{3465(k^2r^2 + 1)^6}$
$r^{-1}g_{l,m}$			
3	3	$\frac{128\sqrt{2}(k^2r^2 - 5/3)r^3k^5\sqrt{\pi}}{5(k^2r^2 + 1)^5}$	$\frac{\frac{128i}{5}\sqrt{2}(k^2r^2 - 5/3)r^3k^5\sqrt{\pi}}{(k^2r^2 + 1)^5}$
3	-3	$\frac{128\sqrt{2}(k^2r^2 - 5/3)r^3k^5\sqrt{\pi}}{5(k^2r^2 + 1)^5}$	$-\frac{\frac{128i}{5}\sqrt{2}(k^2r^2 - 5/3)r^3k^5\sqrt{\pi}}{(k^2r^2 + 1)^5}$
4	3	$-\frac{\frac{512i}{105}k^6r^4\sqrt{30}\sqrt{\pi}}{(k^2r^2 + 1)^5}$	$\frac{512k^6r^4\sqrt{30}\sqrt{\pi}}{105(k^2r^2 + 1)^5}$
4	-3	$\frac{\frac{512i}{105}k^6r^4\sqrt{30}\sqrt{\pi}}{(k^2r^2 + 1)^5}$	$\frac{512k^6r^4\sqrt{30}\sqrt{\pi}}{105(k^2r^2 + 1)^5}$
5	3	0	0
5	-3	0	0
$r^{-1}h_{l,m}$			
3	3	$\frac{128\sqrt{2}(k^2r^2 - 5/3)r^3k^5\sqrt{\pi}}{5(k^2r^2 + 1)^5}$	$\frac{\frac{128i}{5}\sqrt{2}(k^2r^2 - 5/3)r^3k^5\sqrt{\pi}}{(k^2r^2 + 1)^5}$
3	-3	$\frac{128\sqrt{2}(k^2r^2 - 5/3)r^3k^5\sqrt{\pi}}{5(k^2r^2 + 1)^5}$	$-\frac{\frac{128i}{5}\sqrt{2}(k^2r^2 - 5/3)r^3k^5\sqrt{\pi}}{(k^2r^2 + 1)^5}$
4	3	$-\frac{\frac{512i}{105}k^6r^4\sqrt{30}\sqrt{\pi}}{(k^2r^2 + 1)^5}$	$\frac{512k^6r^4\sqrt{30}\sqrt{\pi}}{105(k^2r^2 + 1)^5}$
4	-3	$\frac{\frac{512i}{105}k^6r^4\sqrt{30}\sqrt{\pi}}{(k^2r^2 + 1)^5}$	$\frac{512k^6r^4\sqrt{30}\sqrt{\pi}}{105(k^2r^2 + 1)^5}$
5	3	0	0
5	-3	0	0